NTNU – Trondheim
Norwegian University of
Science and Technology

MPD Heave Lab

CBHP Simulations and Hydraulic Analysis

Andreas Laupstad Boge

Petroleum Geoscience and Engineering
Submission date: June 2013
Supervisor: John-Morten Godhavn, IPT

Norwegian University of Science and Technology
Department of Petroleum Engineering and Applied Geophysics

Abstract

Drilling performed from floating drilling rigs subjected to heave motion may be challenging. As the drillstring is suspended in slips during connection, the entire drillstring follows the motion of the floating rig. In harsh environment with heavy waves, drillsting heave induces severe surge and swab effects down hole. In a narrow pressure window reservoir, this effect might be crucial and worst case scenario is to lose the well. MPD on floating rigs is an approach to solve issues regarding surge and swab effects.

A scaled MPD rig subjected to heave motion has been constructed at NTNU. The objective of the scaled rig is to design an automatic operated choke system to reduce pressure fluctuation due to surge and swab effects on a lab scale. A precise hydraulic model is crucial for a successful experiment. This thesis presents two different hydraulic models for the MPD heave lab. A simplified empirical model is developed based on curve matching from fixed choke experiments, this non-linear model is fairly simple and may be implemented as a controller in the heave lab. CBHP simulations based on the empirical model are performed in this thesis, but the controller has not been tested in the lab. A linear controller has been implemented in the heave lab, which reduced BHP fluctuation up to 64% (Albert, A. 2013).

A sophisticated numerical model has also been developed to analyse hydraulics in the heave lab. The numerical model simulates both flow and pressure throughout the entire heave lab. This model deviates slightly from observed data which is caused by unsteady laminar flow effects and unsteady wall shear stress due to fluid acceleration. The hydraulic analysis address important factors for a real case MPD heave compensation operation, such as; fluid acceleration effect on hydraulic friction factor and flow delay caused by fluid inertia.

There is a significant uncertainty associated with along wellbore parameters, especially the unsteady hydraulic friction factor which depends on properties as wellbore geometry and formation properties. Sufficient downhole pressure sampling is crucial for a MPD heave compensation operation, wired drillpipe is therefore advisable, transmitting up to 57600 bits per second.

Abstrakt

Boring utført fra flytende installasjoner utsatt for hivbevegelse kan være utfordrende. Når borestregen er festet i slips for sammenskruing, vil hele borestrengen følge bevegelsen til den flytende installasjonen. I hardt vær med høye bølger, vil borestrengen utsatt for hivbevegelse skape trykkvariasjoner nedi hulls. I ett smalt trykk-vindu reservoar kan denne effekten være avgjørende og i verste fall ødelegge borehullet. MPD på flytende installasjoner er en tilnærming for og løse problemer relatert til hivbevegelse.

En skalert flytende rig utsatt for hivbevegelse har blitt bygget på NTNU. Objektivet med den skalerte riggen er og designe ett automatisk operert choke system som reduserer nedi hull trykkvariasjoner grunnet hivbevegelse på lab basis. En presis hydraulisk model er avgjørende for eksperimentets utfall. Den oppgaven presenterer to forskjellige hydrauliske modeller for den skalerte laben. En forenklet empirisk modell er utviklet basert på kurve tilpasning fra fikset choke åpning eksperimenter, denne ulineære modellen er forholdsvis enkel og kan bli implementert på hiv laben for og styre choken. CBHP simuleringer basert på den empiriske modellen er gjennomført i denne oppgaven, men modellen har ikke blitt testet på laben. En lineær modell har blitt implementert på hiv-laben for og automatisk styre choken, denne modellen reduserte nedi hull trykkvariasjoner opp til 64% (Albert, A 2013).

En sofistikert numerisk modell har også blitt utviklet for og analysere hydraulikk i hiv laben. Den numeriske modellen simulerer både strømning og trykk gjennom hele hiv laben. Denne modellen avviker noe fra lab data som er grunnet ustødig laminær strømning effekter og ustødig grensesjikt spenninger grunnet strømning akselerasjon. Den hydrauliske analysen påpeker viktige faktorer for en reel hiv kompenserte MPD operasjon, som; akselerert strømnings påvirkning på hydraulisk friksjon faktor og strømning forsinkelse grunnet væske tregheter.

Det er en betydelig usikkerhet knyttet til langs brønnbane parametere, spesielt den ustødige hydrauliske friksjons faktor som er avhengig av brønnbane geometri og formasjons egenskaper. Tilstrekkelig nedi hulls trykk prøvetakning er avgjørende for en hiv kompensert MPD operasjon, kabel borestreng er derfor anbefalt, overfører opp til 57 600 bits per sekund.

Acknowledgement

First I would like to thank my advisor John-Morten Godhavn for guidance and feedback. I would also like to thank Sigbjørn Sangesland, Pål Skalle and Stein Tore Johansen for their opinions on experimental observations and modelling approaches. I would like to thank fellow students Anish Phade, Martin Standal Gleditsch, Anders Albert, Jussi Mikael Aanestad and Robert Drønnen for collaboration in the lab. Espen Øybø for sincerely showing us the lab setup and introducing us to his matlab script.

Last but not least I would like to thank Åge Sivertsen and Jarle Glad for their tremendous help and guidance in the lab.

Contents

1.0 Introduction

This project is a corporation between NTNU: The department of Petroleum Engineering and Applied Geophysics (IPT), the department of Engineering Cybernetics and Statoil ASA. Two students from IPT have been working on this project spring 2013.

1.1 Motivation

The world energy consumption is increasing. Even though research regarding renewable energy is being conducted, the world will depend on oil for years to come. From mid-1970 oil fraction of energy consumption has decreased from 46% to approximately 35%. This trend is likely to continue, but oil independency is not likely to occur just yet. It is mainly around technology regarding stationary purposes there has been a decrease in oil demand. In the transportation sector oil demand has increased from 23% to 28%. The comparative advantage of oil in the transportation sector is huge; alternatives such as biofuel technology are not considered a sufficient replacement yet. Todays proved oil reserves are estimated to last for another 50-60 years. We cannot rely on oil independency by 2060, it is therefore important to continue explore and develop new fields. Most of the easy accessible oil have been produced or proven. About half of the undiscovered reserves are assumed to be located offshore. Arctic regions have lately received political and social attention in Norway, this region is assumed to account for 25% of undiscovered reserves. Figure *1.1* illustrate where produced oil resources, proven oil reserves and undiscovered oil reserves are located worldwide.

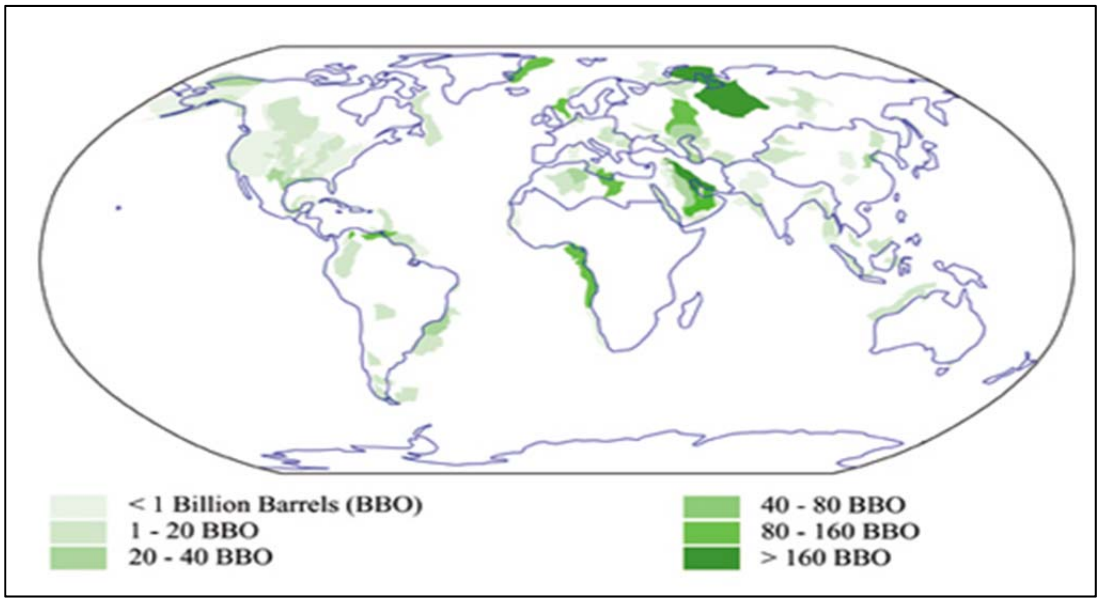

Figure 1.1; Worldwide produced oil resources, proven and undiscovered oil reserves.

The oil industry are moving into harsher environments, drilling into depleted reservoirs to enhance recovery and optimizing economy by drilling more advanced wells. Environment, political restrictions and reservoir conditions require the oil industry to constantly improve technology and safety. To overcome these challenges and requirements “Managed Pressure Drilling” MPD has been developed. MPD is defined as an adaptive drilling process used to more precisely control the annular pressure throughout the well bore.

Numbers of floating rigs are consistently increasing. John Fredriksen’s Seadrill have for example ordered 9 floating rigs for ultra-deep water depths, these are to be delivered from 2013 to 2015. In harsh environments such as offshore Norway, waives can reach a height of 15-20m. A heave compensated top drive is a common technology on floating rigs, but problems erases when the drillstring is suspended in slips during connections. During connections on a floating rig, the drillstring will follow movements of the floating rig. Drillstring heave will cause surge and swab effects down hole. To be able to successfully implement MPD on floating rigs is it important to have a system that can reduce pressure fluctuations down hole throughout the operation.

1.2 Previous Work

The first MPD operation in Norway where carried out in June 2005 by Statoil on Gullfaks C. High pore pressure in the cap rock introduced by water injection made it difficult to drill the well conventionally. Another MPD operation were conducted at Kvitebjørn in 2010, this well was also drilled from a fixed installation rig. Godhavn(2010) presents and discusses results on this MPD operation and control requirements for automatic MPD. Controlling the BHP with MPD on floating rigs has been discussed in several papers; Hannegan et al. (2011), Solvang et al. (2008), Rasmussen and Sangesland (2007). A full scale test has been conducted on Ullrigg in Stavanger, where an automatic control system for heave motion was tested. The test was not successful. A case study of the testing on Ullrigg was written by Landet et al. (2011). Autumn 2011 Camilla Gjengseth and Tollef Svenum presented the design of a lab scaled model for heave motion in “Heave Compensated Manage Pressure Drilling: A Lab Scaled Rig Design.” This model was built at NTNU in Trondheim. Gjengseth and Svenum both wrote their master thesis about the model, and presented commissioning testing and simulation results respectively. Autumn 2012, A. Phade, M. Gleditsch, R. Drønnen, A. Albert, M. Aanestad and A. Boge from NTNU were working with the heave lab. Their work focused on simulations and evaluating lab components and sensor.

1.3 Objective

My master thesis will focus on the heave lab model built at NTNU. The model was initially divided into 3 segments; the surface system, the copper pipe and the actual well with the moving BHA. My master thesis will be a continuation of my specialization project fall 2012 “Experimental Work and Modelling of Surge and Swab Effects”. The objective is to perform experiments and match the pressure model to logged pressure variation in the heave lab. A pressure model for the well is already established, while my master thesis will focus further on the fluid dynamics in the copper pipe and surface system. A model for pressure variations was described by Gjengseth and Svenum, this model will be the fundament for my experiments. In addition to this model will a simplified empirical model be presented. Additional experiments will be performed to evaluate parameters such as system compressibility, copper pipe friction factor and time delay due to pressure propagation. These experimental based parameters will be input values for the pressure model.

1.4 Outline of Thesis

Outline of this thesis is as follows; Chapter 2 is an introduction to MPD as a technology and existing equipment, the MPD heave lab is also presented in this chapter. Chapter 3 presents and evaluates important system parameters such as compressibility, copper pipe friction factor and speed of sound through the copper pipe. Chapter 4 presents derivation of the numerical model and the empirical model, whilst chapter 5 presents its results. Chapter 6 is left as discussion.

2.0 Managed Pressure Drilling

This chapter gives a brief introduction to various types of MPD and most common MPD equipment. The scaled rig constructed at NTNU is briefly introduced in chapter *2.4.*

2.1 MPD Candidates

MPD as a drilling technique is the result of high cost regarding NPT caused by the narrow mud window between pore pressure and fracture pressure. With today's high rig rate, it is essential to reduce the NPT. As defined in the introduction; MPD is an adaptive drilling process to more precisely control the annular pressure profile. When being able to better control the annular pressure, several incidents regarding NPT can be mitigated. Such as; differential sticking and lost circulation – well kick sequence. MPD also enable possibilities for; extending casing points to limit the total number of casings, limiting lost circulation, drilling with total lost returns and increasing the penetration rate. There are various types of MPD techniques and they are listed below.

2.1.1 Constant Bottom Hole Pressure

As a field is depleting, reduced reservoir pressure will change pore pressure, well-bore instability and fracture gradient. As a result the pressure window between the lower and upper stable well-bore pressure decreases. The lower limit is usually the pore pressure and the upper limit is usually fracture pressure. To successfully drill a well, the well-bore pressure must stay within this pressure window boundary. If not; the result might be incidents such as: well bore instability, lost circulation or kick. In a conventional drilling operation the well-bore pressure might change due to change in frictional pressure drop or surge and swab effects. Change in frictional pressure drop occurs when mud circulation is stopped, and surge and swab effects might take place when drilling from a floating rig in harsh weather. In an MPD operation with CBHP as target, actions are taken to mitigate these pressure changes. Equipment used for the operation will be explained in chapter *2.2*, but the concept is as follows: by sealing or releasing annular pressure at surface one can directly control the pressure in the well-bore.

2.1.2 Pressurized Mud-Cap Drilling

Drilling conventionally through a highly fractured reservoir can be difficult due to lost circulation and kicks. The method "mud cap drilling" was first introduced in the Austin Chalk fields to reduce lost time and mud associated with fractured reservoir drilling. The method consisted of bullheading the annulus with heavy mud when lost circulation occurred, to maintain vacuum condition in the upper wellbore section. Water was pumped down inside the drillstring, with no returns to surface. Today's PMCD are quite similar to the method first introduced in Texas. The major difference is that today's PMCD operates with surface pressure. A column of mud that is lighter than required to balance formation pressure is placed within the annulus. A rotating annular seal is introduced to withstand the surface pressure. The advantage of this method is to gather down hole information by monitoring surface pressure. Similar to the concept first introduced in Texas; water is being pumped down the drillstring displacing both water and cuttings into the fractures.

2.1.3 Dual Gradient Drilling

Offshore drilling in deep water causes both rig capacity problems and operational problems for conventional drilling. Marin risers required for drilling at 2000*m* water depth requires large rig capacity, not to mention the amount of drilling fluid required to fill the riser. From an operational aspect is it difficult to weight the mud to stay within boundaries of fracture pressure and pore pressure. Drilling long sections without setting casing, is in many cases impossible. Figure *2.1* below illustrates how many casing points are required to reach TD with 10 000*ft* water depth.

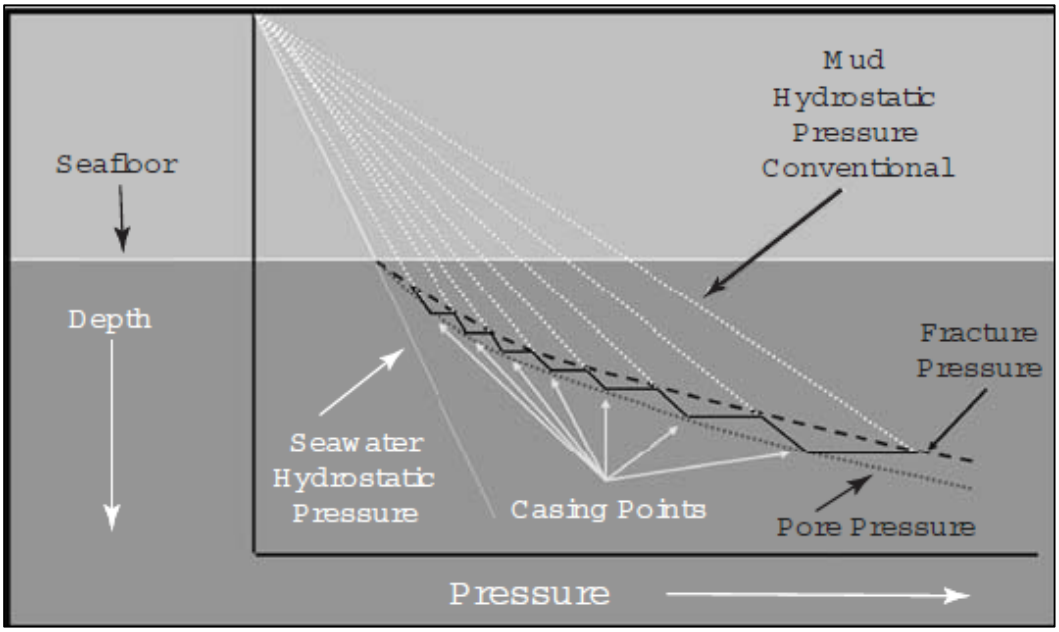

Figure 2.1; Required casing points with 10 000ft water depth.

There are several types of dual gradient systems, but the concept is the same. A dual wellbore gradient is obtained by operating with different drilling fluids within the riser-section and within the actual wellbore. Normally a lighter drilling fluid is used in the riser, to reduce casing points. This is illustrated in figure *2.2*. A riserless system is also available; this system introduces a mud pump placed on the seafloor. The mud pump returns the circulated mud up the return line.

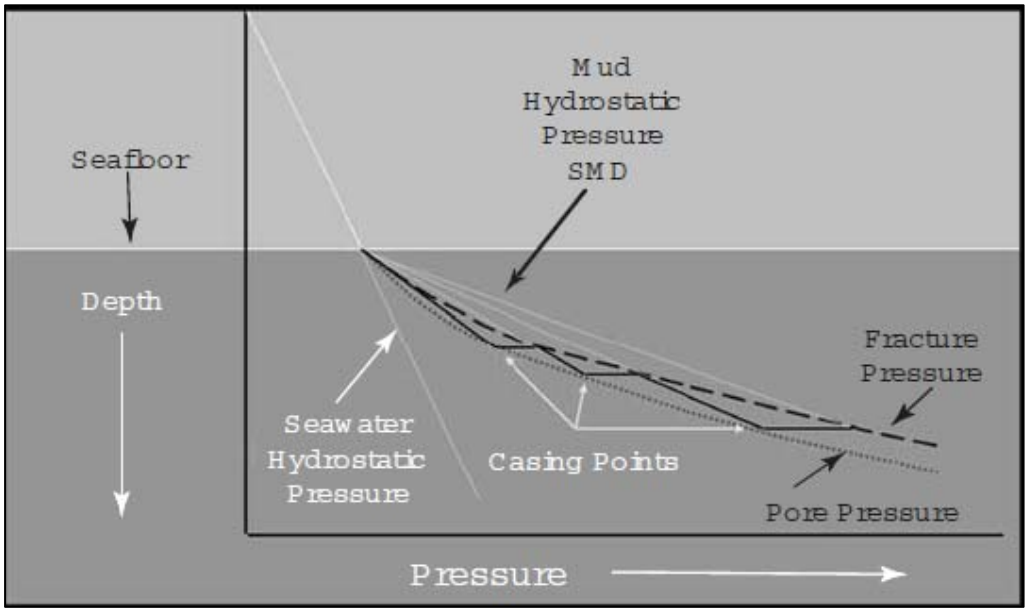

Figure 2.2; reduced casing points with a DG system.

2.2 MPD Equipment

Previous chapter presented different MPD techniques, these concepts requires different equipment than used in a conventional drilling operation. The most common MPD equipment is presented in this chapter.

2.2.1 Rotating Control Device

As discussed in chapter *2.1*, MPD can utilize surface pressure to both control and measure down hole pressure. A rotating control device is designed to seal the annular pressure from atmospheric pressure. Compared to sealing-equipment used in intervention operations, the rotating control device is required to withstand pipe rotation. Two different types of rotating control devices are presented here; a passive system and an active system.

The passive system is a rotating packer that uses an annular seal or “stripper rubber” which is 12.7*mm*-22.2*mm* smaller than the drillpipe. This forms a seal in zero pressure conditions. The passive system is further designed to have increased sealing effect with increased well pressure. Pressure build up in the annulus exerts forces to the seal

element, increasing the seal efficiency. The annular seal assembly rotates with the drillpipe and is locked and sealed into the bearing assembly. The bearing pack is lubricated and cooled by a circulated hydraulic system.

The active system is not supported by the well pressure. The active system is actuated by a hydraulic ram that forces the packer element up against a spherical head, where it seals of against the drillpipe. Two hydraulic systems are implemented; one of them are closing and opening the system, while the second system is used for lubrication and cooling of the bearing packer.

2.2.2 Drilling Choke Manifold

The choke manifold is physically controlling the surface pressure. The mud return flows through a choke at surface, the choke opening determine the surface pressure. If the choke opening is reduced, surface pressure increases. Whilst, an increased choke opening reduce the surface pressure. The choke require flow to control the surface pressure, in a “normal” drilling operation the mud pump is shut off while doing connections. To compensate for stopped circulation, a back-pressure pump is installed to enable pressure control when making up a connection. A continuous circulation system is also developed to enable mud circulation through the drillpipe when making up a connection (not further explained in this project). In a conventional drilling operation, bottom hole pressure varies due to e.g change in flow (change in dynamic pressure). In a CBHP operation the choke manifold is used to reduce pressure fluctuation down hole. When the mud pump are shut off (zero dynamic pressure), back-pressure pump is started and choke opening is decreased to compensate for reduced bottom hole pressure. The choke manifold can be operated manually, semi-automatic or programmable logic controllers (PLC) automatic operated choke. In most CBHP operation an automatic operated choke is required. Wells drilled from floating rigs subjected to heave motion, will experience pressure fluctuation due to surge and swab effects. An automatic operated choke is required to maintain constant bottom hole pressure on floating rigs subjected to heave.

2.3 Heave Motion

Offshore drilling performed from floating rigs subjected to heave is challenging. Harsh weather conditions in the North Sea may impose rig heave excitation close to 13*m*. When the drillstring is suspended in slips, the drillstring will follow the movement of the floating rig. Surge and swab effects caused by rig heave may be severe when drillstring is suspended in slips. Studies show that pulling of pipe creates swab effects of 150-300*psi* (Wagner et al., 1993) and surge effects is ranging between 75-150*psi* (Solvang et al,. 2008). For drilling operations performed in small pressure window reservoirs, severe surge and swab effects might be the difference between a well failure and success. An automatic operated choke will mitigate surge and swab effects.

2.4 Scaled Rig Design

A scaled rig has been constructed at NTNU simulating surge and swab effects on a floating rig subjected to heave motion. Project target is to create an automatic operated choke system to mitigate surge and swab effects simulated in the lab. The scaled rig can be divided into three main components; the actual well, the 900*m* tubing and the surface equipment. Figure *2.3* below illustrates the lab design.

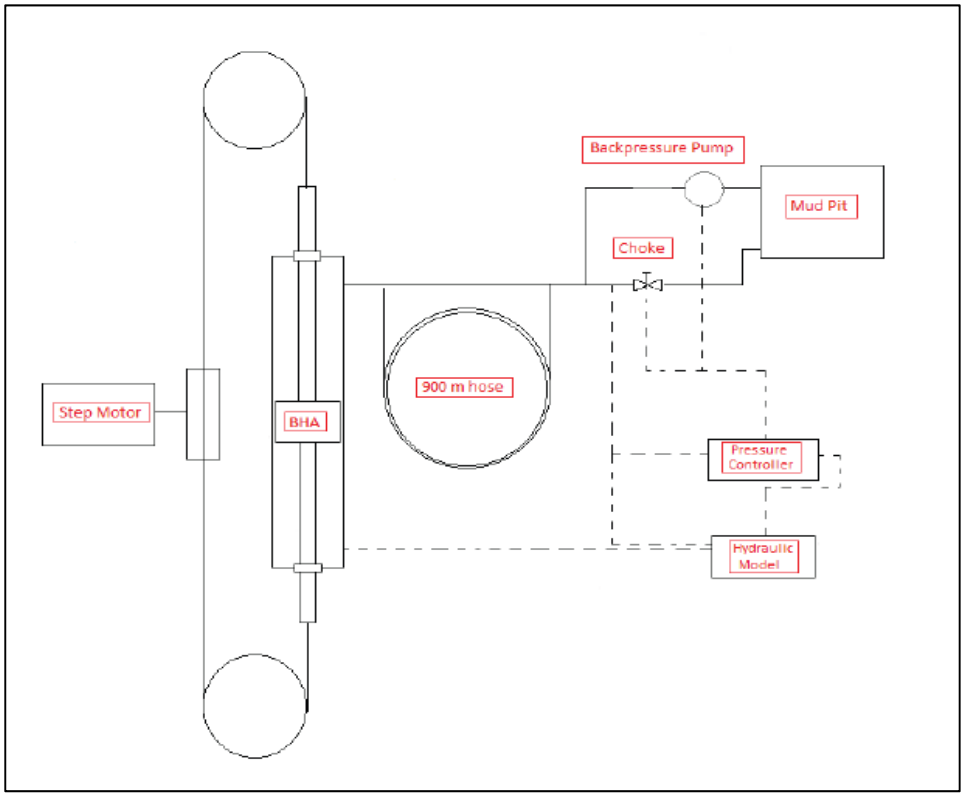

Figure 2.3; MPD heave lab design, figure is adapted from "Heave Compensated Managed Pressure Drilling: A Lab Scaled Rig Design" written by Tollef Svenum and Camilla Gjengseth.

2.4.1 The well

The actual well (referred to as "the well" in this project) consists of a step motor, a 42.53mm ID PVC pipe and a BHA. The well is placed vertically, and the step motor is moving the BHA up and down in the well; simulating surge and swab effects. Figure *2.4* below gives a more detailed configuration of the well. Measurements in figure *2.4* are taken autumn 2012, different OD BHA`s have been tested (test results are presented in "MPD Heave Lab: Experimental work and Modelling of Surge and Swab Effects). *P1* and *P2* are the two pressure sensors within the well, used to measure pressure drop over the BHA in the well. Picture 2.1 below is a photograpgy of the actual well in the MPD heave lab.

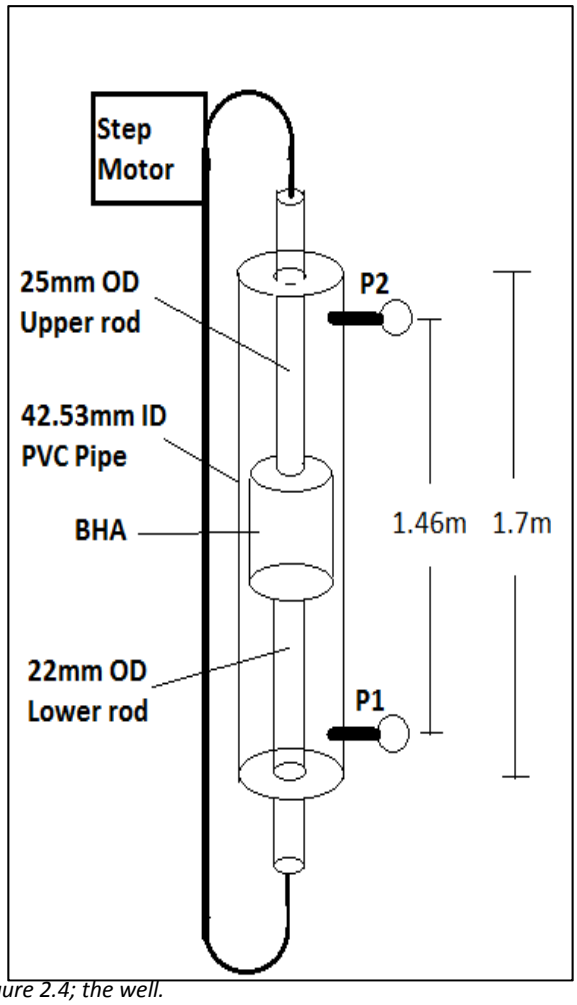

Figure 2.4; the well.

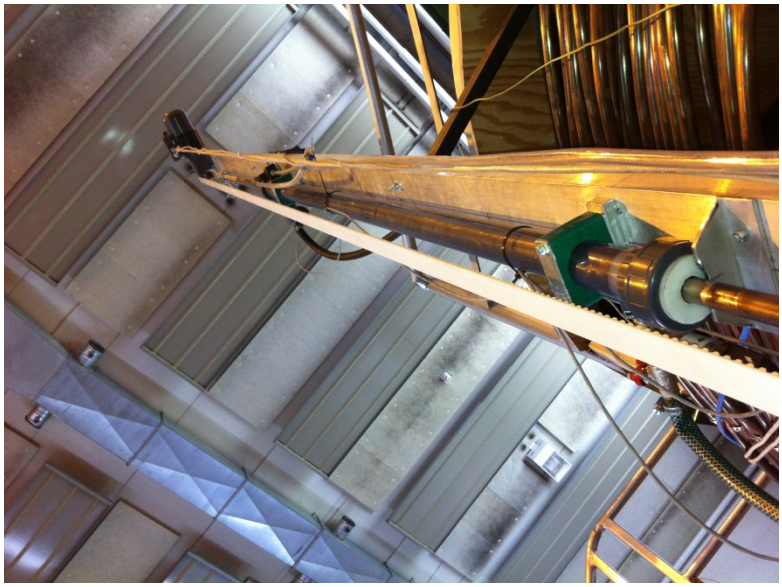

Picture 2.1; the actual well in the MPD heave lab.

2.4.2 The Copper Pipe

The 900*m* long tubing (referred to as “the copper pipe” in this project) is a 900*m* long coiled copper pipe. Of practical and economic reasons was it no possible to drill a 900*m* long vertical well. A 900*m* long coiled copper pipe was therefore included to simulate the upper 900*m* of the well. An important aspect within CBHP drilling, is the time delay caused by pressure propagation. Pressure propagates with the velocity of sound in the respective fluid. This phenomena cause a time delay from when counteractive pressure regulating is performed at surface until it is recognized down hole. The 900m long copper pipe was included to simulate this time delay. Picture 2.2 below illustrate the 900*m* long copper pipe installed in the MPD heave lab.

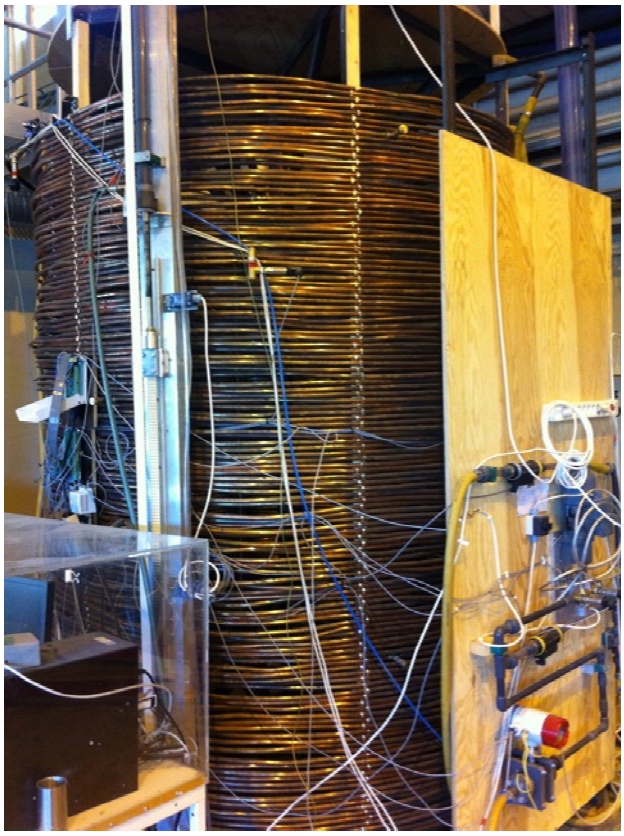

Picture 2.2; copper pipe

2.4.3 Surface Equipment

The surface equipment consists of; the choke, the back-pressure pump, “the mud pit” and the hydraulic model. The surface equipment is aimed to control the pressure within the well. The back-pressure pump is consistently circulating water from “the mud pit” through the choke. The choke opening can determine the pressure upstream the choke, thereby controlling the pressure in the well. Surge effects increases the BHP, by reducing surface pressure, BHP can be maintained constant. Swab effects decreases the BHP, increased surface pressure can maintain CBHP. Maintaining constant pressure in the well requires accurate surface pressure. An automatic operated choke is therefore

required to maintain constant pressure in the well. Picture 2.3 below illustrates the actual choke installed in the MPD heave lab.

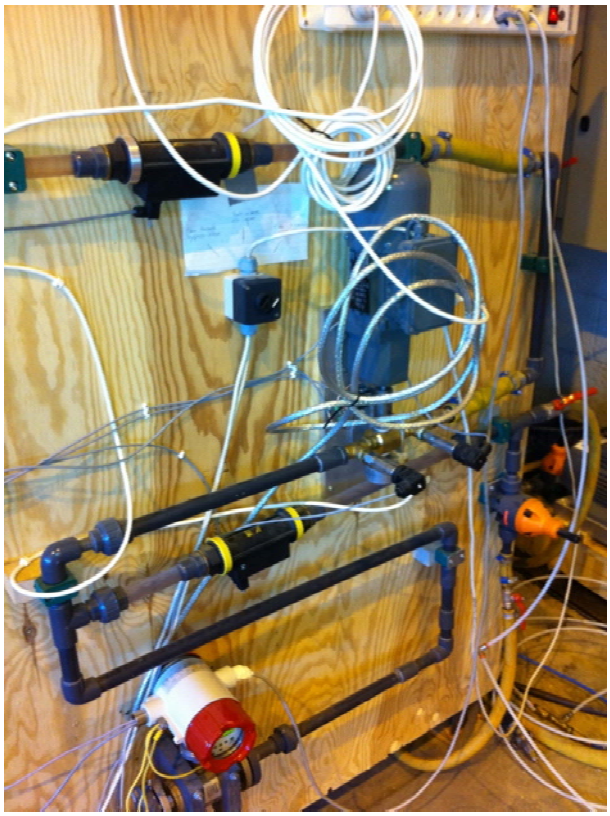

Picture 2,3; Choke system.

2.4.4 BHA Oscillation

The oscillating BHA string simulates Surge and Swab effects induced by pipe movement for a floating rig subjected to heave motion. A Simulink program has been developed to control the step-motor moving the BHA. It is possible to simulate endless variations of pipe movement with the Simulink program. However; all modelling presented in this thesis is based on a simple sinusoidal pipe movement. The BHA position is given by equation *2.4.1*. The BHA velocity and acceleration is by definition the derivative and double-derivative of the BHA position and are given by equation *2.4.2* and *2.4.3* respectively.

$$z_{string}(t) = A_{string} \sin\left(\frac{2\pi\, t}{T_{string}}\right) + E_{string} \qquad (2.4.1)$$

$$v_{string}(t) = \frac{2\pi A_{string}}{T_{string}} \cos\left(\frac{2\pi\, t}{T_{string}}\right) \quad (2.4.2)$$

$$a_{string}(t) = -A_{string}\left(\frac{2\pi}{T_{string}}\right)^2 \sin\left(\frac{2\pi t}{T_{string}}\right) \quad (2.4.3)$$

Where A_{string} is the amplitude of the BHA oscillation, T_{string} is the period of the oscillation and E_{string} is the equilibrium point of the BHA motion.

3.0 System specifications and Parameters

This chapter presents system specifications and calibration of sensors installed in the MPD Heave Lab. Furthermore are relevant system parameters evaluated, such as; compressibility, copper pipe friction factor and speed of sound.

3.1 System Specifications and Sensors Calibration

Previous chapter presented three categories for which the Heave Lab may be divided into. These are the well, the copper pipe and the surface equipment. Besides are there several rubber hoses connecting the different lab components together, these rubber hoses are installed of practical reasons. Various types of flow and pressure sensors are located around the Heave lab for detailed analyses. Schematic below illustrate where the different sensors are located and how the different lab components are connected.

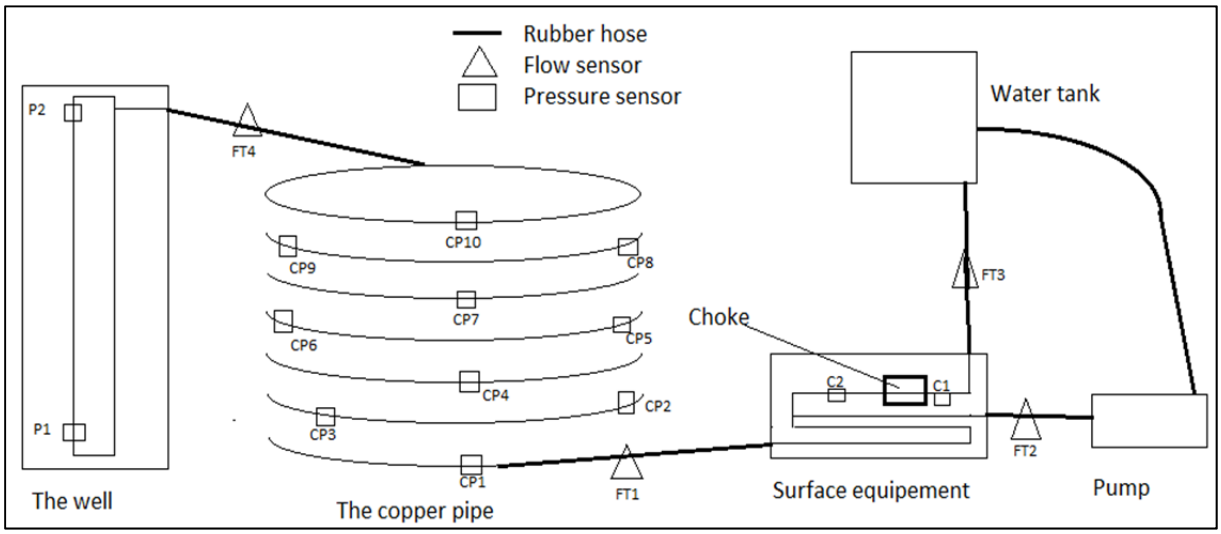

Figure(3.1); lab setup.

3.1.1 Volumes and Lengths

Rubber hoses connect both well to copper pipe and copper pipe to surface equipment. Well fluid is being displaced through these flexible rubber hoses, and they are therefore an important part of the system in terms of compressibility. The well-copper pipe hose consists of two different rubber hoses; a 13*mm* ID hose and a 19*mm* ID hose. Detailed pipe lengths and volumes are given in table *3.1* below.

Component	Tubular	lenght [m]	ID [mm]	volume [L]
Copper pipe	16mm ID Copper pipe	893.69	16	179.69
Well-CP hose	Yellow 19mm ID rubber hose	1.3	19	0.37
	Black 13mm ID rubber hose	2.25	13	0.3
CP-surface eq	Yellow 19mm ID rubber hose	1.61	19	0.46
Well	Ref: Figure (2.4)			1.32
total				182.14

Table (3.1); System lengths and volumes.

It is important to evaluate the system volume upstream the choke, for accurate compressibility calculations presented in chapter *3.2*. Furthermore; accurate hose and copper pipe lengths are presented in this sub-chapter which is important for pressure drop evaluation. The system has been drained and measured to confirm the total volume. System drainage was performed by aid of a 10*barg* air pressure system, and resulted in a total volume of 180*L*. The discrepancy between measured and calculated volume equates to 1.1%. This discrepancy is likely caused by deviation from copper pipe nominal inner diameter. In further calculations, measured volume of 180*L* is assumed correct.

3.1.2 Pressure Sensor Calibration

Prior to performing any heave lab experiments have all pressure sensors been calibrated and evaluated. All 14 pressure sensors mounted on the heave lab system ranges from 0*barg* to 16*barg*, figure *3.1* illustrate where the different sensors are located. Each pressure sensor transmits a current of 4*mA* when measuring 0*barg* and 20*mA* for 16*barg*. A resistance of 500*Ω* is installed, which transforms the signal to range between 2*V* and 10*V*. This gives the following relation between pressure *P* and voltage *U*; $P = 2 \times (U - 2)$. Where pressure *P* is given in barg and voltage *U* is given in *V*.

A static test was performed to evaluate the hydrostatic pressure relation between the various sensors. Calibration of *P1* and *P2* located within the well is presented in “MPD Heave Lab: Experimental Work and Modelling of Surge and Swab Effects” by A. Boge. Since sensors *P1* and *P2* have already been calibrated, can remaining sensors can be calibrated against *P1* or *P2*. In this calibration test was *P2* used as the reference pressure. The entire system was pressurized to 10*barg*, water was then released to gradually decrease the pressure in the isolated system. Graph *3.1* illustrates how *P2* changed while gradually decreasing the system pressure.

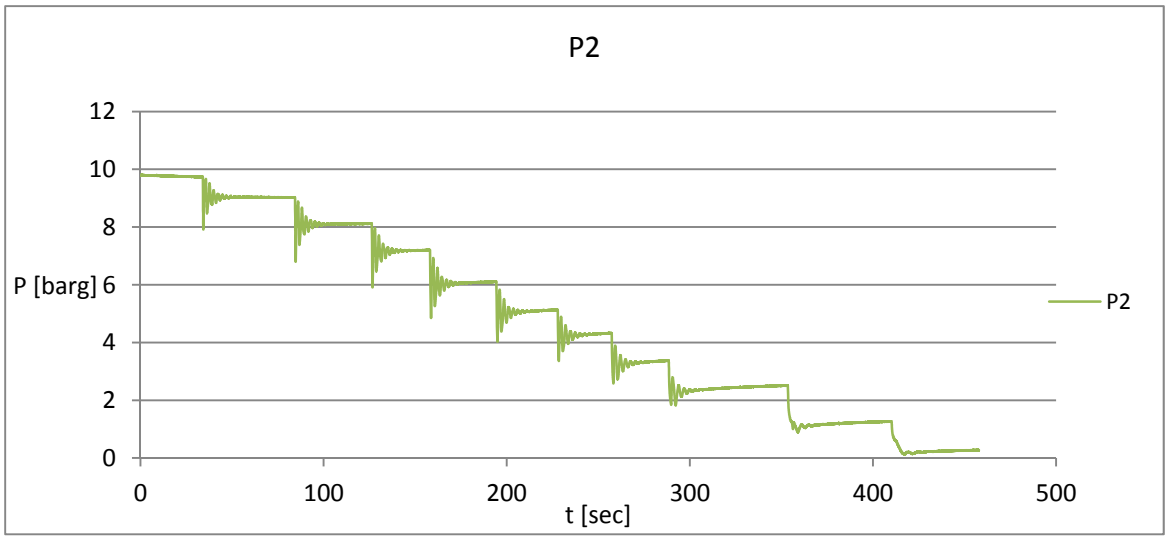

Graph(3.1); pressure response while releasing water from an isolated system.

Graph *3.1* illustrate how the pressure was decreased from 10*barg* to 0*barg*, the graph clearly illustrate severe pressure fluctuation in the transition zones. The pressure fluctuations are caused by pressure waves being reflected within the closed system. This phenomena is further discussed in chapter *4.1.4*. Water density is assumed constant with varying pressure (discussed in chapter *3.2*), the hydrostatic pressure between all pressure sensors are therefore constant for this experiment. Hydrostatic pressure difference between each pressure sensor is calculated from $\Delta P_{hyd} = \rho g \Delta h$, where ΔP_{hyd} is given in Pa, water density ρ is given in $^{kg}/_{m^3}$, g equates 9.81 $^{m}/_{s^2}$ and height difference Δh is given in *m.* Table *3.2* below presents sensor height above ground level h_{ground}, height difference from pressure sensor *P2*; Δh_{P2-CPi}, and theoretical pressure difference between the respective pressure sensor and *P2*.

sensor	h (ground) [m]	Δh [m]	P(hyd) [Pa]
CP1	0.1	3.95	38680
CP2	0.3	3.75	36721
CP3	0.6	3.45	33784
CP4	0.85	3.2	31335
CP5	1.2	2.85	27908
CP6	1.53	2.52	24677
CP7	1.85	2.2	21543
CP8	2.18	1.87	18312
CP9	2.5	1.55	15178
CP10	2.73	1.32	12926
P1	2.35	1.7	16647
P2	4.05	0	0
C1	1.02	3.03	29671
C2	1.02	3.03	29671

Table(3.2); pressure sensor specifications.

Theoretical hydrostatic pressure difference presented in table *3.2* has been used to calibrate all pressure sensors, given *P2*. The pressure-voltage relations have been altered to match theoretical values and measured values. Table *3.3* presents modified pressure-voltage relations and average pressure differences between the respective sensor and *P2* over the 450*sec* testing period.

sensor	P-U relationship	Measured average P(hyd) [Pa]
CP1	P=2*(U-2)	38381
CP2	P=2*(U-1.98)	36590
CP3	P=2*(U-1.83)	33845
CP4	P=2*(U-1.975)	31701
CP5	P=2*(U-2)	28934
CP6	P=2*(U-2.015)	25328
CP7	P=2*(U-2)	20250
CP8	P=1.99*(U-2.01)	18507
CP9	P=2*(U-2)	16591
CP10	P=2*(U-2)	12243
P1	P=1.988*(U-2)	16142
P2	P=2*(U-2)	0
C1	P=1.995*(U-2)	30338
C2	P=2*(U-1.805)	30326

Table(3.3); Pressure-Voltage relation and average pressure differences between each sensor and P2.

Graphs *3.2* through *3.4* below presents all measured sensor values throughout the testing period. Each sensor is represented as the pressure difference between the respective sensor and *P2*. Constant water density results in constant hydrostatic pressure; this is reflected in graphs plotted below. In graphs *3.2* through *3.4* are pressure disturbances in the transition zones quite dominating, however; hydrostatic pressure trends are clearly illustrated.

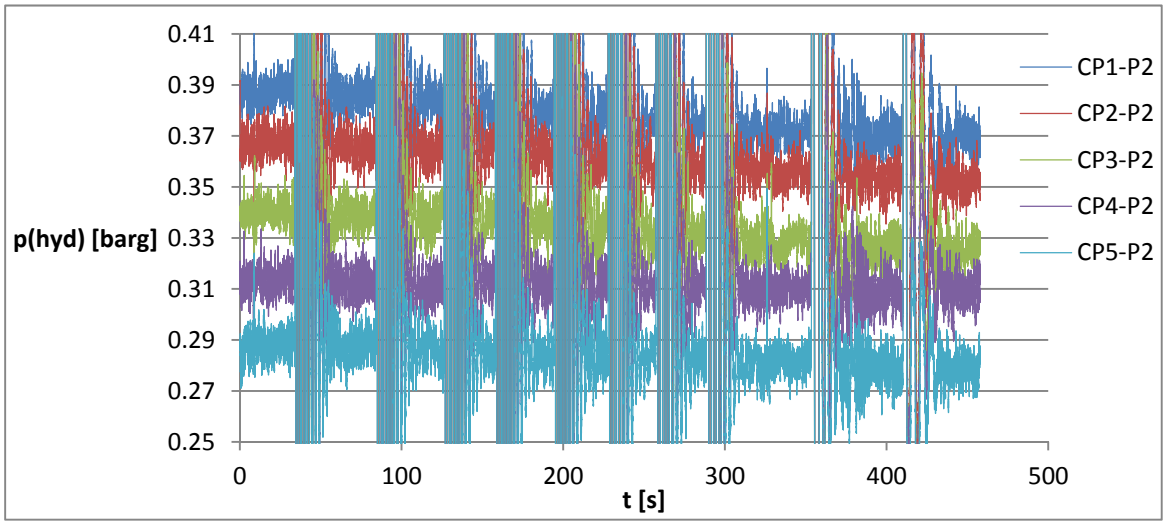

Graph(3.2); measured pressure difference between P2 and CP1,CP2,CP3,CP4 and CP5.

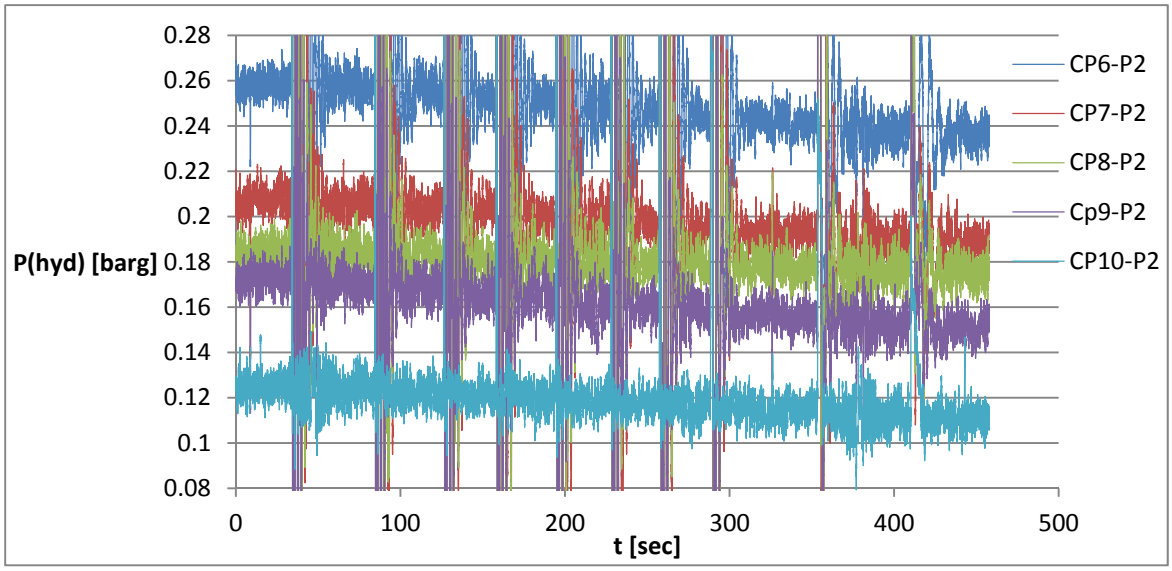

Graph(3.3); measured pressure difference between P2 and CP6,CP7,CP8.CP9 and CP10.

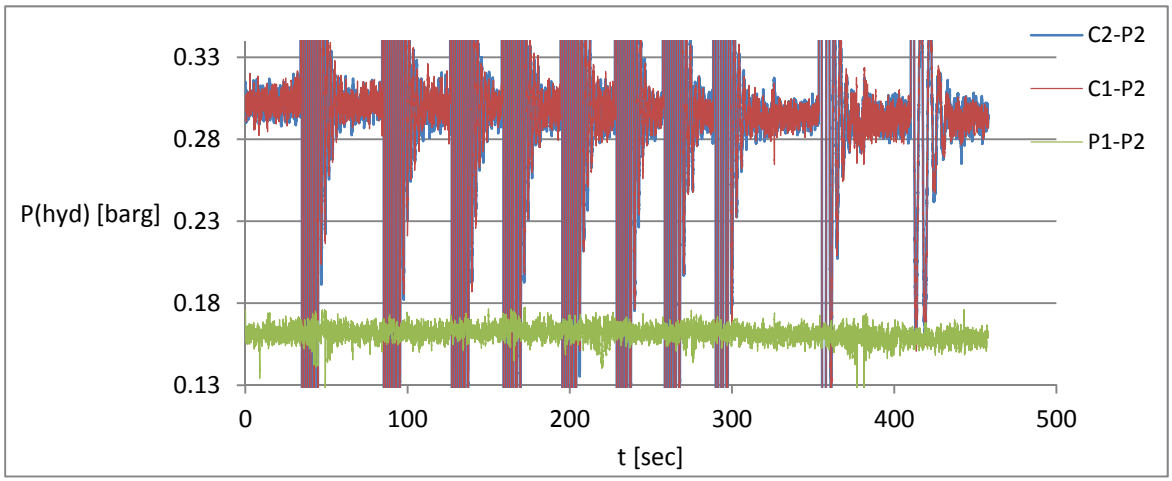

Graph(3.4); measured pressure difference between P2 and C2,C1 and P1.

3.1.3 Flowmeter Calibration

There are currently 3 flowmeters installed on the heave lab system. Figure *3.1* illustrate where the different flowmeters are located. Flowmeter *FT4* measuring displaced flowrates from the well is as of now (june, 2013) not installed. Both *FT2* and *FT3* are mechanical flowmeters, measuring flow based on a rotating spinner device. *FT1* is a magnetic inductive flowmeter, which is capable of measuring flow in both directions. FT1 is programmed to measure flowrates ranging from 0*LPM* to 6*LPM*. Higher flowrates than 6*LPM* are not expected when running the BHA, for a period of T_{string}=3*sec* maximum flowrate equates to;

$$FT1_{max} = v_{string,max}\Delta A_{ur-lr} = Max\left(\frac{2\pi A_{string}}{T_{string}}\cos\left(\frac{2\pi t}{T_{string}}\right)\right)\frac{\pi}{4}\left({D_{ur}}^2 - {D_{lr}}^2\right)$$

$$= \frac{2\pi\times 0.4}{3}\,\frac{\pi}{4}\,(0.025^2 - 0.022^2) = 9.28\times 10^{-5}\,{}^{m^3}/_{s} = 5.57LPM.$$ *FT1* transmits a current of 4*mA* for 0*LPM* and 20*mA* for 6*LPM*. This signal is converted to 2*V* and 10*V* respectively by a 500*Ω* resistor. This gives the following relation between measured signal *U* in voltage and flowrate *FT1* in *LPM*; $FT1 = 0.75\times(U-2)$. *FT2* and *FT3* transmits a current of 4*mA* for 0*LPM* and 20*mA* for 100*LPM*, which is also converted to voltage by a 500*Ω* resistor. The signal received by *FT2* and *FT3* is theoretically converted to *LPM* by the following expression; $FT2 = FT3 = 12.5\times(U-2)$.

Several experiments have been performed to evaluate the flowmeters, the first experiment was performed to evaluate the accuracy of *FT1*. In this experiment was water steadily pumped through *FT1* and collected in a bucket, which was weighted after 30 seconds of flowing. The flowrate was also read from the flowmeter display for each flowrate. Measured data from the flow experiment is listed in table *3.4.* Not surprisingly does column 3 and 4 coincide, where column 3 represents data read from the flowmeter display. Data in column 4 is an average value of signals transmitted to the computer, transmitted signals are plotted in graph *3.5*. Weighted values listed in column 2 are reasonable close to the other measurements considering the difficulty of conducting a measurement in exactly 30 seconds.

flow	Weighted flow *LPM*	from display *LPM*	average data
1	0.428	0.41	0.409
2	1.304	1.29	1.287
3	2.676	2.64	2.647
4	4.278	4.2	4.214
5	5.364	5.32	5.330

Table(3.4); flowrate data for FT1.

The second experiment was performed to calibrate *FT2* with respect to *FT1*, flow ranging from 8*LPM* to approximately 28*LPM* was measured. Water was pumped through both *FT1* and *FT2*, which is connected in series. Even though *FT1* is programmed to reach saturation level at 6*LPM*, is the *FT1* display capable of displaying higher flowrates.

Flowrates read from the *FT1* display have been used to calibrate *FT2*, these data are listed in column 2 of table *3.5*. These measurements have been used to alter the voltage-flowrate relation for *FT2*. The improved voltage-flowrate relation is found in table *3.6*. Average flowrates over the testing period is found in column 3 of table *3.5*. Some discrepancies are present between *FT1* and *FT2*, these discrepancies are likely caused by inaccurate *FT2* measurements. The mechanical *FT2* device is not as accurate as the magnetic inductive flowmeter.

flow	FT1 values *LPM*	average data *LPM*
1	8.21	8.351
2	11.46	11.612
3	15.75	15.869
4	19.8	19.799
5	24.87	24.598
6	28.11	27.633

Table(3.5); flowrate data read from the FT1 display and average values for FT2.

Measurements obtained from experiment 1 are plotted in graph *3.5* below, where measurements from both *FT1* and *FT2* are presented. *FT2* values are plotted based on calibration conducted in experiment 2. Experiment 1 reveals the inaccuracy of *FT2* for flowrates lower than 4*LPM*. For even lower flowrates does *FT2* indicate zero flow. This error is caused by an insufficient fluid-momentum to overcome the torque required to rotate the mechanical spinner *FT2*. However; *FT2* is installed to measure flowrates from the pump expected in the range of 20*LPM* and 30*LPM*, this low flowrate inaccuracy of *FT2* is therefore not an issue for the heave lab.

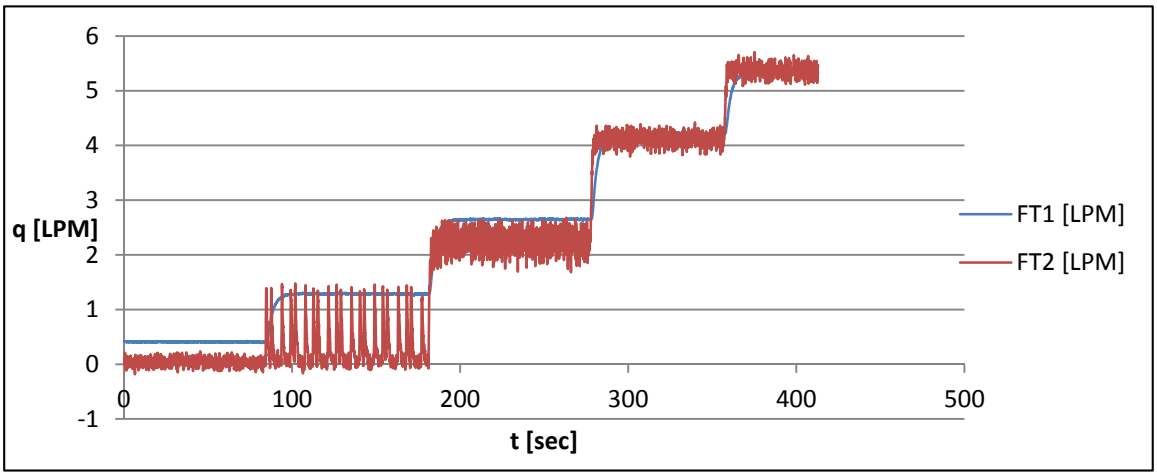

Graph(3.5); Flowrate from calibration experiment 1.

In calibration experiment 3 was the choke open as opposed to experiment 1 and 2. The entire flowrate was forced through *FT2* and *FT3*, enabling calibration of *FT3*. By means of *FT2* was *FT3* calibrated similar to calibration procedure in experiment 2. The altered voltage-pressure relation for *FT3* is also listed in table *3.6*. Graph *3.6* illustrate

that flow measurements obtained by *FT2* and *FT3* matches for the entire flow interval. The percentage discrepancy between *FT2* and *FT3* does not exceed 3% for the entire interval.

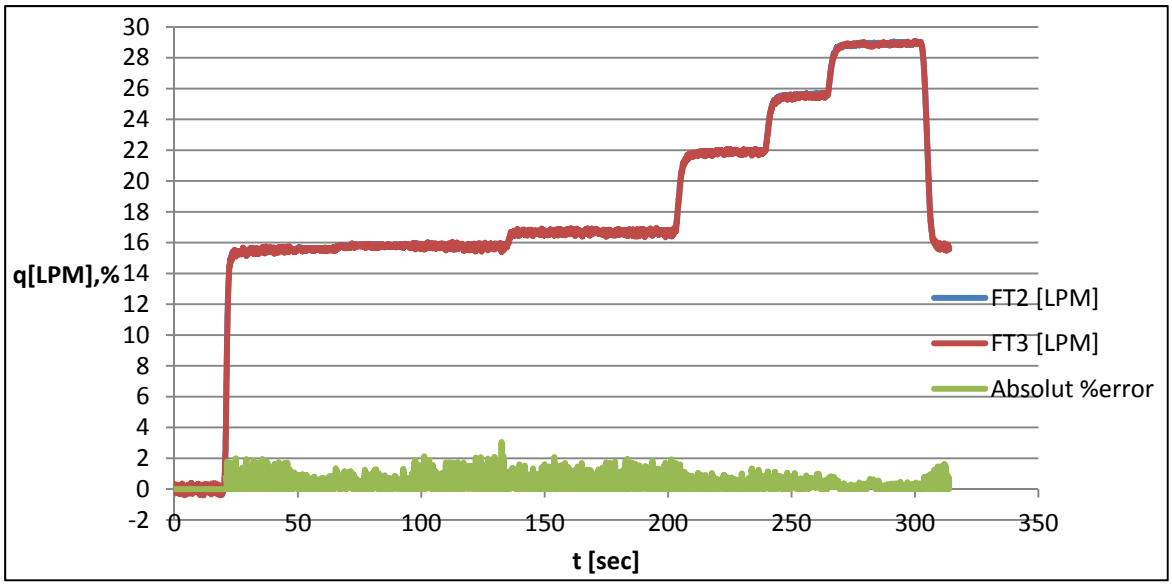

Graph(3.6); measured flowrates by FT2 and FT3, and % discrepancy between FT2 and FT3.

Sensor	P/U relationship
FT1	P=0.75*(U-2)
FT2	P=11.53*(U-2.178)
FT3	P=11.62*(U-1.876)

Table(3.6); pressure voltage relation for all flowmeters.

3.2 Compressibility

Compressibility is a measure of relative volume change within in a fluid or solid, subjected to a change in pressure. Water is used as drilling fluid in the MPD heave lab. Water is usually assumed incompressible and the compressibility effect is therefore neglected when calculating fluid flow. Graph *3.7* below illustrates how water compressibility varies with pressure.

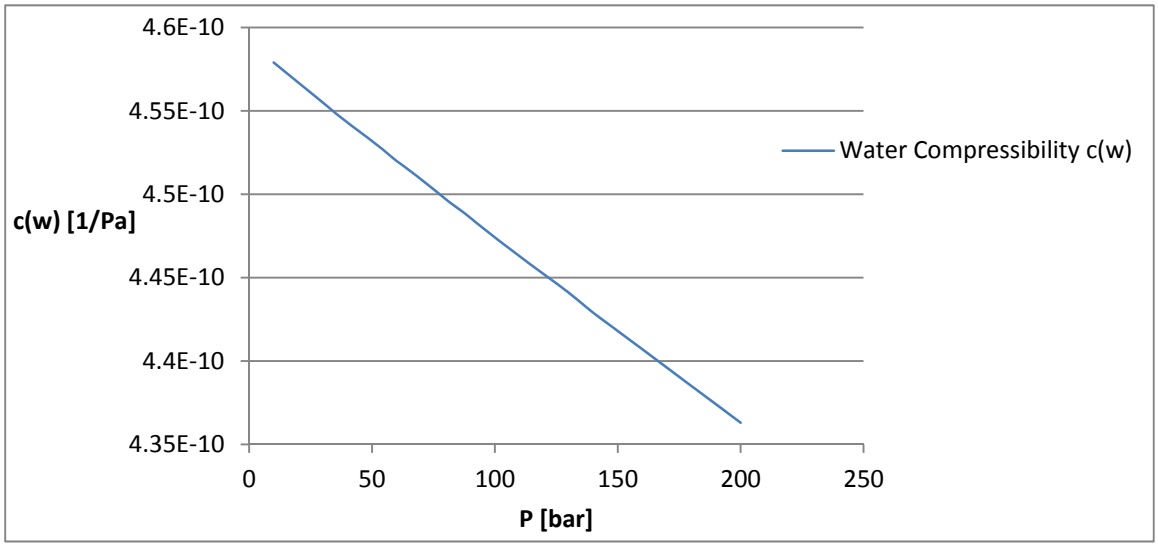

Graph(3.7); water compressibility

Assuming a water compressibility of $4.55 \times 10^{-10}\ Pa^{-1}$, compressibility effect has a small influence on fluid flow. Approximately 1*bar* pressure drop is expected through the copper pipe, when running the BHA string with a 9*sec* period. Assuming one control-volume throughout the 893.7*m* long copper pipe, average pressure increase equates to 0.5*bar* when fluid flow is initiated. Volume change within the control-volume then equal

$\Delta V_{comp} = c_w V \Delta P = c_w \frac{\pi}{4} {D_{cp}}^2 L_{cp} \Delta P$

$= 4.55 \times 10^{-10} \times \frac{\pi}{4} \times\ 0.016^2 \times 893.7 \times 0.5 \times 10^5 = 4.09 \times 10^{-6}\ m^3$.

For a 0.4*m* BHA string Amplitude and 24.4*mm* OD lower rod (initially installed), the displaced volume within the well equates to $q_{disp} = \frac{\pi}{4} \left({D_{ur}}^2 - {D_{lr}}^2\right) 2A_{string} =$

$\frac{\pi}{4}(0.025^2 - 0.0244^2) \times 2 \times 0.4$

$1.86 \times 10^{-5}\ m^3$. This means that approximately 20% of the fluid flow would be compressed rather than flowing through the copper pipe.

Autumn 2012; fluid flow experiments were briefly presented in “MPD Heave Lab: Experimental Work and Modelling of Surge and Swab Effects” by A. Boge. Experiments proved zero flow downstream the copper pipe for string periods T_{string} equal or higher than 9*sec* for a 24.4*mm* OD lower rod. These results contradict with calculation above. System compressibility is therefore evaluated to further investigate the compressibility effect.

3.2.1 System Compressibility

The displaced water is flowing through rubber hoses and the copper pipe. Though water compressibility is a known physical property, flexible hoses and pipes will change the effective water compressibility within its respective medium. Establishing an accurate fluid flow model, effective water compressibility must be determined within both the rubber hose and copper pipe. Two experiments have been performed, of practical reasons; one was performed for an isolated rubber hose system, whilst the other one was performed for the entire system (copper pipe and rubber hose). In both experiments, the isolated system was pressurized to a desired level and a measured fluid mass was then released through a valve. Pressure responses for both experiments are plotted in graph *3.8* and *3.9* below.

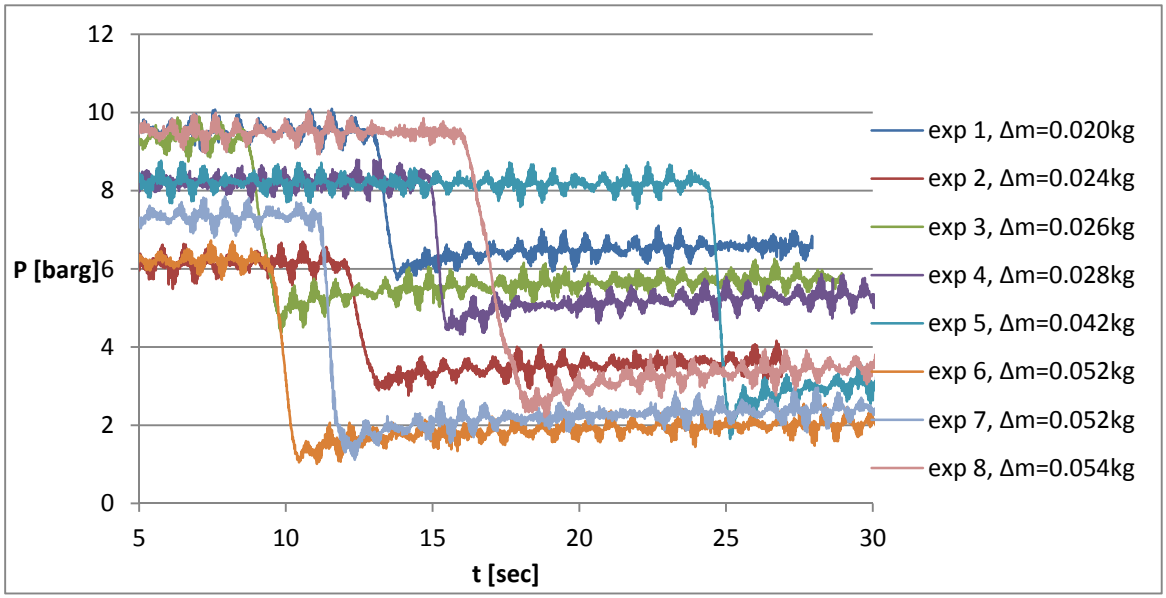

Graph(3.8), Rubber hose pressure response for a released fluid mass Δm

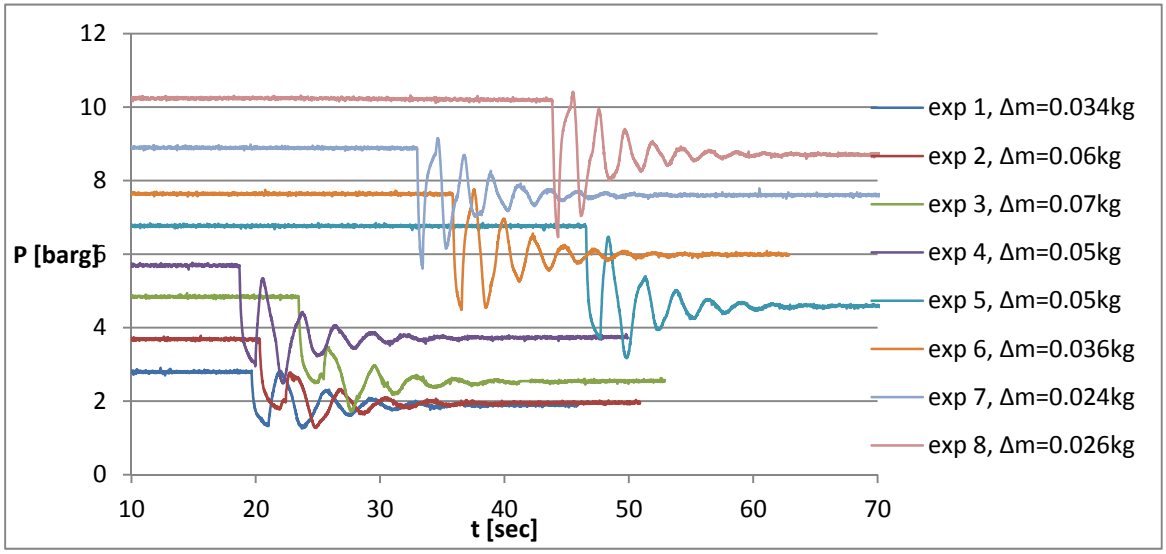

Graph(3.9); Entire system pressure response for a released fluid mass Δm

Pressure data plotted above are used to calculate each system`s respective compressibility. Pressure data plotted in graph *3.9* above also illustrate the phenomenon of pressure propagation and system resonance. The imposed pressure wave created in the well reach the choke, and creates a reflected wave that moves in the opposite direction of the original pressure wave. This cause the pressure in the well to fluctuate for a certain time before all energy within the pressure wave is absorbed. System resonance is further discussed in chapter *4.1.4*. Stabilized pressure change together with released volume *ΔV* and system volume *V* is used to calculate compressibility from equation 3.2.1.

$$c_f = -\frac{1}{V}\frac{dV}{dP} \approx -\frac{1}{V}\frac{\Delta V}{\Delta P} \tag{3.2.1}$$

Where c_f is given in Pa^{-1}, *V* and *ΔV* are given in $m^3$and *ΔP* is given in *Pa*. Compressibility is assumed independent of temperature in our system (assumed constant temperature), but dependent of pressure. In table *3.7* and *3.8* below are stabilized pressure values (plotted in graph *3.8* and *3.9*) listed together with calculated compressibility. Water density *ρ* is assumed constant; the increased system compressibility is not a result of varying density but flexible hoses and piping. Experiment performed with the rubber hose; a 5.54*m* long 19*mm* ID hose was pressurized. Volume within the rubber hose equates to $V = \frac{\pi}{4} {D_{hose}}^2 L_{hose} = \frac{\pi}{4} 0.019^2 \times 5.54 = 1.57 \times 10^{-3}\ m^3$.

Experiment	Δm [kg]	ρ [kg/m^3]	ΔV [m^3]	V [m^3]	P(i) [barg]	P(end) [barg]	ΔP [bar]	p(ave) [barg]	c(f) [1/Pa]
1	0.02	998.2	2.004E-05	1.57E-03	9.54	6.59	2.95	8.07	4.32E-08
2	0.024	998.2	2.404E-05	1.57E-03	6.17	3.59	2.58	4.88	5.94E-08
3	0.026	998.2	2.605E-05	1.57E-03	9.35	5.74	3.60	7.54	4.60E-08
4	0.028	998.2	2.805E-05	1.57E-03	8.30	5.35	2.95	6.83	6.05E-08
5	0.042	998.2	4.208E-05	1.57E-03	8.22	3.39	4.82	5.81	5.55E-08
6	0.052	998.2	5.209E-05	1.57E-03	6.24	2.03	4.21	4.13	7.88E-08
7	0.052	998.2	5.209E-05	1.57E-03	7.35	2.44	4.92	4.90	6.74E-08
8	0.054	998.2	5.410E-05	1.57E-03	9.49	3.69	5.80	6.59	5.94E-08

Table(3.7); compressibility and pressure data for the rubber hose

Experiment	Δm [kg]	ρ [kg/m^3]	ΔV [m^3]	V [m^3]	P(i) [barg]	P(end) [barg]	ΔP [bar]	p(ave) [barg]	c(f) [1/Pa]
1	0.034	998.2	3.41E-05	0.18	2.80	1.90	0.90	2.35	2.10E-09
2	0.06	998.2	6.01E-05	0.18	3.68	1.96	1.73	2.82	1.93E-09
3	0.07	998.2	7.01E-05	0.18	4.84	2.54	2.30	3.69	1.70E-09
4	0.05	998.2	5.01E-05	0.18	5.69	3.73	1.96	4.71	1.42E-09
5	0.05	998.2	5.01E-05	0.18	6.76	4.60	2.17	5.68	1.28E-09
6	0.036	998.2	3.61E-05	0.18	7.64	5.99	1.65	6.81	1.22E-09
7	0.024	998.2	2.40E-05	0.18	8.88	7.61	1.28	8.24	1.05E-09
8	0.026	998.2	2.60E-05	0.18	10.19	8.71	1.49	9.45	9.74E-10

Table(3.8); compressibility and pressure data for the entire system

3.2.2 Compressibility Parameters.

In this sub chapter method of least squares presented in Appendix C is used to find a linear relation between compressibility and pressure listed in table *3.7* and *3.8*. In matrices $\boldsymbol{X}_{hose}$ and $\boldsymbol{Y}_{hose}$ below; data listed in table *3.7* is rearranged to meet requirements in Appendix C.

$$\boldsymbol{X}_{hose} = \begin{bmatrix} 1 & 4.13 \\ 1 & 4.88 \\ 1 & 4.90 \\ 1 & 5.81 \\ 1 & 6.59 \\ 1 & 6.83 \\ 1 & 7.54 \\ 1 & 8.07 \end{bmatrix} \qquad \boldsymbol{Y}_{hose} = \begin{bmatrix} 7.88 \times 10^{-8} \\ 5.94 \times 10^{-8} \\ 6.74 \times 10^{-8} \\ 5.55 \times 10^{-8} \\ 5.94 \times 10^{-8} \\ 6.05 \times 10^{-8} \\ 4.60 \times 10^{-8} \\ 4.32 \times 10^{-8} \end{bmatrix}$$

$$\boldsymbol{X^T X} = \begin{bmatrix} 1 & 1 & 1 & 1 & 1 & 1 & 1 & 1 \\ 4.13 & 4.88 & 4.90 & 5.81 & 6.59 & 6.83 & 7.54 & 8.07 \end{bmatrix} \begin{bmatrix} 1 & 4.13 \\ 1 & 4.88 \\ 1 & 4.90 \\ 1 & 5.81 \\ 1 & 6.59 \\ 1 & 6.83 \\ 1 & 7.54 \\ 1 & 8.07 \end{bmatrix} =$$

$$\begin{bmatrix} 8 & 48.75 \\ 48.75 & 310.67 \end{bmatrix}$$

$$(\boldsymbol{X}^T\boldsymbol{X})^{-1} = \frac{1}{8 \times 310.67 - 48.75 \times 48.75} \begin{bmatrix} 310.67 & -48.75 \\ -48.75 & 8 \end{bmatrix} = \begin{bmatrix} 2.85 & -0.45 \\ -0.45 & 0.07 \end{bmatrix}$$

$$\boldsymbol{X}^T\boldsymbol{Y} = \begin{bmatrix} 1 & 1 & 1 & 1 & 1 & 1 & 1 & 1 \\ 4.13 & 4.88 & 4.90 & 5.81 & 6.59 & 6.83 & 7.54 & 8.07 \end{bmatrix} \begin{bmatrix} 7.88 \times 10^{-8} \\ 5.94 \times 10^{-8} \\ 6.74 \times 10^{-8} \\ 5.55 \times 10^{-8} \\ 5.94 \times 10^{-8} \\ 6.05 \times 10^{-8} \\ 4.60 \times 10^{-8} \\ 4.32 \times 10^{-8} \end{bmatrix} =$$

$$\begin{bmatrix} 4.70 \times 10^{-7} \\ 2.77 \times 10^{-6} \end{bmatrix}$$

$$\boldsymbol{\beta}_{hose} = (\boldsymbol{X^T X})^{-1}\boldsymbol{X}^T\boldsymbol{Y} = \begin{bmatrix} 2.85 & -0.45 \\ -0.45 & 0.07 \end{bmatrix} \begin{bmatrix} 4.70 \times 10^{-7} \\ 2.77 \times 10^{-6} \end{bmatrix} = \begin{bmatrix} 1.02 \times 10^{-7} \\ -7.11 \times 10^{-9} \end{bmatrix}$$

Beta values calculated above gives following relation between compressibility and pressure, in equation *3.2.2* compressibility $c_{f,hose}$ is given in *1/Pa* and pressure *P* is given in *barg*.

$$c_{f,hose} = 1.02 \times 10^{-7} - 7.11 \times 10^{-9}P \qquad (3.2.2)$$

The same method is applied to compressibility data for the entire system, this the gives following beta values; $\boldsymbol{\beta}_{system} = \begin{bmatrix} 2.30 \times 10^{-9} \\ -1.54 \times 10^{-10} \end{bmatrix}$. Linear relation between $c_{f,system}$ and pressure *P* is given in equation *3.2.3*.

$$c_{f,system} = 2.30 \times 10^{-9} - 1.54 \times 10^{-10} P \qquad (3.2.3)$$

Graph *3.10* and *3.11* below presents measured compressibility from table *3.7* and *3.8*. Regression curves determined above are plotted together with the measured values.

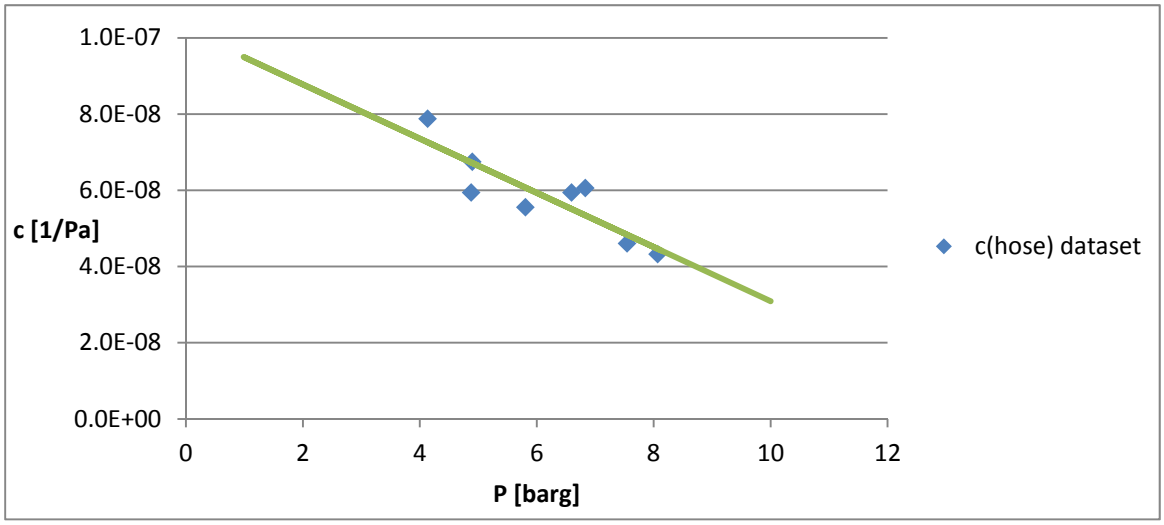

Graph(3.10);compressibility data and linear relation between $c_{f,hose}$ and P for rubber hose.

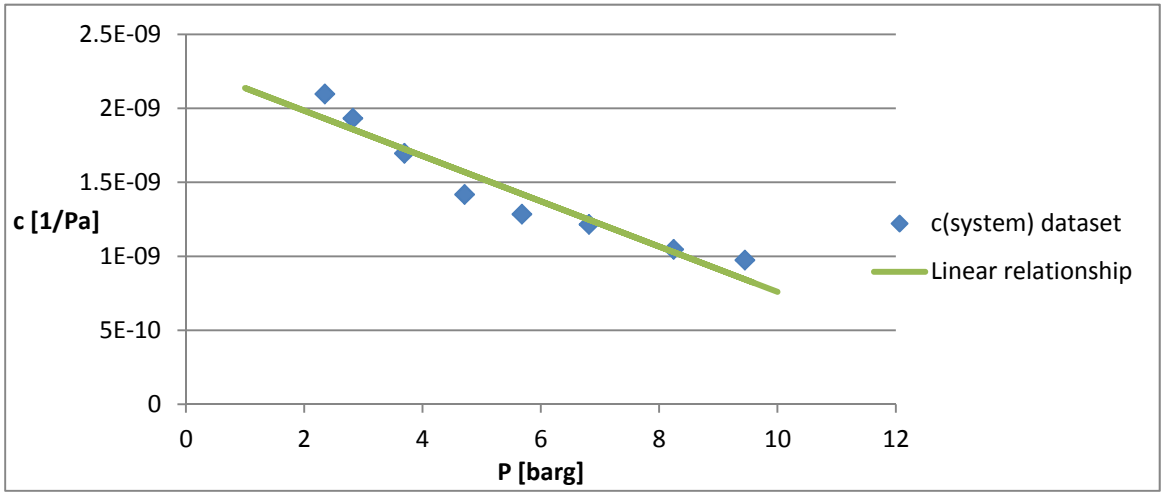

Graph(3.11); Compressibility data and linear relation between $c_{f,system}$ and P for entire system

Effective compressibility within the copper pipe is calculated from volumetric fractions. $\sum x_i c_i = c_{system}$. Where x_i and c_i denotes copper pipe and rubber hose properties.

$$x_{cp} = \frac{V_{cp}}{V_{cp}+V_{hose}}, x_{hose} = \frac{V_{hose}}{V_{hose}+V_{cp}}$$

$$\sum x_i c_i = \frac{0.1766}{0.1766+2.058\times10^{-3}} c_{f,cp} + \frac{2.058\times10^{-3}}{0.1766+2.058\times10^{-3}} c_{f,hose} = c_{f,system}$$

Solving equation above with respect to $c_{f,cp}$ compressibility within the copper pipe is obtained.

$$c_{f,cp} = 1.14 \times 10^{-9} - 7.29 \times 10^{-11} P \quad (3.2.4)$$

3.3 Copper Pipe Friction Factor

BHA heave motion will cause fluid to be displaced through the copper pipe and to surface. A significant pressure loss occurs over the BHA, but frictional pressure loss through the copper pipe is also an important attribute that have to be addressed. Depending on the heave motion characteristics, fluid flow through the copper pipe will experience both laminar and turbulent flow properties. Flow characteristics are of huge importance to the frictional pressure drop, it is therefore important to evaluate the frictional pressure drop for both laminar and turbulent flow within the copper pipe. Flow characteristics depend on geometry, surface roughness, flow velocity, surface temperature and type of fluid. Experimental work by Osborne Reynolds concluded that the flow regime depends mainly on the ratio of inertial forces to viscous forces. The Reynolds number is given by equation *3.3.1*.

$$Re = \frac{inertial\ forces}{Viscous\ forces} = \frac{\rho v_{avg} D}{\mu} \quad (3.3.1)$$

For most applications is the flow regime laminar for $Re < 2300$, turbulent for $Re > 4000$ and transitional in between. In our experiments are the fluid flow expected to be both laminar and turbulent, depending on the BHA heave motion. Graph *3.12* below illustrates how the Reynolds numbers are varying for a 12*sec* period and a 4.5*sec* period with an 0.40*m* amplitude.

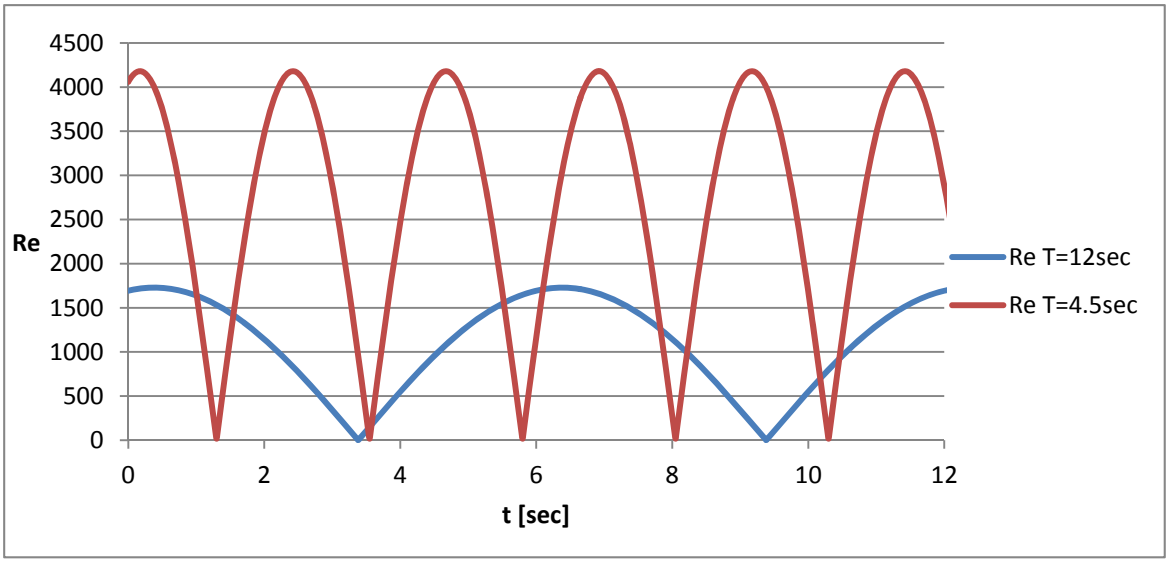

Graph(3.12); Reynolds number for fluid flow through the copper pipe, T_{string}=12sec and T_{string}=4.5sec.

Graph *3.12* above illustrate that fluid flow through the copper pipe is laminar for the entire cycle when the BHA is moving with a period equal to $T_{string} = 12sec$. When T_{string}=4.5sec is the fluid flow partly laminar and partly turbulent.

Of practical reasons; pressure loss through a conduit for all types of fully developed fluid flow is expressed by equation *3.3.2*. Where ΔP_L is the pressure loss over the flow interval, *L* is the length of the interval, *D* is the pipe inner diameter, *ρ* is fluid density, v_{avg} is average fluid velocity within the pipe and *f* is the Darcy-Weisbach friction factor. All parameters are given in SI-units.

$$\Delta P_L = f \frac{L}{D} \frac{\rho \, v_{avg}{}^2}{2} \tag{3.3.2}$$

For Laminar fluid flow within a circular straight pipe section a simple expression can be derived for the friction factor. The friction factor for laminar fluid flow is given by equation *3.3.3*. This equation shows that the friction factor is a function of the Reynolds number only and independent of surface roughness.

$$f_{SL} = \frac{64}{Re} \tag{3.3.3}$$

For turbulent flow within a circular straight pipe section, the friction factor calculation becomes more difficult. Friction factor correlation for turbulent flow is based on experimental work, the most recognized friction factor correlation is known as the Colebrook equation. The friction factor for turbulent flow is given by equation *3.3.4*, which is an implicit equation for the friction factor. Friction factor for turbulent flow is dependent on surface roughness.

$$\frac{1}{\sqrt{f_{ST}}} = -2\log\left(\frac{\varepsilon/_D}{3.7} + \frac{2.51}{Re\sqrt{f_{ST}}}\right) \quad (3.3.4)$$

In equation *3.3.4*; all parameters are given in SI-units and ε represents the equivalent roughness value for the respective pipe material. The equivalent roughness value ε equates to approximately 0.0015mm for copper. The famous Moody chart found below presents the Darcy-Weisbach friction factor for a wide range of Reynolds numbers and pipe roughness values.

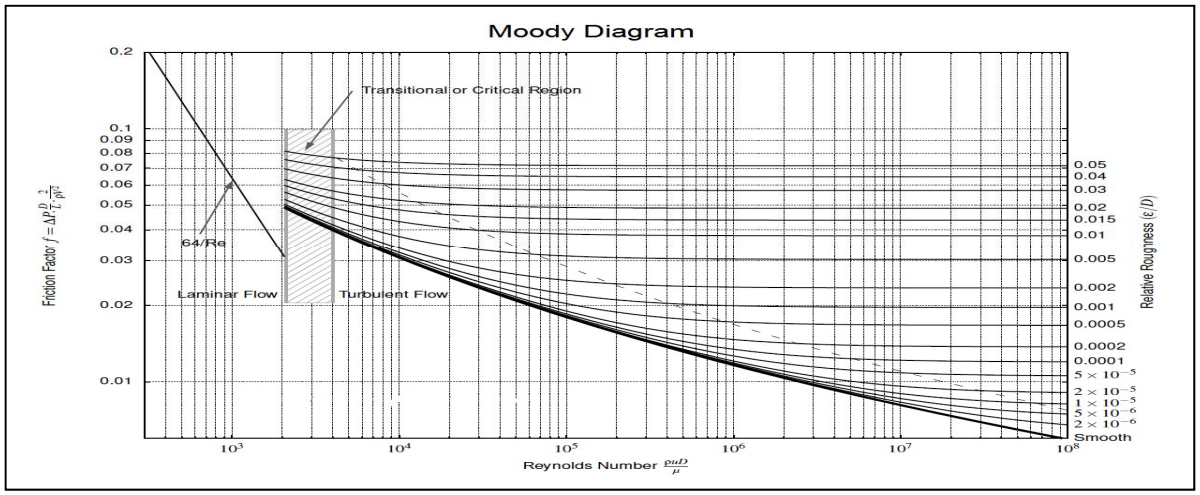

Graph(3.13); Moody chart; graphical representation of the Darcy-Weisbach friction factor.

3.3.1 Friction Factor for Coiled Pipe.

The heave lab consists of an approximately 900*m* long coiled pipe, which represent the upper part of a wellbore. In an actual drilling operation friction factor correlation presented above may be used to calculate frictional pressure loss throughout the well. However; in our lab, the coiled copper pipe is subjected to different friction factors than presented above.

In a straight pipe section; the fluid velocity is uniform at a given radial distance from the centre axis. For fluid flow in a coiled pipe section a secondary flow effect affects the flow regime. Secondary flow by definition is perpendicular to the desired flow direction, and is in this case driven by centrifugal forces. This effect cause higher fluid velocity along the outer wall of coil, as fluid is moving towards the outer wall of the coil creating counter-rotating vortices an increase in pressure loss is experienced over the coiled pipe section. Figure *3.2* and *3.3* below illustrates the difference in secondary flow effects for a straight pipe section and a coiled pipe section.

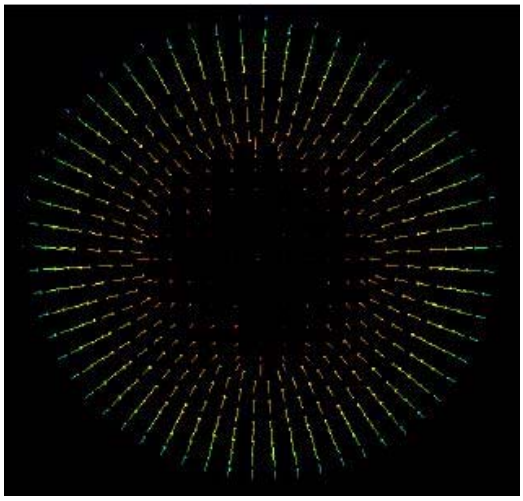

Figure(3.2); straight pipe section

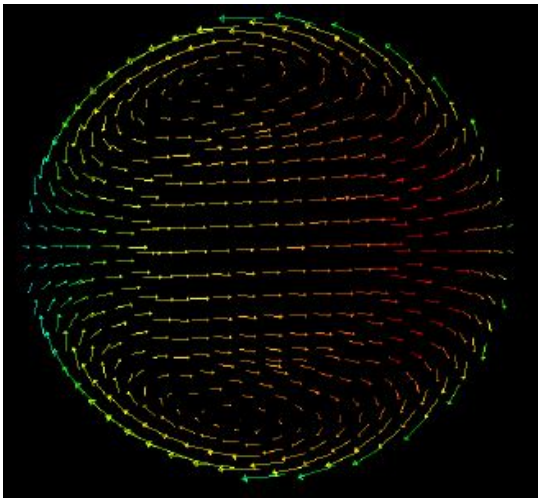

Figure(3.3); coiled pipe section

Experiments and theoretical work concerning friction factor within a coiled pipe has been discussed by several researchers, e.g Dean, White, Srinivasan et al. and Ito. In this project friction factor correlations presented by White and Ito respectively is used for further evaluation. Friction factor for laminar fluid flow for a Newtonian fluid within a coiled pipe is given by equation *3.3.5* White, C.M., 1929.

$$\frac{f_{CL}}{f_{SL}} = \left\{1 - \left[1 - \left(\frac{11.6}{N_{De}}\right)^{0.45}\right]^{1/0.45}\right\}^{-1} \tag{3.3.5}$$

Equation *3.3.5* is only valid for $12 < N_{De} < 2000$, where N_{De} is the Dean number and is calculated from equation *3.3.6*. Where R_{cp} is radius of the copper pipe and R_c is radius of the coil.

$$N_{De} = Re\left(\frac{R_{cp}}{R_c}\right)^{1/2} \tag{3.3.6}$$

Friction factor for turbulent fluid flow of a Newtonian fluid within a coiled pipe is given by equation *3.3.7*, Ito, H., 1959.

$$f_{CT} = \left(\frac{R_{cp}}{R_c}\right)^{1/2}\left\{0.029 + 0.304\left[Re\left(\frac{R_{cp}}{R_c}\right)^2\right]^{-0.25}\right\} \tag{3.3.7}$$

Equation *3.3.7* is only valid for $300 > Re\left(\frac{R_{cp}}{R_c}\right)^2 > 0.034$. Substituting equation *3.3.3* into equation *3.3.5*, equation *3.3.8* is obtained for friction factor within a coiled pipe for a laminar flow regime.

$$f_{CL} = \frac{64}{Re}\left\{1 - \left[1 - \left(\frac{11.6}{N_{De}}\right)^{0.45}\right]^{1/0.45}\right\}^{-1} \quad (3.3.8)$$

Steady state flow experiments were performed to evaluate the friction factor in the heave lab copper pipe. The BHA was kept steady, and a relief valve below *P1* in figure *3.1* was used to choke the flow as the pump effect was kept constant. Flow rates and pressure was registered to evaluate the friction factor for a wide range of flow rates. Graph *3.14* and *3.15* below presents pressure regimes within the copper pipe for a laminar flow experiment and a turbulent flow experiment.

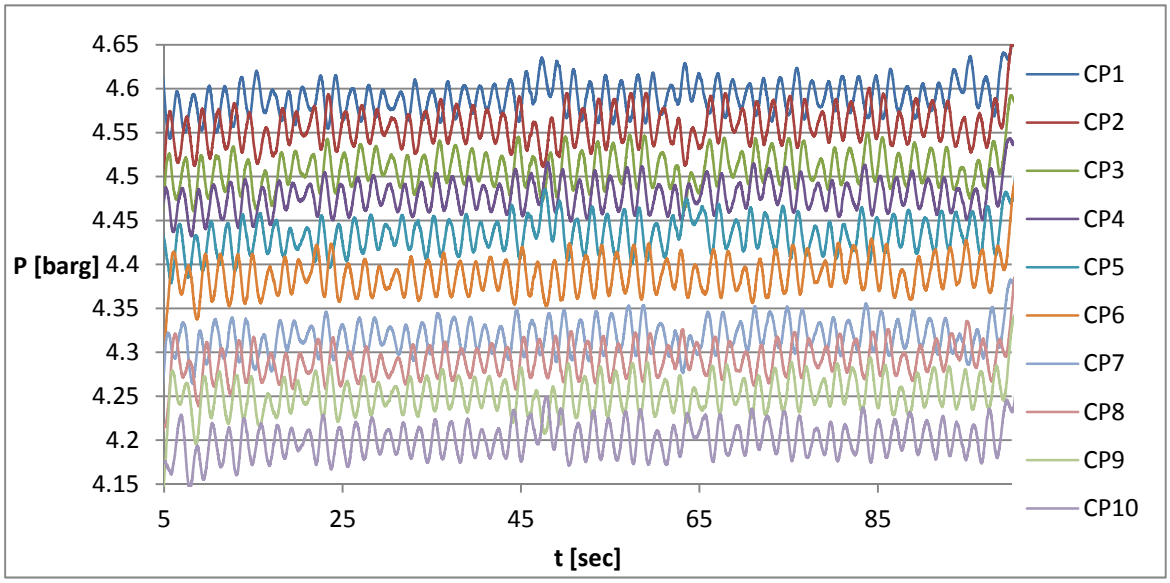

Graph(3.14); pressure profile for a steady state laminar flow experiment, flowrate=0.87LPM and Re=1148.

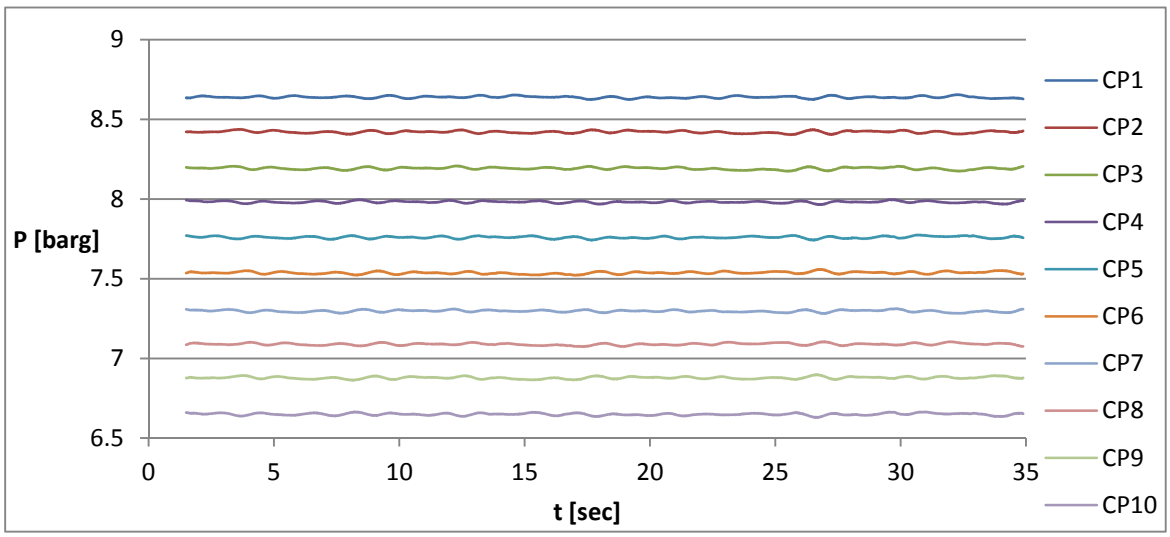

Graph(3.15); pressure profile for a steady state turbulent flow experiment, flowrate=4.94LPM and Re=6540.

Similar flow experiments have been performed for various flow rates, data for all experiments are presented in table *3.9* below. All measured data in table *3.9* are average values over the testing period. The differential height between *CP1* and *CP10* equates to 2.63*m*, this hydrostatic pressure contribution have been accounted for in calculations presented below. Friction factor *f measured* is calculated from equation *3.3.2*.

flowrate [LPM]	Re	ΔP (CP1-CP10) [bar]	P(hyd) [bar]	ΔP(L) [bar]	f measured
0.21	278	0.279	0.258	0.021	0.254
0.3	397	0.298	0.258	0.041	0.237
0.78	1033	0.378	0.258	0.120	0.103
0.80	1056	0.382	0.258	0.124	0.102
0.87	1149	0.389	0.258	0.132	0.091
1.03	1364	0.434	0.258	0.176	0.087
1.14	1504	0.443	0.258	0.186	0.075
1.25	1658	0.475	0.258	0.218	0.073
1.28	1695	0.497	0.258	0.240	0.076
1.43	1897	0.511	0.258	0.253	0.064
1.55	2052	0.561	0.258	0.303	0.066
1.64	2171	0.587	0.258	0.330	0.064
2.15	2846	0.731	0.258	0.473	0.053
2.97	3932	0.982	0.258	0.724	0.043
3.77	4991	1.322	0.258	1.064	0.039
4.44	5878	1.686	0.258	1.429	0.038
4.94	6540	1.990	0.258	1.732	0.037
8.16	10803	4.628	0.258	4.370	0.034

Table(3.9); pressure data, Re, flowrates and friction factor obtained from steady state flow experiments.

In graph *3.17* and *3.18* below, measured friction factor is compared to both straight pipe and coiled pipe friction factor correlations presented above. Laminar flow experiments are presented in graph *3.16* together with friction factor calculated from equation *3.3.3* and *3.3.5*. Turbulent flow experiments are presented in graph *3.17* together with friction factor calculated from equation *3.3.4* and *3.3.7*. In friction factor calculations presented in graph *3.16* and *3.17* is coiled pipe radius $R_c = 1.077m$, tubular radius $R_{cp} = 0.008m$ and equivalent roughness value $\varepsilon = 0.0015mm$.

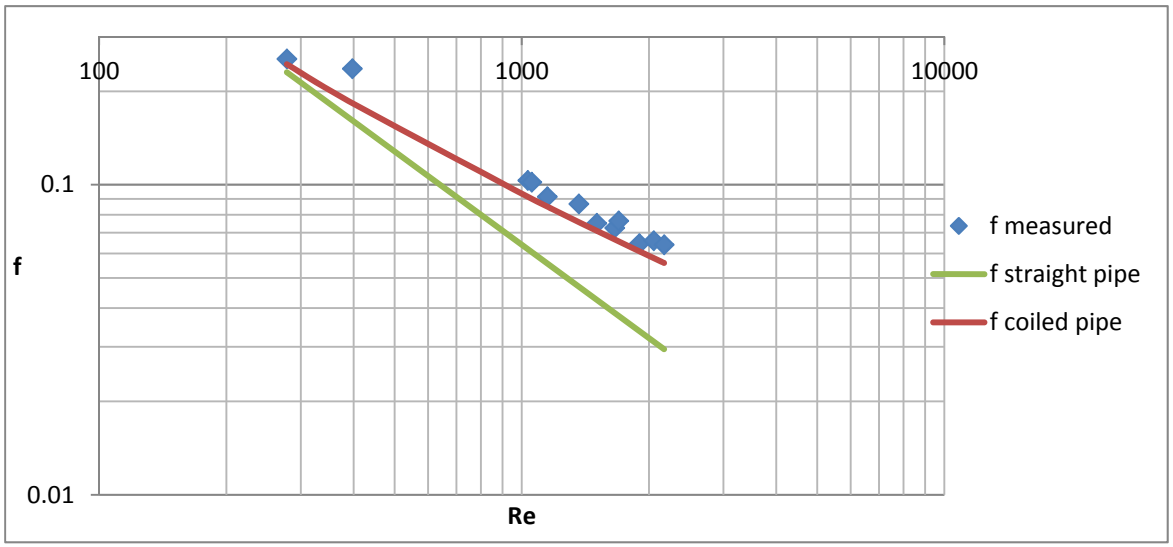

Graph(3.16); log-log coordinate of measured friction factor and calculated friction factors for laminar flow.

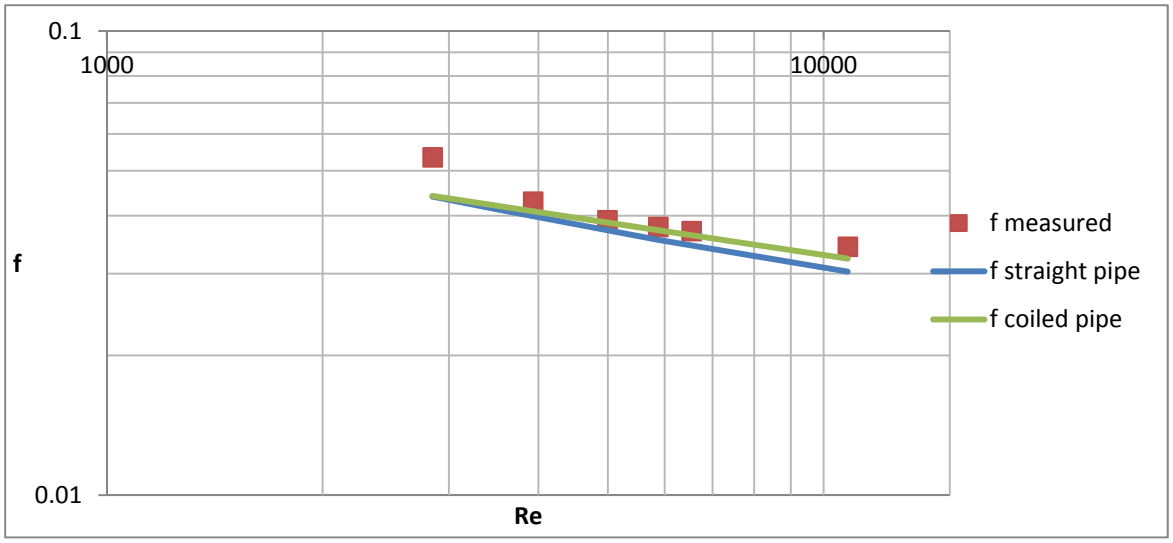

Graph(3.17); log-log coordinate of measured friction factor and calculated friction factors for turbulent flow.

Both plots above clearly illustrate that a coiled pipe friction factor correlation is a better approximation than a straight pipe friction factor correlation. However; discrepancies between the coiled pipe friction factor correlation and measured data is present. This can be explained from inaccurate data readings, the heave lab copper pipe is not a perfect circular coiled pipe, an equivalent roughness value ε of 0.0015mm is assumed and transitional flow regime effects for $2300 < Re < 4000$ have been neglected.

A simplified friction factor correlation based on empirical data is derived to account for discrepancies present in the heave lab copper pipe. To simplify further pressure drop calculations, one friction factor correlation is derived to be valid for both laminar and turbulent flow. Data listed in column 1 and 2 of table *3.10* approximates a straight line in log-log coordinates for $1000 < Re < 6500$. Graph *3.12* illustrate that the expected flow regime within the copper pipe satisfy this criterion. Reynolds number exceeds the lower

limit for a marginal time. However; negligible frictional pressure losses are associated with low Reynolds number, therefore does the straight line approximation not contribute to any pressure loss modelling error of significance. Linear regression of the logarithmic values listed in table *3.10* is performed to obtain the empirical friction factor correlation. Logarithmic values of Reynolds number and measured friction factor are found in table *3.10*.

Re	f measured	Log(Re)	Log(f measured)
1033	0.103	3.014	-0.986
1056	0.102	3.024	-0.992
1149	0.091	3.060	-1.039
1364	0.087	3.135	-1.062
1504	0.075	3.177	-1.124
1658	0.073	3.220	-1.140
1695	0.076	3.229	-1.117
1897	0.064	3.278	-1.190
2052	0.066	3.312	-1.181
2171	0.064	3.337	-1.194
2846	0.053	3.454	-1.272
3932	0.043	3.595	-1.368
4991	0.039	3.698	-1.408
5878	0.038	3.769	-1.422
6540	0.037	3.816	-1.431

Table(3.10); logarithmic values of Reynolds number and measured friction factor obtained from experiments.

Regression method presented in Appendix C is used to find the empirical relation between the Reynolds number and friction factor.

$$\boldsymbol{X}_f = \begin{bmatrix} 1 & 3.014 \\ 1 & 3.024 \\ 1 & 3.060 \\ 1 & 3.135 \\ 1 & 3.177 \\ 1 & 3.220 \\ 1 & 3.229 \\ 1 & 3.278 \\ 1 & 3.312 \\ 1 & 3.337 \\ 1 & 3.454 \\ 1 & 3.595 \\ 1 & 3.698 \\ 1 & 3.769 \\ 1 & 3.816 \end{bmatrix} \quad \boldsymbol{Y}_f = \begin{bmatrix} -0.986 \\ -0.992 \\ -1.039 \\ -1.062 \\ -1.124 \\ -1.140 \\ -1.117 \\ -1.190 \\ -1.181 \\ -1.194 \\ -1.272 \\ -1.368 \\ -1.408 \\ -1.422 \\ -1.431 \end{bmatrix}$$

$$\boldsymbol{\beta}_f = (\boldsymbol{X}_f{}^T \boldsymbol{X}_f)^{-1} \boldsymbol{X}_f{}^T \boldsymbol{Y}_f = \begin{bmatrix} 0.705 \\ -0.569 \end{bmatrix}$$

From calculated beta values, following relation is valid for the Reynolds number and friction factor.

$Log(f_{emp}) = 0.705 - 0.569 \times Log(Re) \rightarrow$

$Log(f_{emp}) = \mathrm{Log}(10^{0.705}) - \mathrm{Log}(Re^{0.569}) \rightarrow Log(f_{emp}) = Log\left(\frac{10^{0.705}}{Re^{0.569}}\right)$

By raising both sides to the power of ten, a simplified empirical relation is derived for the copper pipe friction factor. Equation *3.3.9* is valid for $1000 < Re < 6500$.

$$f_{emp} = \frac{10^{0.705}}{Re^{0.569}} \tag{3.3.9}$$

In graph *3.18* is the measured friction factor plotted together with the empirical friction factor in a log-log coordinate.

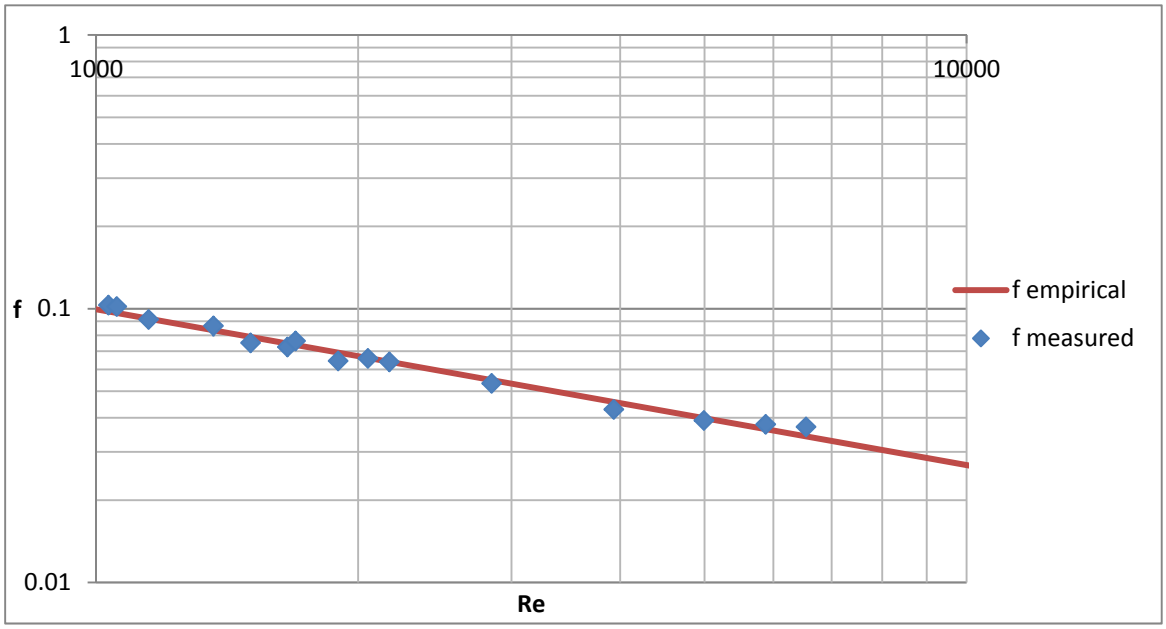

Graph(3.18); measured friction factor and empirical friction factor correlation.

The discrepancy between measured friction factor and each respective friction factor correlation have been evaluated. The discrepancy have been interpreted as an absolute error term, the absolute error term is calculated from equation *3.3.10*.

$$\varepsilon_{error} = |f_{measured} - f_{correlation}| \tag{3.3.10}$$

The standard deviation calculated from equation *3.3.11* is used to evaluate the different correlation from equation *3.3.7, 3.3.8* and *3.3.9*.

$$SD = \sqrt{\frac{1}{N}\sum(\varepsilon_{error,i} - \varepsilon_{error,avg})^2} \quad (3.3.11)$$

Where N is the number of datapoints and $\varepsilon_{error,avg}$ is the average value of all ε_{error}. The standard deviations comparing the different correlations to the measured friction factor are listed in table *3.11*.

Correlation	relationship	SD
White, C.M	$f_{CL} = \frac{64}{Re}\left\{1 - \left[1 - \left(\frac{11.6}{N_{De}}\right)^{0.45}\right]^{1/0.45}\right\}^{-1}$	0.00297
Ito, H	$f_{CT} = \left(\frac{R_{cp}}{R_c}\right)^{1/2}\left\{0.029 + 0.34\left[Re\left(\frac{R_{cp}}{R_c}\right)^2\right]^{-0.25}\right\}$	0.003393
Empirical	$f_{emp} = \frac{10^{0.705}}{Re^{0.569}}$	0.001721

Table(3.11); standard deviations for discrepancies between measured data and each respective correlation.

Standard deviations listed in table *3.11* illustrate that the empirical relation is slightly better than the correlations developed by White, C.M and Ito, H. The fact that the heave lab copper pipe is not a perfect circular coiled pipe amongst others, is the reason why the empirical friction factor correlation is better for our system. The empirical friction factor correlation also has the advantage that it is valid for both laminar and turbulent flow.

3.4 Speed of Sound

An important aspect in all CBHP operations is the effect of time delay caused by pressure propagation. Operational dependent parameters cause a time delay from when the actual pressure change occur downhole to the pressure change is registered at surface and visa versa. This phenomenon makes it more difficult to accurately control the BHP at floating rigs subjected to heave motions, as the surface pressure needs to be managed prior to the actual pressure change downhole. The heave lab well and the surface equipment is separated by an approximately 900*m* long copper pipe to simulate this time delay, and needs therefore to be evaluated.

Pressure waves propagate with the speed of sound through a given fluid. In fluids the sound consists of compression waves, determined by fluid's compressibility and density. The speed of sound through a fluid is given by equation *3.4.1*.

$$a = \sqrt{\frac{1}{c\rho}} \tag{3.4.1}$$

Where *c* is the fluid compressibility and *ρ* is the fluid density. In chapter *3.2.1* were 8 experiments presented to evaluate the compressibility within the entire system (ref: graph *3.9*). From the same data obtained in that experiment is it possible to investigate time delay through the copper pipe. From experiment number 3 presented in graph *3.9*, have several pressure sensors been plotted and presented in graph *3.19*.

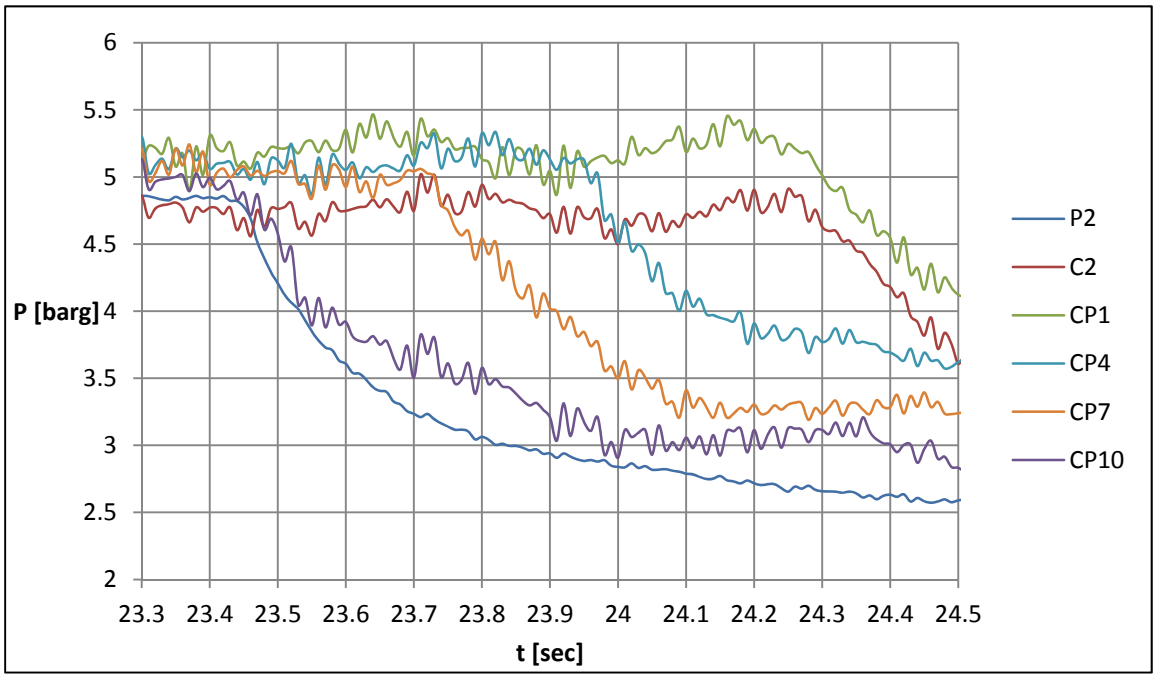

Graph(3.19); pressure readings for an isolated system subjected to a small water release through valve in the well.

As expected is the pressure decrease first registered at *P2* where the small water volume was released. Thereafter is the pressure decrease registered by the other pressure

sensors as the pressure wave reaches the other sensors. Graph *3.19* illustrate that the pressure sensors located at the inlet and outlet of the copper pipe (*CP1* and *CP10*) reacts simultaneously as *P2* and *C2* respectively. The rubber hoses between these elements are flexible and subjected to a higher compressibility factor, but there is negligible time delay through them due to their short length. It takes approximately $0.81sec$ from when the pressure decrease is registered by *CP10* to the pressure wave reach *CP1*. The time delay through the copper pipe is measured and plotted in graph *3.20* for all 8 experiments presented in chapter *3.2.1*. Speed of sound through the copper pipe is calculated from equation *3.4.1* and used to calculate the time delay through the copper pipe. Equation *3.2.4* is used to calculate the compressibility within the copper pipe.

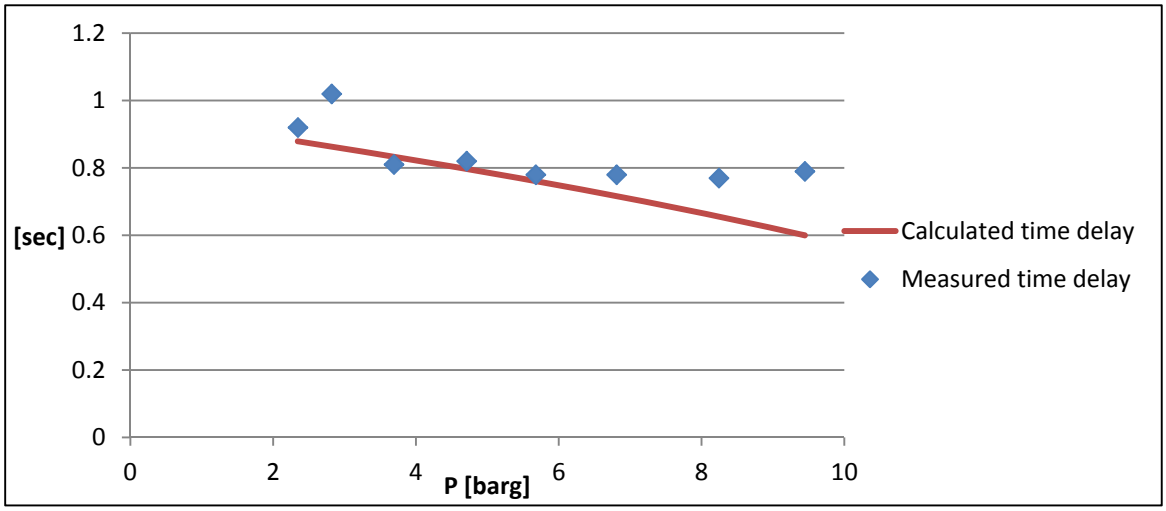

Graph(3.20); calculated and measured time delay through the copper pipe.

The measured data illustrate a slight decrease in time delay with increasing pressure, but the calculated time delay decreases more rapidly. Even though the compressibility used in the calculation is measured for this system, is there a discrepancy between measured and calculated time delay. It is reasonable to believe that the actual tubing profile and curvature influence the pressure propagation.

4.0 Pressure and Flow Modelling

This chapter presents two different models for the MPD heave lab. A simplified empirical model is presented in chapter *4.5*, this model presents a simple method of how to estimate the pressure in the MPD Heave Lab well. A more advanced numerical model is derived and presented in chapters *4.1* through *4.4*.

4.1 Model Assumptions

4.1.1 Newtonian Fluid and Viscosity

The fluid used in the rig model is water; water follows the rheology of a Newtonian fluid. The viscous forces present in a Newtonian fluid are characterized by the fluid viscosity. The linear relationship between the fluid shear stress and viscosity is given by equation *4.1.1*

.

$$\tau = \mu \frac{du}{dy} \tag{4.1.1}$$

Viscosity of a Newtonian fluid is only dependent on temperature and pressure. Water is most dependent on temperature, and due to small pressure variations in our model, viscosity can be assumed independent of pressure. Graph *4.1* below adapted from the project “Heave Compensated Managed Pressure Drilling: A Lab Scaled Rig Design” by Tollef Svenum and Camilla Gjengseth illustrates how water viscosity varies with temperature.

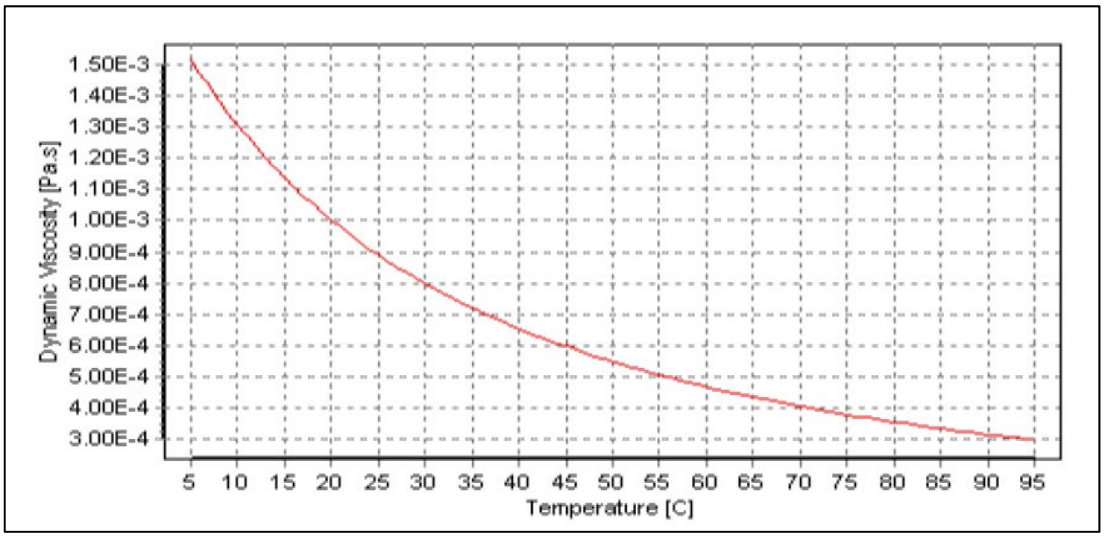

Graph 4.1; Water viscosity (Pas) as function of temperature deg C.

4.1.2 Constant Pump Flowrate, *FT2*

The backpressure-pump was briefly introduced in chapter *2.4.3*, it is necessary to consistently pump fluid through the choke to be able to control the surface pressure. When the BHA string is subjected to heave motion does the fluid flowrate through the choke depend on both displaced fluid in the well and the flowrate from the pump (*FT1* and *FT2*). While the displaced fluid flowrate depend on the heave motion, is it possible to adjust the flowrate from the pump. The backpressure pump effect is proportional to both flowrate and pressure difference between inlet and outlet of the pump $P_{pump} = q\Delta p \frac{1}{\eta_t}$, $\eta_t$is the total pump efficiency. The surface pressure will fluctuate with both fixed and automatically controlled choke opening, which will influence the outlet pressure of the pump. Our pump is designed to operate with a constant pump effect P_{pump}, as the outlet pressure varies so will the flowrate delivered by the pump.

The pipeline between the pump and the choke was initially designed with an air accumulator. The highly compressible gas within the accumulator caused huge variation in flowrate delivered from the pump, as fluid from the pump was accumulated in the compressed accumulator volume. The pump effect equation presented above may be rearranged to; $q = \frac{P_{pump}\eta_t}{\Delta p}$. For a given heave motion characteristics is Δp given by the system, whilst $\eta_t$is a given pump constant. From the equation rearrangement above is it clear that a larger pump effect P_{pump} will cause a lesser flowrate fluctuation with a given pressure fluctuation. Pump flowrate *FT2* is plotted below for 3 different cases; with an accumulator, with a pump effect equal to approximate 70% and with 100% pump effect when subjected to a BHA heave motion of $T_{string} = 6sec$.

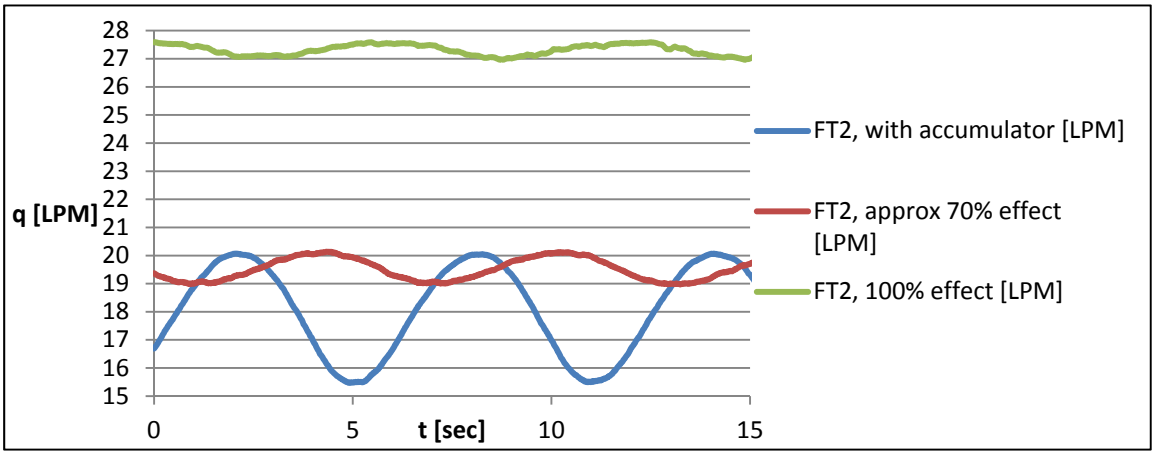

Graph(4.2); Flowrate delivered from the back-pressure pump with;1. Accumulator, 2. 70% and 3. 100% pump effect.

In the measurements presented above is it clear that a high pump effect without any accumulator will deliver the most stable flowrate. With a 100% pump effect will the flowrate fluctuate with approximately $\pm 0.3LPM$, whilst for 70% pump effect and with

an accumulator will the flowrate fluctuate with approximately $\pm 0.6 LPM$ and $\pm 2.3 LPM$ respectively. For a BHA heave motion of $T_{string} = 6\ sec$ is the maxmimum and minimum displaced flowrate equal to $\pm 3.4 LPM$ (*FT1* measurements found in chapter *5.1*). The flowrate fluctuation from the pump when delivering at 100% is less than 10% of displaced flowrate. Therefore is the flowrate from the pump assumed to be constant for further calculations and all experiments are performed with a 100% pump effect.

4.1.3 Constant Pressure Downstream of the Choke, *C1.*

The pressure downstream the choke needs to be large enough to bring the fluid back to the watertank located at the top of the scaled-rig. The watertank is located approximately 2*m* above the choke, the pressure downstream the choke therefore needs to overcome both hydrostatic pressure and frictional pressure loss. The total flowrate pumped back to the watertank consists of both displaced well fluid and flowrate from the pump. The displaced flow from the well fluctuates with approximately $\pm 3.4 LPM$ for $T_{string} = 6 sec$. Whit a constant flowrate from the pump equal to approximately $27 LPM$, is the total flow fluctuation through the choke $\pm 3.4 LPM$. This maximum flow fluctuation equates to only $\frac{3.4}{27} = 12.5\%$ of the total flow. Due to a relatively small change in flowrate through the choke is the frictional pressure loss back to the watertank assumed constant, and the same goes for the hydrostatic pressure. Pressure downstream the choke *C1* is plotted below for $T_{string} = 12, 9, 7$ and *5 sec* and with maximum flowrate from the pump equal to $27 LPM$. Graph *4.3* illustrates that *C1* is fairly constant except for some pressure peaks which is likely caused by disturbances.

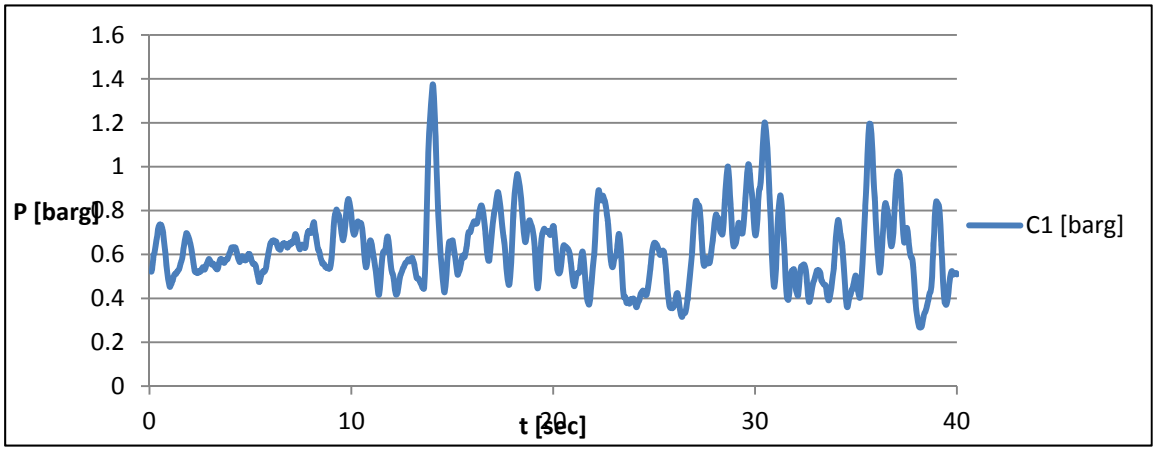

Graph(4.3); Pressure downstream choke C1 for $T_{string} = 12,9,7\ and\ 5 sec$ and maximum pump flowrate.

4.1.4 Negligible System Resonance

In chapter *3.4* was it discussed how pressure propagates through a medium with the speed of sound. An important aspect that needs to be evaluated in a system with propagating waves is the system resonance. As the pressure wave is created at one end and travel through the system to the other end point, the pressure wave might be fully reflected, fully absorbed or somewhere in between. In the most extreme case the pressure wave is totally reflected, which creates a reflected wave with the same speed and amplitude as the imposed pressure wave. This creates a standing wave with maximum oscillation twice the amplitude of the original wave at each antinodes and no displacement at the nodes. Figure *4.1* below illustrate the case of total reflection.

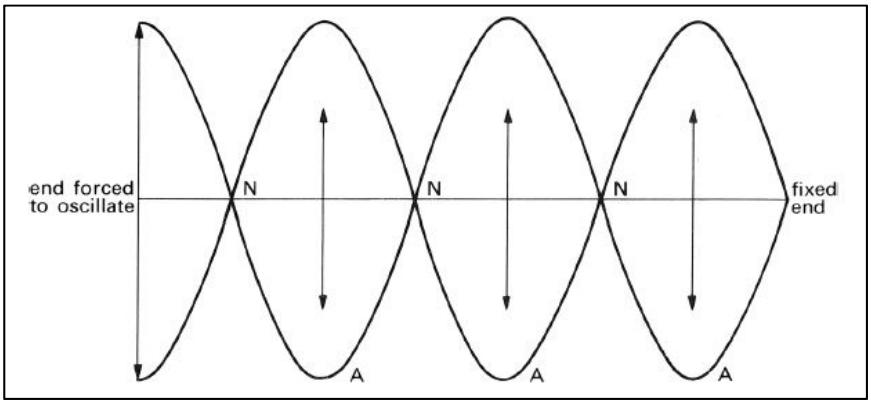

Figure(4.1); Standing wave caused by total reflection.

System resonance is investigated in detail and presented in “Disturbance Attenuation in Managed Pressure Drilling Using Impedance Matching and an Experimental Lab Setup“ by M. Gleditsch for the heave lab system. He found a significant increase in BHP fluctuation for given values of choke angel and heave motion characteristics for a closed system without the backpressure pump running. Furthermore does his report conclude that a much lesser system resonance is observed with the backpressure pump running as the pressure wave is likely being absorbed in the pump.

4.1.5 Additional Assumptions

- Compressibility assumed independent of pressure.
- Water density assumed constant.
- Speed of sound assumed independent of pressure.

4.2 Numerical Flow Modelling

The oscillating BHA String causes fluid to be displaced in the well and throughout the copper pipe. BHA surge effects reduce the annular volume in the well, which force the fluid to flow out of the well and through the copper pipe. Whilst BHA swab effects increase the annular volume in the well and thereby causes fluid to flow from surface through the copper pipe and into the well. The fluid flow in and out of the well is proportional to the BHA string velocity, given by equation *4.2.1*. BHA string velocity is defined as positive when moving upwards, similar is flowrate defined as positive when flowing out of the well and to surface.

$$q_{disp}(t) = -v_{string}(t)\frac{\pi}{4}\left({D_{ur}}^2 - {D_{lr}}^2\right) \quad (4.2.1)$$

Where q_{disp} is given in ${m^3}/{s}$, v_{string} is given in ${m}/{s}$ and D_{ur} and D_{lr} is the diameter of the upper rod and lower rod respectively given in *m.*

Water is usually assumed to be an incompressible fluid. However, our system has proven to be influenced of compressibility effects. This is discussed in chapter *3.2*, where effective compressibility was found to be approximately four times the value of water compressibility within the copper pipe. This is caused by expansion and compression of the actual copper pipe as the pressure varies, accordingly does this influence the flowrate within the copper pipe. When comparing BHA string velocity and *FT1* readings (displaced flowrate measured at surface) a significant time delay of fluid flow is found in the copper pipe. Remaining part of this sub-chapter will derive a model for the flowrate and compare the model to measured data.

The principle of mass conservation is used to derive a model for the flowrate. As discussed in chapter *3.2* is it reasonable to assume a constant fluid density and compressibility is assumed independent of pressure. A numerical model based on 81 control volumes is used to calculate the fluid flowrate throughout the copper pipe. The sinusoidal pressure distribution will cause accumulated fluid volume within each control volume to change accordingly. Each control volume is denoted with the integer *i,* and the 82 control volume boundaries are denoted with the integer *j.* Utilizing the principle of mass conservation with constant fluid density gives the following relationship for flowrate q_j at each boundary.

$$q_j(t) = q_{j+1}(t) - \Delta p_{i=j}(t)\alpha_{cp}L_{cv} \quad , \quad j \in 1,2,\dots,81 \quad (4.2.2)$$

Where Δp_i is the average pressure change within control volume *i* given in ${}^{pa}/_{s}$, α_{cp} is the expansion factor of the copper pipe in ${}^{m^3}/_{m\ Pa}$ and L_{cv} is the length of the control volume equal to $\frac{893.6}{81} = 11.03m$. By definition is q_{82} the flowrate at the boundary between the copper pipe and the well. The rubber hose connecting the copper pipe to the well has been accounted for by using the system compressibility factor rather than the copper pipe compressibility factor, this gives following boundary conditions $q_{82}(t) = q_{disp}(t)$ and $q_1(t) = FT1_{calc}$(t). The expansion factor is simply calculated from the system compressibility factor and copper cross-sectional area, $\alpha_{cp} = c_{f,system}\, A_{cp} = c_{f,system}\, \frac{\pi}{4}\, {D_{cp}}^2 = 1.37 \times 10^{-9}\, \frac{\pi}{4}\, 0.016^2 = 2.76 \times 10^{-13}\ {}^{m^3}/_{m\ Pa}$.

Where an average pressure of 6 barg is assumed in the system and the system compressibility is calculated from equation *3.2.3*. For $j = 1,2,3, \ldots,81$ equation *4.2.2* can be divided into 81 linear equations, this equation system is solved by adding together all right-hand terms and left-hand terms respectively. This gives the following relationship between q_{82} and q_1.

$$q_1(t) = q_{82}(t) - \alpha_{cp} \Delta L_{cv} \sum_{i=1}^{81} \Delta p_i(t) \qquad (4.2.3)$$

Figure *4.2* below gives an illustration of the sensors, control volumes and boundary conditions.

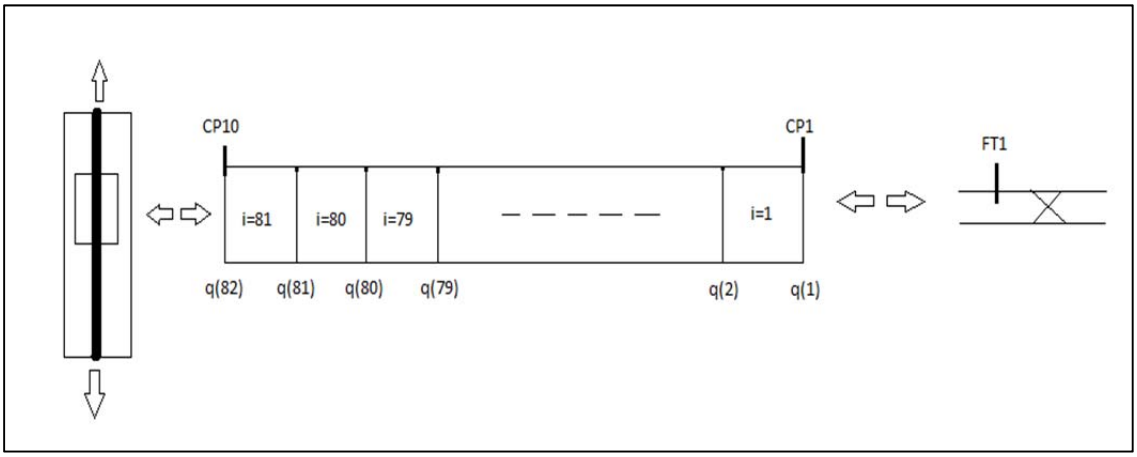

Figure(4.2); Illustration of control volumes, sensors and boundary conditions related to the flow model.

The pressure change within the control volume Δp_i is used to calculate how large amount of the flowrate is accumulated in the control volume. Δp_i used in this analysis is an average value in the control volume, Δp_i is calculated from equation *4.2.4* where the respective pressure values are found at each control volume boundary, further

discussed in next chapter. The pressure variation throughout the copper pipe registered by the pressure sensors is further discussed in chapter *4.3*.

$$\Delta p_i(t) = \frac{\frac{P_{i,t+\Delta t_{step}} + P_{i+1,t+\Delta t_{step}}}{2} - \frac{P_{i,t-\Delta t_{step}} + P_{i+1,t-\Delta t_{step}}}{2}}{2\Delta t_{step}} \qquad (4.2.4)$$

Where Δt_{step} is time steps used in the model, the MPD heave lab computer register data at intervals of 0.01 sec. Further calculations are therefore performed with time steps equal to 0.01 sec.

4.2.1 Flow Calculations Based on Real Pressure Readings

The flow model presented above has been tested with 9 control volumes based on real pressure readings to evaluate the flow model. The BHA string was oscillated with constant amplitude of 0.4m and different heave periods T_{string} equal to 12sec, 9sec, 6sec and 5sec. BHA string velocity, copper pipe pressure and *FT1* was logged to evaluate the flow model. In graphs *4.4* through *4.7* are displaced flowrate calculated from equation *4.2.1*, logged flowrate at surface *FT1* and calculate flowrate at surface from equation *4.2.3* plotted for periods equal to 12sec, 9sec, 6sec and 5sec respectively.

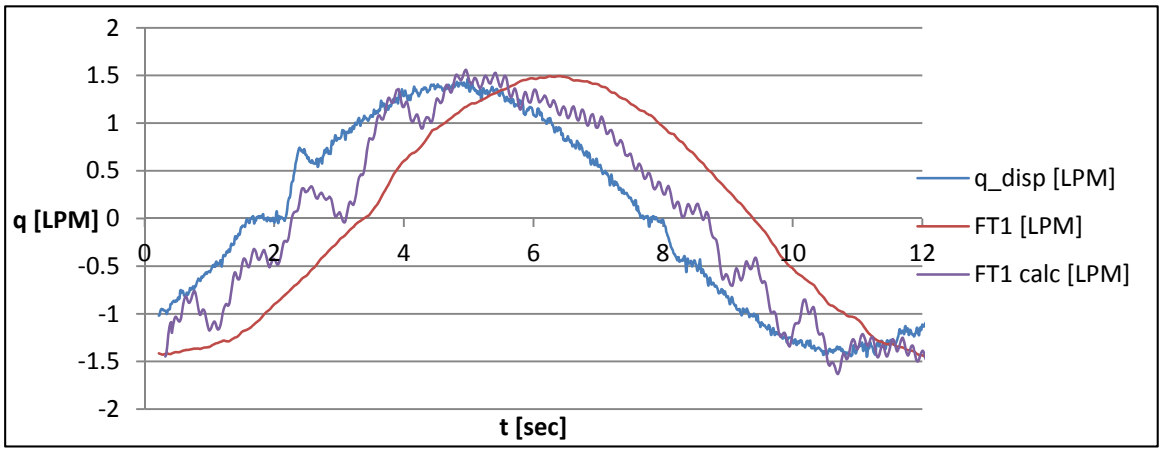

Graph(4.4); flow calculations and measurements for $T_{string} = 12sec$.

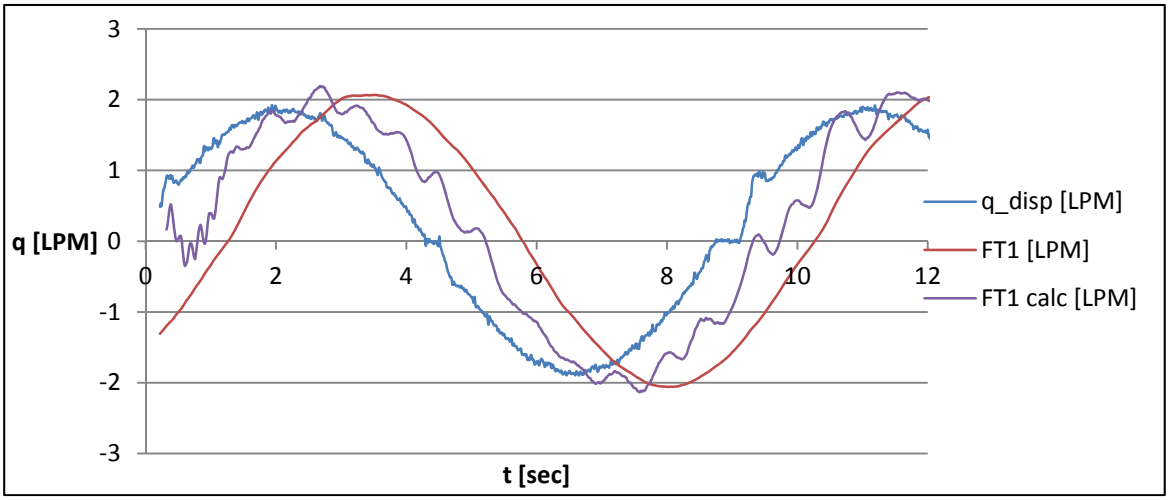

Graph(4.5); flow calculations and measurements for $T_{string} = 9\ sec.$

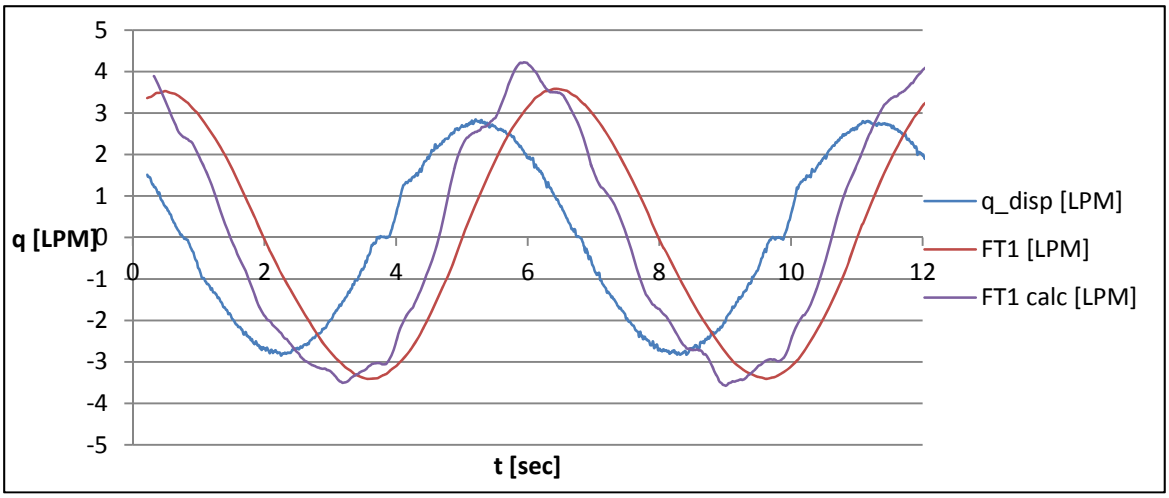

Graph(4.6); flow calculations and measurements for $T_{string} = 6\ sec.$

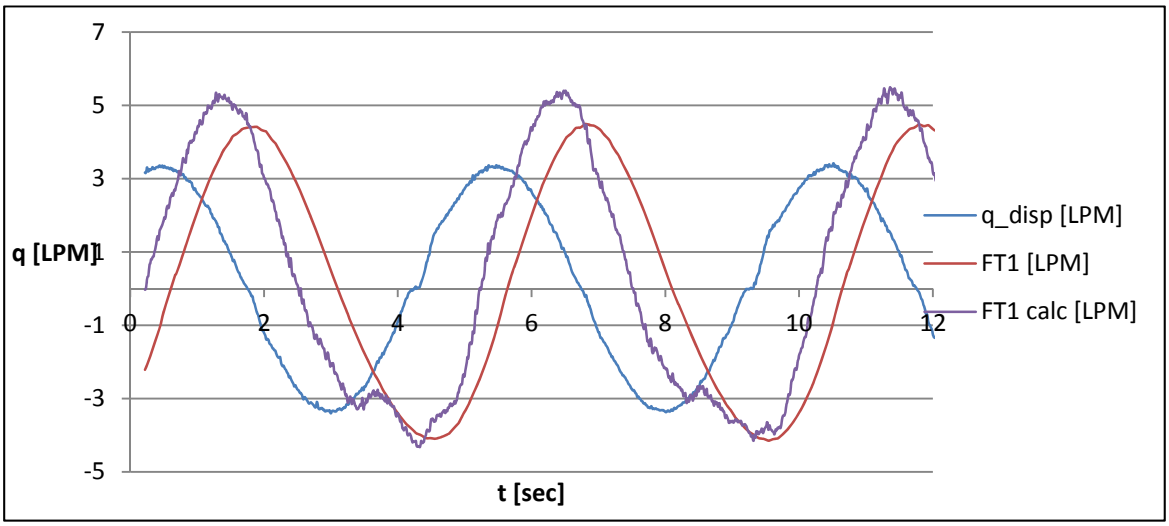

Graph(4.7); flow calculations and measurements for $T_{string} = 5\ sec.$

Calculations presented above do not match the observed data. The time delay induced by flowing through the approximately 900*m* long copper pipe is longer than calculated from equation *4.2.3*, and graph *4.6* and *4.7* illustrates larger amplitude of calculated flowrate than measured. The later issue may be explained from bad assumptions regarding the compressibility factor. In this analysis is the compressibility factor assumed independent of pressure which is not entirely correct, as the compressibility factor decreases with increasing pressure. The Matlab code presented in chapter *4.4* have been used to evaluate the time delayed flow based on real pressure reading inputs as presented above. Table *4.1* below presents measured time delay from observed data, time delay caused by compressibility effects and a third column which is the difference between measured and calculated time delay.

T	Measured time delay	Calculated time delay	Measured - calculated time delay
12	1.7	0.83	0.87
11	1.6	0.84	0.76
10	1.5	0.86	0.64
9	1.4	0.93	0.47
8	1.6	1	0.6
7	1.55	1.05	0.5
6	1.6	1.12	0.48
5	1.64	1.16	0.48

Table(4.1); Measured time delay, Calculated time delay and Calculated time delay subtracted from measured time delay.

Table *4.1* illustrate that the additional time delay presented in column 3 is most dominating for smaller oscillation frequencies. The flow characteristics are laminar throughout the entire period for smaller oscillation frequencies, and partly laminar for bigger oscillation frequencies. One possible explanation for the additional time delay is due to the flow characteristics itself. This is further discussed in the next sub-chapter.

4.2.2 Unsteady Laminar Flow

The oscillating pressure profile caused by the heave motion of the BHA string force the fluid to constantly change flow direction and acceleration. If the heave motion is slow enough, the fluid velocity profile will have the characteristics of a parabolic velocity profile, also referred to as a Poiseuille profile. If the BHA string on the other hand is oscillated more frequently but still is characterised by laminar flow, the fluid velocity changes direction more rapidly and causes distortion of the parabolic fluid velocity profile. The inertia of the fluid in the central core of the pipe causes the fluid flowrate to lag behind the applied pressure profile. A useful parameter to evaluate the extent to

which the fluid velocity profile is characterised by a parabolic velocity profile, is the Womersley number α. For a sinusoidal pressure profile of angular frequency ω, pipe diameter *D* and kinematic viscocity *v* is the Womersley number α given by equation *4.2.5*.

$$\alpha = \frac{D}{2}\sqrt{\frac{\omega}{\nu}} = \frac{D}{2}\sqrt{\frac{\frac{2\pi}{T}}{\frac{\mu}{\rho}}} = \frac{D}{2}\sqrt{\frac{2\pi\rho}{T\mu}} \tag{4.2.5}$$

At Womersley number in the range of 1-3 does the fluid flowrate start to lag behind the applied pressure, and the phase delay only keeps increasing with increasing Womersley number. Figure *4.3* below illustrate some fluid velocity profiles for different Womersley numbers as function of radial distance and phase.

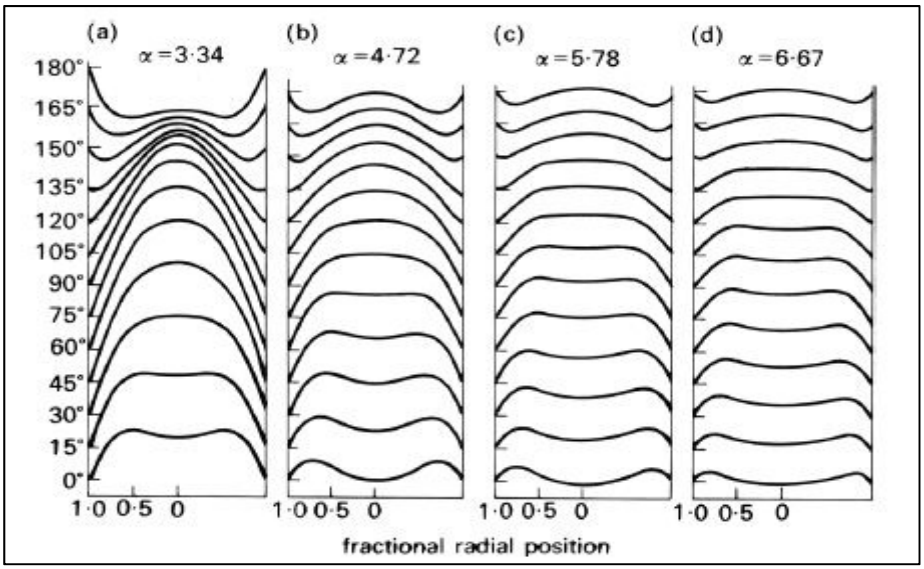

Figure(4.3); Fluid velocity profile for varies Womersley numbers.

Fluid flowrate is assumed laminar for Reynolds number lower than 2300. Maximum flowrate within the heave lab copper pipe assumed to be laminar is calculated from equation *3.3.1*, $v_{max,lam} = \frac{Re\ \mu}{\rho\ D_{cp}} = \frac{2300\times0.001}{998.2\times0.016} = 0.144\ ^{m}/_{S} \rightarrow q_{max,lam} = v_{max,lam}\ A_{cp} = 0.144\ \frac{\pi}{4}\ 0.016^2 = 2.89\times10^{-5}\ ^{m^3}/_{S}$. Equation *4.2.1* can be used to calculate the minimum BHA string period T_{string} that satisfies laminar flow throughout the entire cycle. $q_{max,lam} = \max(v_{string})\frac{\pi}{4}\ ({D_{ur}}^2 - {D_{lr}}^2) \rightarrow \frac{2\pi A_{string}}{T_{string,min}} = \frac{q_{max,lam}}{\frac{\pi}{4}({D_{ur}}^2-{D_{lr}}^2)} \rightarrow T_{string,min} = \frac{\frac{\pi^2}{2}A_{string}({D_{ur}}^2-{D_{lr}}^2)}{q_{max,lam}} = \frac{\frac{\pi^2}{2}\times0.4\ (0.025^2-0.022^2)}{2.89\times10^{-5}} = 9.61sec$. The only graph presented in previous sub-chapter that satisfies laminar flow throughout the entire cycle is graph *4.4*,

where $T_{string} = 12sec$. The Womersley number for $T_{string} = 12sec$ can be calculated from equation 4.2.5, $\alpha = \frac{D}{2}\sqrt{\frac{2\pi\rho}{T\mu}} = \frac{0.016}{2}\sqrt{\frac{2\pi\times998.2}{12\times0.001}} = 5.78.$

The Womersley number calculated above, indicate unsteady laminar flow through the copper pipe for $T_{string} = 12\ sec$. The additional time delay measured and presented in graph *4.4* is therefore likely to the result of unsteady flow. For $T_{string} < 9.61\ sec$ is the fluid regime within the copper pipe partly transitional and turbulent. Transitional flow characteristics are assumed to be a combination of laminar and turbulent flow. Remaining experiments presented in previous sub-chapter (graph *4.5*, *4.6* and *4.7*) is partly laminar and transitional. The effect of unsteady flow is a possible explanation for additional time delays present for these experiments as well.

4.3 Numerical Pressure Modelling

Pressure drop over the BHA has been carefully evaluated and simulated in "Experimental Work and Modelling of Surge and Swab Effects" by A. Boge. An automatic controlled choke system requires an accurate pressure model for the entire system. It is therefore important to evaluate the pressure drop through the remaining parts of the system, specially the copper pipe where most of the pressure drop occurs. Chapter *4.2* presented a flow model for the copper pipe, this flow model will be used to calculate the pressure drop through the copper pipe.

The pressure drop through the copper pipe is caused by both acceleration and instantaneous velocity of the fluid. The frictional pressure loss caused by instantaneous velocity has been carefully investigated and presented in chapter *3.3*. The pressure difference through the copper pipe caused by fluid acceleration is derived from Newton's second law.

$$\sum F_{res} = ma_f \rightarrow \Delta P_{acc}A = \rho A \Delta L a_f \rightarrow \Delta P_{acc} = \rho \Delta L a_f \qquad (4.3.1)$$

Where all parameters are given in consistent SI-units, ΔL is the length of the pipe segment and a_f is the fluid acceleration. Fluid flow modelling illustrated that fluid velocity depends on both position and time, hence do also fluid acceleration depend on the same variables. Similar to fluid flow calculations are therefore pressure drop also calculated from a numerical basis. Equation *4.2.2* defines how to calculate the flowrate

through each control volume boundary *j.* This boundary flowrate is used to calculate the average fluid velocity within the control volume *i,* fluid velocity is given by equation *4.3.2*.

$$v_{f,i}(t) = \frac{q_{j=i}(t)+q_{j=i+1}(t)}{2A_{cp}} = \frac{q_{j=i}(t)+q_{j=i+1}(t)}{\frac{\pi}{2}D_{cp}{}^2} \quad (4.3.2)$$

Furthermore is the fluid acceleration approximation within control volume *i* given by equation *4.3.3*, which is a reasonable approximation for $\Delta t_{step} = 0.01sec$, where Δt_{step} is the numerical time step.

$$a_{f,i}(t) = \frac{v_i(t+\Delta t)-v_i(t-\Delta t)}{2\Delta t_{step}} \quad (4.3.3)$$

Chapter *3.4* presents time delays in a dynamic system caused by pressure propagation. It is important to account for this time delay effect when calculating pressure drop through the copper pipe. The numerical model used in this analysis is divided into 81 control volumes. Time delay through each control volume equates to, $\Delta t_{p-prop,cv} = \frac{0.81sec}{81} = 0.01sec$.

The average velocity and acceleration terms presented above are used to calculate pressure drop through each control volume *i.* This pressure drop is again used to calculate pressure at each control volume boundary *j.* Control volume boundary pressure P_j is calculated from equation *4.3.4.*

$$P_{j+1}(t) = P_j\left(t + \Delta t_{p-prop,cv}\right) + \Delta P_{L,i=j}(t) + \Delta P_{acc,i=j}(t) + \Delta P_{hyd,i=j},\ j \in 1,.,81 \quad (4.3.4)$$

In equation *4.3.4* are all variables given in *Pa.* The hydrostatic pressure term $\Delta P_{hyd,i}$ is calculated based on a constant inclination of the copper pipe. The vertical distance between the outlet and inlet of the copper pipe equates to $\Delta h_{cp} = 2.73 - 0.1 = 2.63m$ (ref; table *3.2*). The vertical distance between each control volume boundary equates to $\Delta h_{i,cv} = \frac{2.63}{81} = 0.032m$. Notice from equation *4.3.4* that $P_{j+1}(t) = P_j\left(t + \Delta t_{p-prop,cv}\right) + \cdots \underset{equiv}{\Longleftrightarrow} P_{j+1}\left(t - \Delta t_{p-prop,cv}\right) = P_j(t) + \cdots$which is the correct term, since the pressure pulse starts propagating in the well and propagates with decreasing *j* numbers. The pressure calculation is in other words performed in the opposite direction of pressure propagation. This mathematical approach is chosen due to the following boundary condition; $P_1(t) = C2(t) + \rho g \Delta h_{CP1-C2}$, which is further discussed in the next sub-chapters.

4.3.1 Boundary Condition – Choked Flow

The surface equipment consists of several physical components such as the backpressure-pump, the watertank and the choke, previously presented in chapter *2.4.3*. The pressure upstream the choke *C2* is controlled by 4 parameters; *FT1*, *FT2*, *C1* and choke characteristics. A detailed analysis of the choke pressure is given in "Heave Compesated managed pressure drilling – Lab experiments" by A, Phade, where following choke characteristic equation is presented.

$$K_v = \frac{q}{\sqrt{\Delta P}} \tag{4.3.5}$$

Where K_v is the choke characterisation parameter, which is constant for a given choke opening. q is the flowrate through the choke opening, given in $^{m^3}/_{hr}$ and $\Delta P = C2 - C1$, is given in *bar.* Flowrate through the choke consists of both displaced well fluid and flowrate from the backpressure pump (ref; figure *3.1*). Rearranging equation *4.3.5* and substituting with *FT1* and *FT2*, following equation is obtained for *C2*.

$$C2(t) = \left(C1 + \left(\frac{FT1_{calc}(t)\times 3600 + FT2\times {}^{60}/_{1000}}{K_v}\right)^2\right) * 1 \times 10^5 \tag{4.3.6}$$

Where $C2(t)$ is given in *Pag,* C1 is a measurement in barg, $FT1_{calc}(t)$ is presented in chapter *4.2*, *FT2 is* a measurement in *LPM* and K_v is the choke characteristics. Both *FT2* and *C1* measurements are presented in chapter *4.1*. Prior to experiments presented in chapter *5.1* was a simple steady flow experiment conducted to determine K_v. The pump was turned on to deliver maximum flow, as required in chapter *4.1*, and a 50 degree opening was chosen for the choke. Both *C1* and *C2* were measured to determine the K_v value. *FT2, C1* and *C2* are plotted below for the experiment.

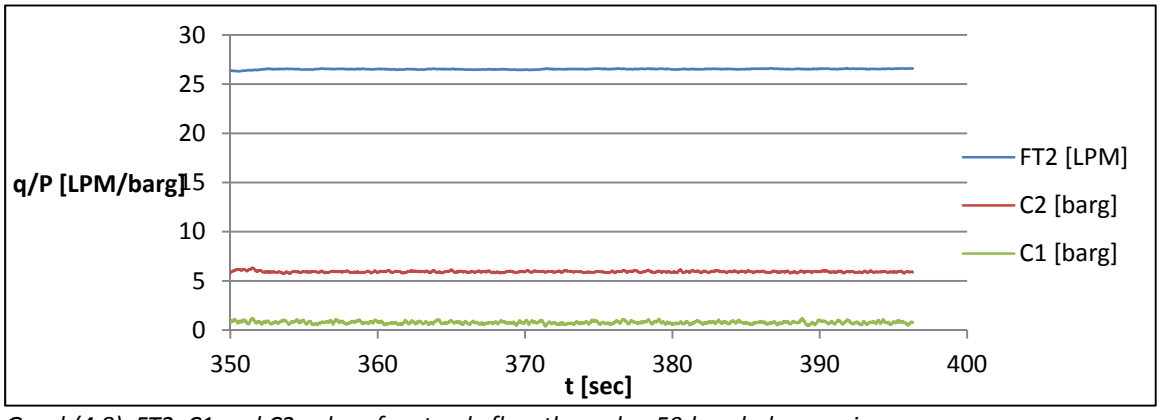

Graph(4.8), FT2, C1 and C2 values for steady flow through a 50deg choke opening.

As expected are all values plotted above fairly constant. Average values of plotted variables equates to $FT2_{ave} = 26.53LPM = 1.59\,^{m^3}/_{hr}$, $C1_{ave} = 0.77barg$ and

$C2_{ave} = 5.93barg$. Equation *4.3.5* is used to calculate the K_v value for a 50 degree choke opening; $K_{v,50deg} = \frac{q}{\sqrt{\Delta P}} = \frac{1.59}{\sqrt{5.93-0.77}} = 0.7$.

4.3.2 Minor Pressure Losses.

The fluid is displaced through varies components from the well to surface. Between the well and copper pipe, and between the copper pipe and the choke are varies components installed such as rubber hoses, pipe-bends and flowmeters with reduced ID. These components will influence the overall pressure drop. These minor pressure losses are not analysed in this project, but have been accounted for by empirical approximation. Graph *4.9* illustrates how the pressure drop varies through the components described above for $T_{string} = 12, 9, 7 \text{ and } 5\ sec$. The pressure drop between the copper pipe and the choke is empirical evaluated from *C2* and *CP1*, whilst pressure drop between the well and the copper pipe is evaluated from *P2* and *CP10*.

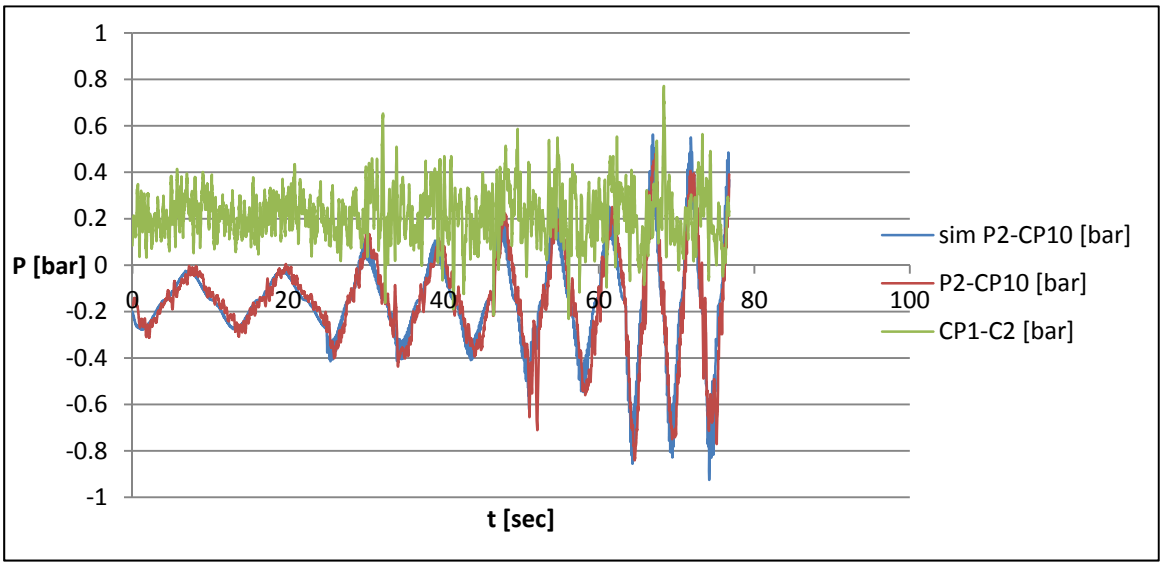

Graph(4.9); measured and empirical approximated minor pressure losses for T=12, 9, 7 and 5 sec.

Graph *4.9* illustrate that the pressure drop between the choke and the copper pipe is fairly constant and equal to 0.2*bar*. A large portion of this pressure difference is simply caused by hydrostatic pressure as the vertical distance between *C2* and *CP1,* $\Delta h_{CP1-C2} = 0.92m$. In further calculation are *C2* and *CP1* related through a simple hydrostatic relationship independent of fluid velocity and acceleration. The pressure drop between

the well and the copper pipe however; depends on the flowrate, which is clearly illustrates in graph *4.9*. An empirical relationship is determined to relate *P2* and *CP10,* given by equation *4.3.7*.

$$\Delta P_{P2-CP10} = 100000 \times (10{v_{hose}}^{1.75} - 0.15) \quad (4.3.7)$$

Where all units are given in consistent SI-units, and v_{hose} is the fluid velocity through the 19*mm* ID rubberhose connecting the well and copper pipe. v_{hose} is calculated from equation *4.3.8*.

$$v_{hose} = \frac{q_{disp}(t)}{\frac{\pi}{4}{D_{hose}}^2} \quad (4.3.8)$$

The largest portion of the pressure loss between the well and the copper pipe likely occurs in the connection point between the well and the rubber hose. A larger annulus area of $9.3cm^2$ is reduced to a narrow $1.33cm^2$ cross sectional hose area, which induces an entrance region subjected to pressure loss.

4.4 Matlab Script – Iterative Model

The two previous chapters present two different models of how to calculate flow and pressure respectively. Both these models depend on each other; an iterative model has been developed to calculate both flow and pressure throughout the scaled rig. Figure *4.4* below illustrates how the iterative model is looped, this model is found in Appendix A.

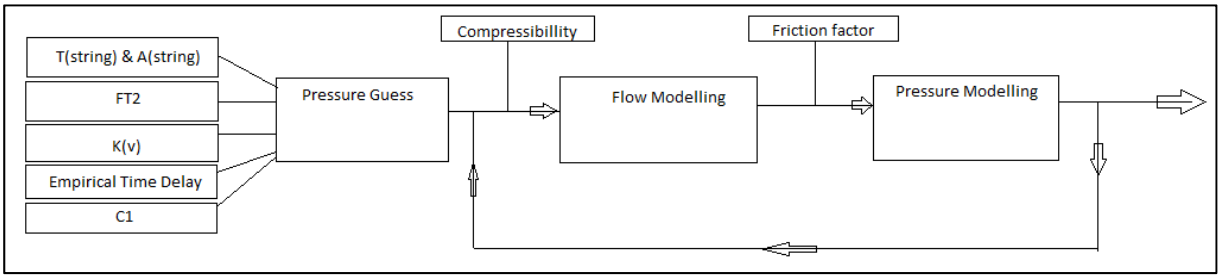

Figure(4.4); Iterative model to calculate flow and pressure.

The iterative model requires an initial pressure guess to start the iteration process. Similar to the pressure modelling presented in chapter *4.3*, is the pressure guess based

on the boundary condition *C2*. $C2_{guess}$ is calculated on the assumption that the magnitude of the flowrate displaced through the copper pipe is conserved, but phase shifted based on the empirical time delay (table *4.1*). The displaced flowrate which flows through the choke is then given by equation *4.4.1*.

$$FT1_{guess} = -\frac{2\pi A_{string}}{T_{string}} \cos\left(\frac{2\pi\, t}{T_{string}} - \frac{2\pi\, \Delta t_{flow}}{T_{string}}\right) \frac{\pi}{4} \left({D_{ur}}^2 - {D_{lr}}^2\right) \times 60000 \qquad (4.4.1)$$

Where the cosine term is the velocity of the BHA string (found in equation *2.4.2*), but time shifted with Δt_{flow} and $FT1_{guess}$ is given in *LPM*. From the initial guess of displaced flowrate through the choke can $C2_{guess}$ be calculated from equation *4.3.6.* From the assumption of a phase shifted flowrate through the copper pipe, is also flow velocity dependent on both time and position. The flow velocity through the copper pipe is assumed to be linearly phase shifted from the well to the choke.

$$v_{f,i\_guess}(t) = \frac{q_{disp}(t - \frac{81-i}{81}\Delta t_{flow})}{\frac{\pi}{4}{D_{cp}}^2} \qquad (4.4.2)$$

The initial pressure guess throughout each control volumes are given by equation *4.4.3*, with the following boundary condition $P_{1,guess}(t) = C2_{guess}(t) + \rho g \Delta h_{CP1-C2}$.

$$P_{j+1}(t) = P_j(t) + 0.05 v_{f,i_{guess=j}}(t) - \Delta P_{hyd,i=j},\ j \in 1,2,\dots,81 \qquad (4.4.3)$$

Graph *4.10* below presents the initial pressure guess throughout the copper pipe at each pressure sensor location. The initial pressure guess is calculated based on following parameters; $T_{string} = 9sec, A_{string} = 0.4m, FT2 = 27LPM, K_v = 0.74, C1 = 0.6barg$ and $\Delta t_{flow} = 1.4\ sec$.

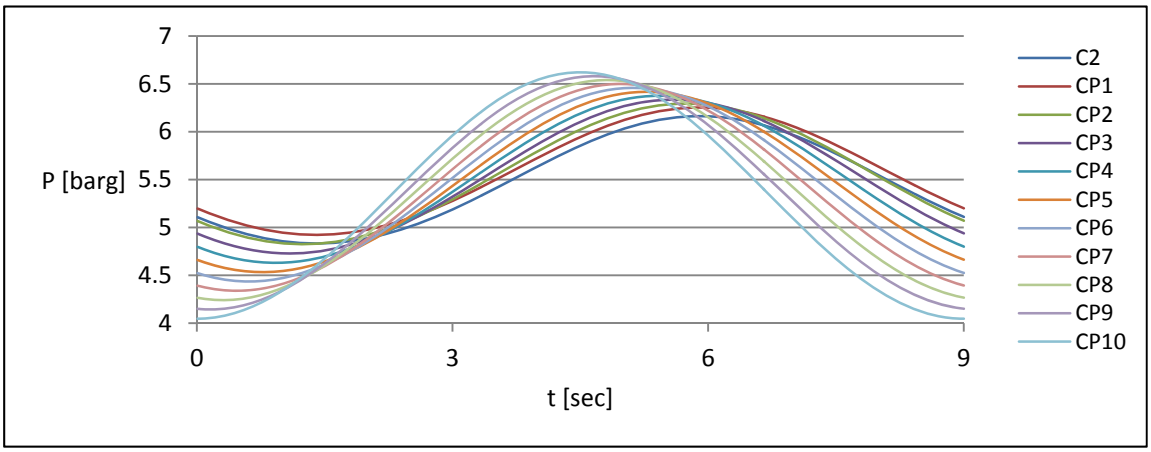

Graph(4.10); initial pressure guess.

The initial pressure guess is used to calculate the flow profile throughout the copper pipe, as described in chapter *4.2*. Chapter *4.2* highlights the effect of fluid inertia, and how calculated time delay based on compressibility diverse from measured time delay. The Matlab Code account for this modelling error, and phase shifts the flow profile to match the measured time delay. Furthermore is the calculated flow profile used to calculate pressure throughout the heave lab system, as described in chapter *4.3*. The Matlab Script presented in "MPD Heave Lab: Experimental Work and Modelling of Surge and Swab Effects" by A, Boge is also included to calculate pressure in the bottom of the well *P1.* Results of the Matlab Script are compared with measured pressure and flow, and are presented in chapter *5.1*.

4.5 Empirical Pressure Model

An Empirical Model has been developed to simplify the relationship between surface pressure and BHP. This model is only valid for the dimensions present in the MPD Heave Lab. The Empirical model is developed based on curve matching from measured data in the lab. 8 experiments have been conducted to develop this model, the BHA has been oscillated with periods ranging from $T_{string} = 12sec$ to $T_{string} = 5sec$ and $A_{string} = 0.4m$. Similar to the initial pressure guess presented in chapter *4.4*, is the magnitude of the displaced flowrate through the copper pipe assumed conserved but phase shifted. The displaced flowrate through the choke is then calculated from equation *4.4.1*, and the choke pressure is calculated from equation *4.3.6*. As previously discussed is the largest part of pressure drop found in the copper pipe. In this empirical model is the entire pressure drop through the copper pipe estimated based on one single control volume. The representative flowrate through the control volume is assumed to be phase shifted one half of the total time delay listed in table *4.1*.Representative flowrate through the single control volume is calculated from equation *4.5.1*.

$$q_{emp} = -\frac{2\pi A_{string}}{T_{string}} \cos\left(\frac{2\pi t}{T_{string}} - \frac{2\pi \Delta t_{flow}}{2T_{string}}\right) \frac{\pi}{4} \left({D_{ur}}^2 - {D_{lr}}^2\right) \quad (4.5.1)$$

The fluid velocity through the control volume is calculated from $q = vA$, where A is the copper pipe cross-sectional area. Substituting this expression into equation *4.5.1,* is following relationship obtained for fluid velocity through the control volume.

$$v_{emp}(t) = -\frac{2\pi A_{string}}{T_{string}} \cos\left(\frac{2\pi t}{T_{string}} - \frac{2\pi \Delta t_{flow}}{2T_{string}}\right) \frac{{D_{ur}}^2 - {D_{lr}}^2}{{D_{cp}}^2} \quad (4.5.2)$$

From the velocity term above is the fluid acceleration derived. The fluid acceleration through the control volume is the derivative of the fluid velocity. The fluid acceleration through the control volume is found in equation *4.5.3.*

$$a_{emp}(t) = \frac{dv_{emp}}{dt} = \left(\frac{2\pi}{T_{string}}\right)^2 A_{string} \sin\left(\frac{2\pi t}{T_{string}} - \frac{2\pi \Delta t_{flow}}{2T_{string}}\right) \frac{{D_{ur}}^2 - {D_{lr}}^2}{{D_{cp}}^2} \quad (4.5.3)$$

An empirical approximation of pressure drop through the copper pipe has been based on the acceleration and velocity terms. This approximation has been found by empirical investigating *C2* and *P2*. The empirical relationship between *P2* and *C2* is found below.

$$\Delta P_{cp,emp} = 6a_{emp}(t) + 41v_{emp}(t)^{1.75} - 0.1 \quad (4.5.4)$$

Where v_{emp} and a_{emp} are given by equation *4.5.2* and *4.5.3*, $\Delta P_{cp,emp}$ is given in bar. Equation *4.3.6* and *4.5.4* have been used to calculate *C2* and *P2* respectively. Calculated values are plotted below together with measured data. Graph *4.11* illustrate experiments with $T_{string} = 12, 11, 10$ and $9sec$ and $A_{string} = 0.4m$, while graph *4.12* illustrate experiments performed with $T_{string} = 8, 7, 6$ and $5\ sec$. In addition was all experiments performed with following parameters; $FT2 = 27LPM, C1 = 0.6barg$ and $K_v = 0.74$.

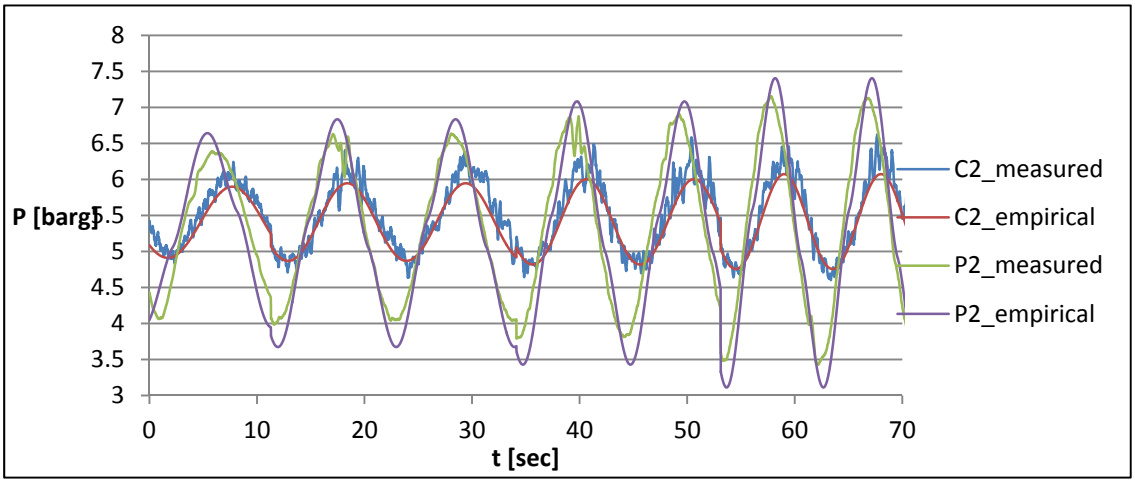

Graph(4.11); measured and calculated values for C2 and P2 for $T_{string} = 12, 11, 10$ *and* $9sec$.

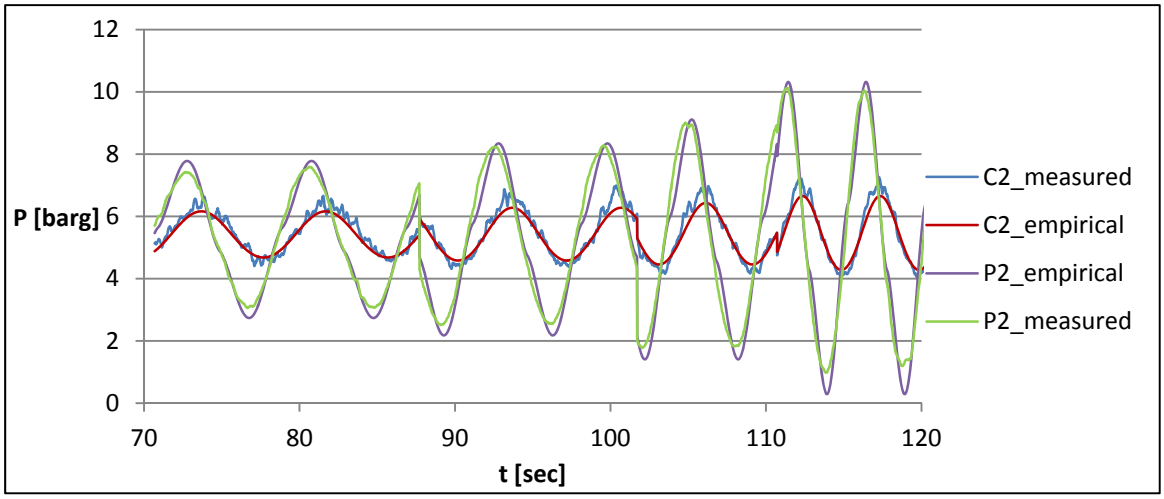

Graph(4.12); measured and calculated values for C2 and P2 for $T_{string} = 8, 7, 6 \; and \; 5 \; sec.$

An empirical relationship between *P1* and *P2* was found in "MPD Heave Lab: Experimental Work and Modelling of Surge and Swab Effects" by A. Boge. The empirical relationship between *P1* and *P2* for the 40.89*mm* OD BHA is given by equation *4.5.5*.

$$\Delta P_{w,emp} = -1.63 v_{string}(t) + 0.15 \tag{4.5.5}$$

BHP is found by adding together all pressure drops to the surface pressure. BHP is given by equation *4.5.6*.

$$P_{BH,emp} = C2 + \Delta P_{cp,emp} + \Delta P_{w,emp} \tag{4.5.6}$$

Calculated BHP and measured BHP is plotted in graph *4.13* and *4.14* for all 8 experiments described above. The absolute discrepancy between measured and calculated pressure is also plotted.

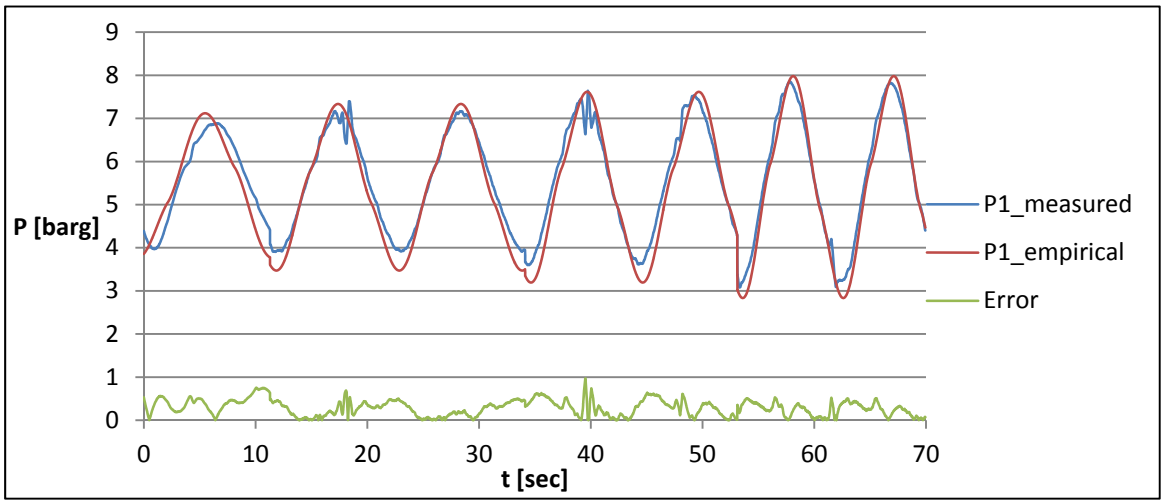

Graph(4.13); Measured and calculated BHP for $T_{string} = 12, 11, 10 \; and \; 9 sec.$

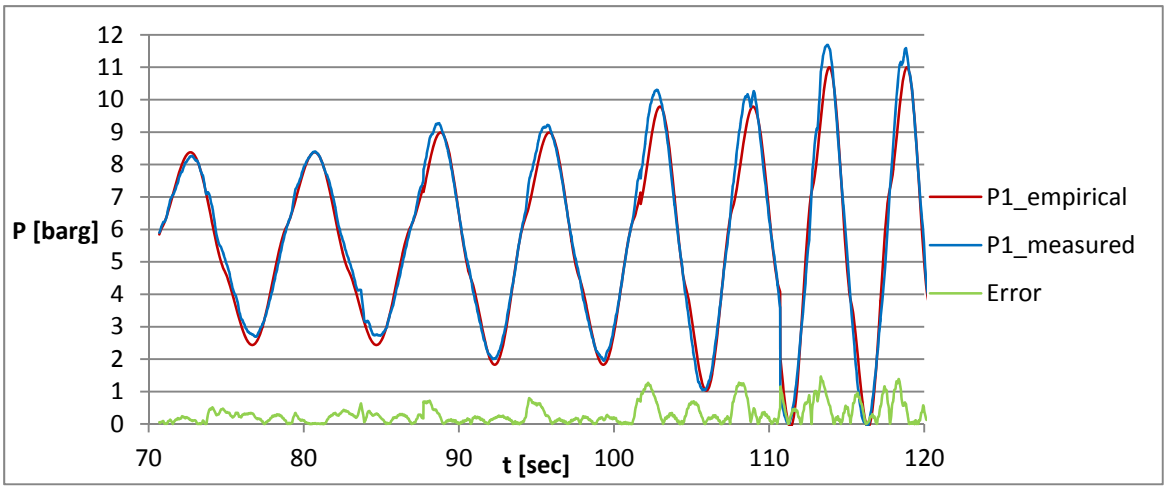

Graph(4.14); Measured and calculated BHP for $T_{string} = 8, 7, 6 \; and \; 5sec$.

Largest discrepancy between measured and calculated pressure equates to $1.46bar$. This discrepancy is found when the BHA is oscillated with a period of $T_{string} = 5sec$, the discrepancy accounts for a total of 25% of the total pressure fluctuation.

5.0 Results

This chapter presents measured data and simulations results. Chapter *5.1* compares the Matlab Script found in Appendix A with measured data. Chapter *5.2* presents calculated choke opening based on the empirical model found in chapter *4.5*.

5.1 Heave Experiments with Fixed Choke Angle

This chapter presents and compares measured lab data and simulation data from the Matlab Script found in Appendix A. 8 experiments have been performed in the MPD Heave Lab with various oscillation frequencies. The BHA string was oscillated with periods from 12sec to 5sec, changing the string period with 1sec for every experiment. It was decided to not perform any experiments with a string period lower than 5sec as the BHP exceeded 11barg. The oscillation amplitude was kept constant at 0.4m. All experiments were performed with a constant choke angel of 50deg and the backpressure-pump was running at 100% effect. More detailed input parameters are found in table *5.1* below. For experiments presented in the following sub-chapters are 4 graphs presented, measured and simulated values of: 1. Displaced flowrate in the well and at surface, 2. Pressure at *C2* and *CP10,* 3. BHP, 4. Discrepancy between measured and simulated BHP.

Parameter	value	unit
A_{string}	0.4	m
Kv	0.74	
FT2	27	LPM
C1	0.6	barg
Δt_{calc_res}	0.01	sec
cv	81	
E_{string}	0.4	m
D_{ur}	25	mm
D_{lr}	22	mm
L_{BHA}	350	mm
D_{BHA}	40.89	mm
t_{cling}	0.18	mm
D_{well}	42.53	mm
α_{cp}	2.70E-13	$m^3/m\,Pa$
D_{cp}	16	mm
$D_{rubberhose}$	19	mm
L_{cp}	893.6	m
L_{cv}	11.03	m
ρ	998.2	kg/m^3
μ	0.001	Pa s
$\Delta t_{p-prop,cv}$	0.01	sec

Table (5.1); input parameters for all simulation results presented in chapter 5.1.

5.1.1 Experiment 1, $T_{string} = 12sec.$

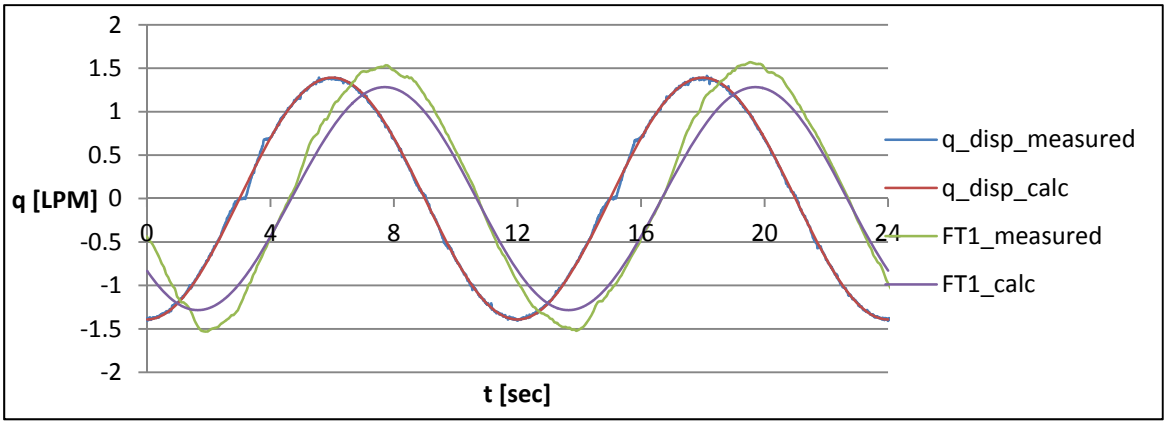

Graph(5.1); Displaced flowrate in the well and at surface for $T_{string} = 12sec.$

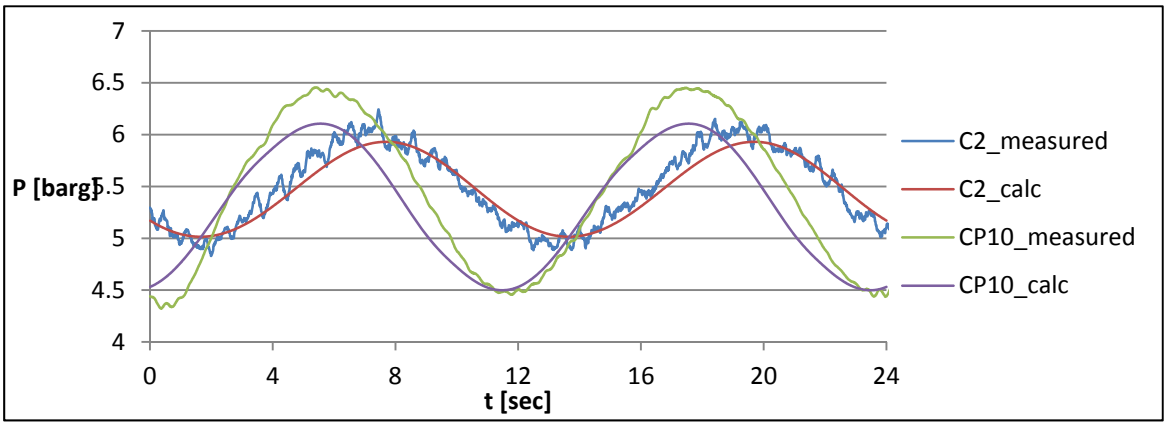

Graph(5.2); Measured and simulated C2 and CP10 for $T_{string} = 12sec.$

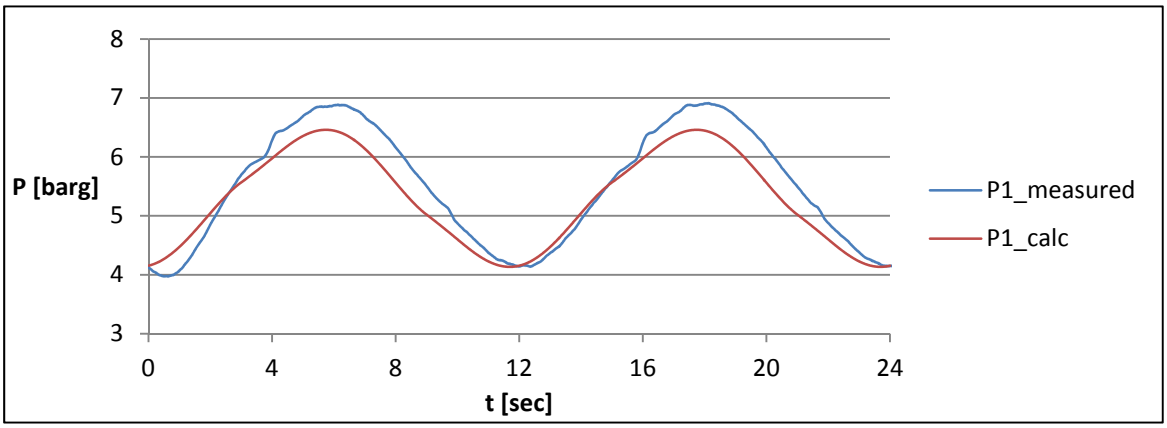

Graph(5.3); Measured and simulated BHP for $T_{string} = 12sec.$

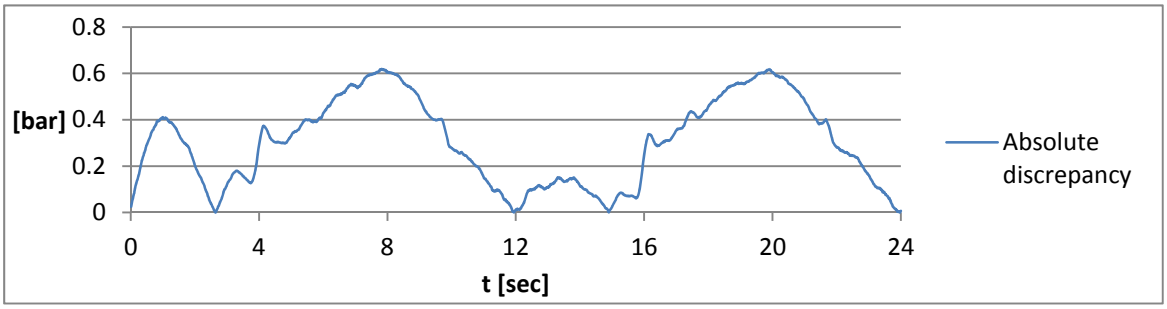

Graph(5.4); Discrepancy between measured and simulated BHP for $T_{string} = 12sec.$

5.1.2 Experiment 2, $T_{string} = 11sec.$

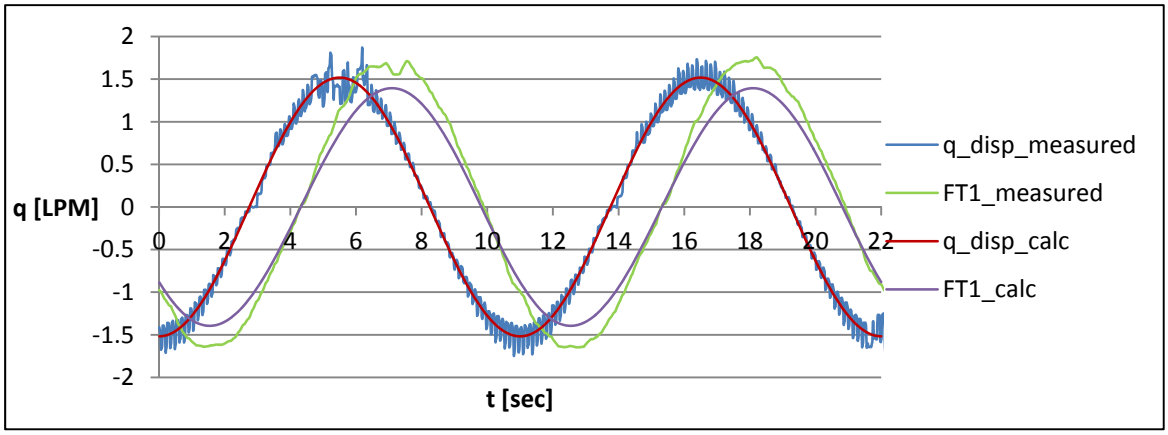

Graph(5.5); Displaced flowrate in the well and at surface for $T_{string} = 11sec.$

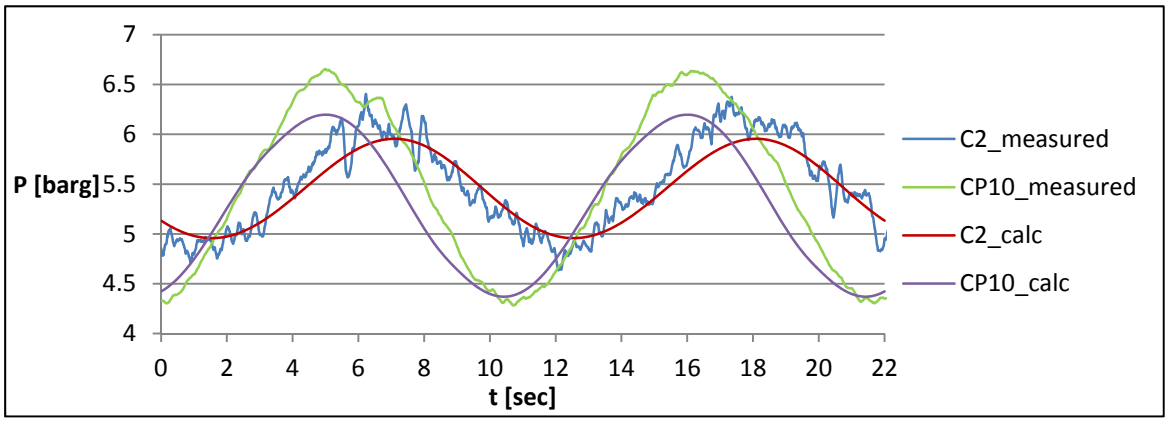

Graph(5.6); Measured and simulated C2 and CP10 for $T_{string} = 11sec.$

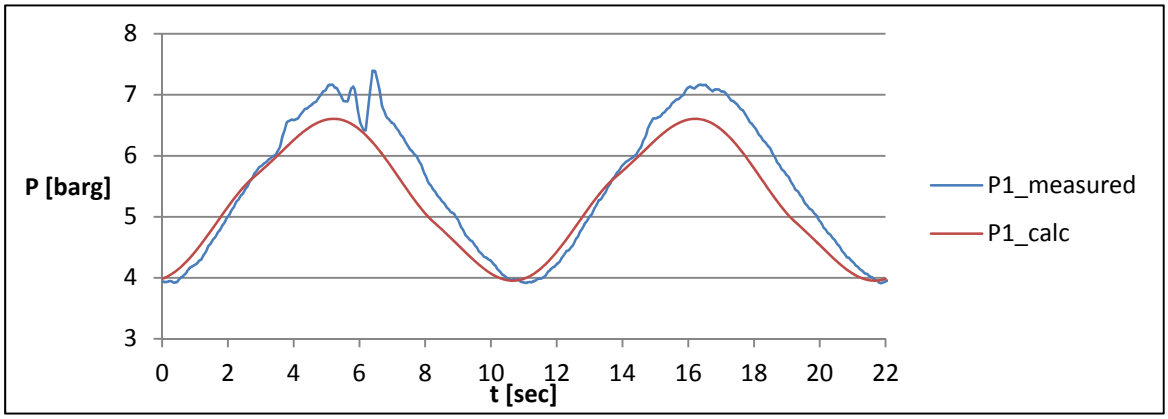

Graph(5.7); Measured and simulated BHP for $T_{string} = 11sec.$

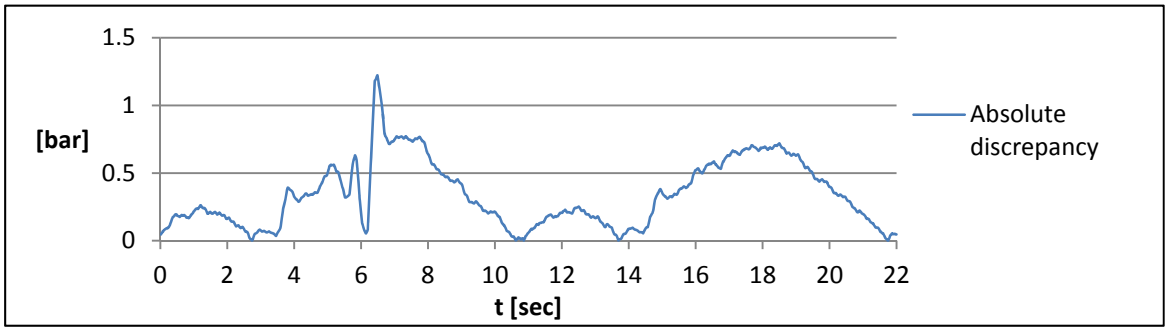

Graph(5.8); Discrepancy between measured and simulated BHP for $T_{string} = 11sec.$

5.1.3 Experiment 3, $T_{string} = 10sec.$

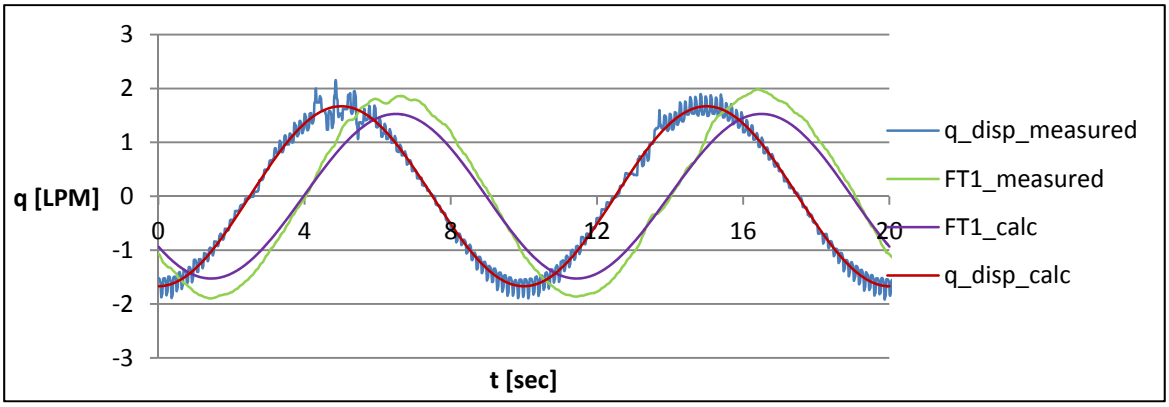

Graph(5.9); Displaced flowrate in the well and at surface for $T_{string} = 10sec.$

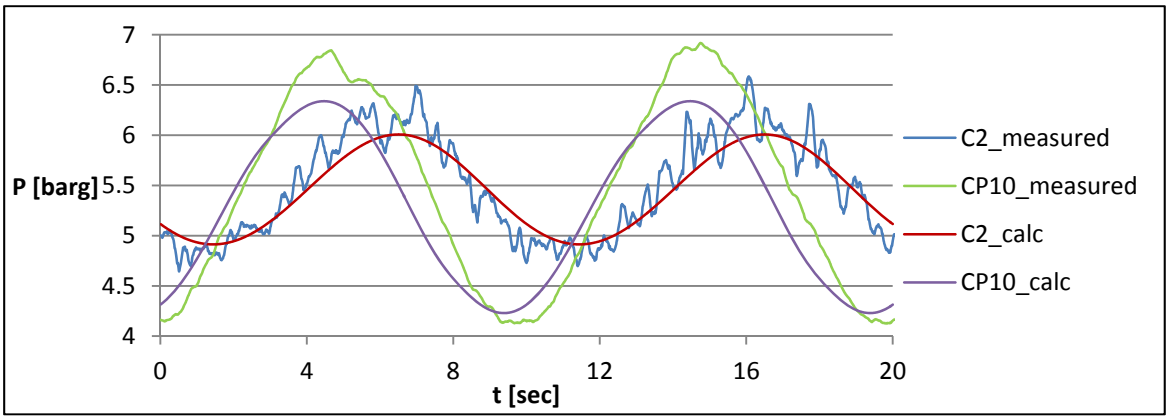

Graph(5.10); Measured and simulated C2 and CP10 for $T_{string} = 10sec.$

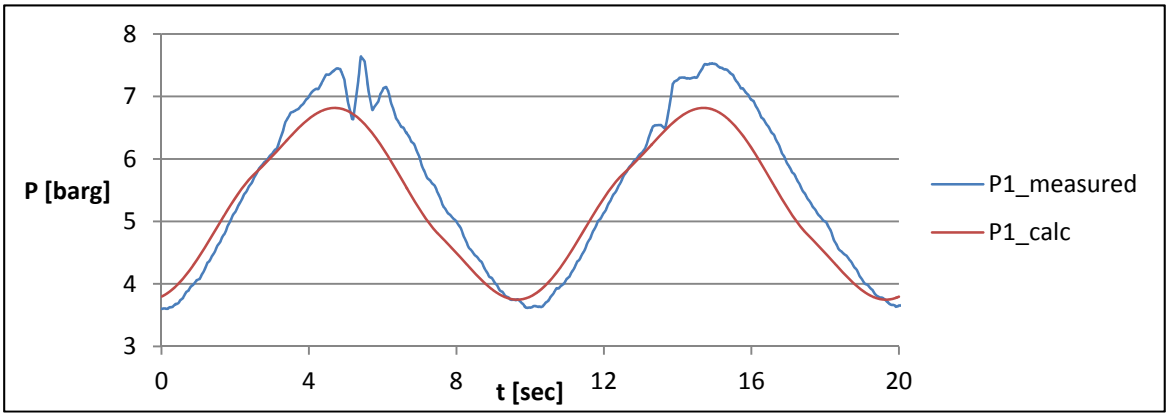

Graph(5.11); Measured and simulated BHP for $T_{string} = 10sec.$

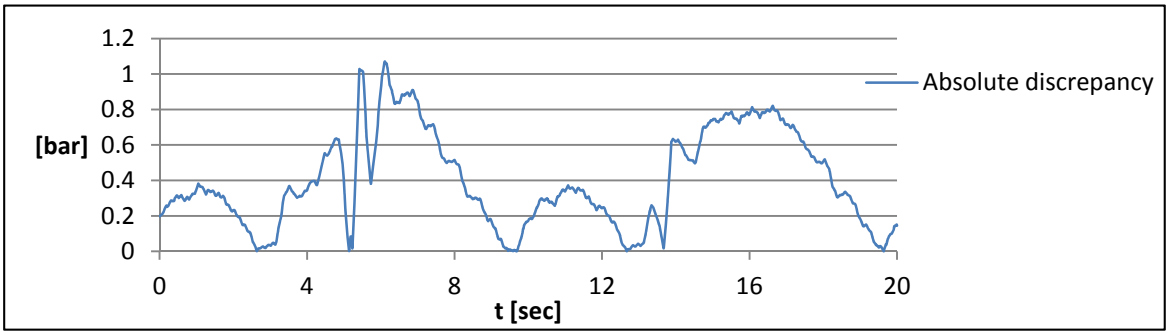

Graph(5.12); Discrepancy between measured and simulated BHP for $T_{string} = 10sec.$

5.1.4 Experiment 4, $T_{string} = 9sec.$

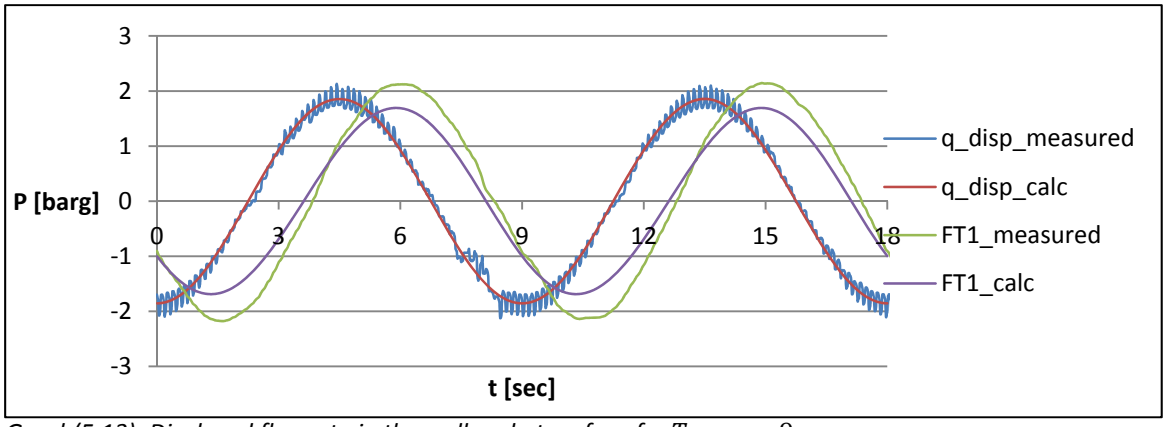

Graph(5.13); Displaced flowrate in the well and at surface for $T_{string} = 9sec.$

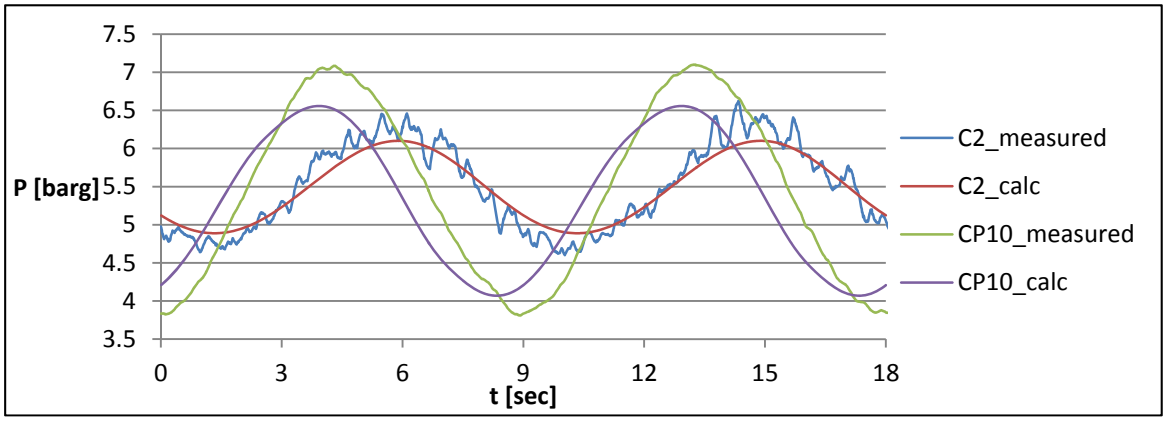

Graph(5.14); Measured and simulated C2 and CP10 for $T_{string} = 9sec.$

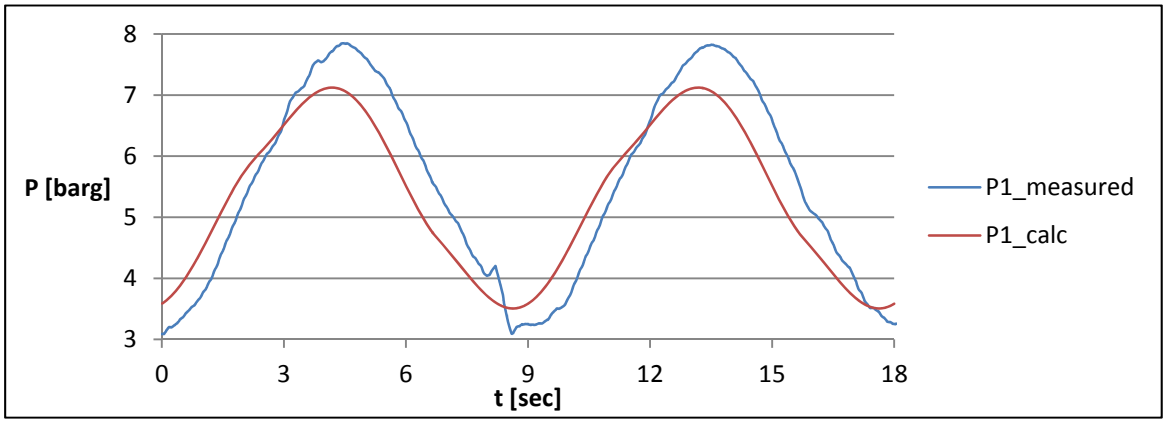

Graph(5.15); Measured and simulated BHP for $T_{string} = 9sec.$

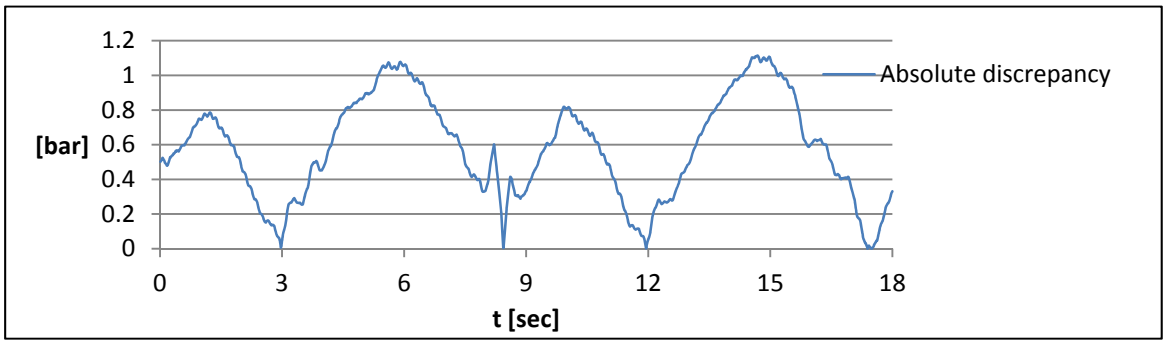

Graph(5.16); Discrepancy between measured and simulated BHP for $T_{string} = 9sec.$

5.1.5 Experiment 5, $T_{string} = 8sec.$

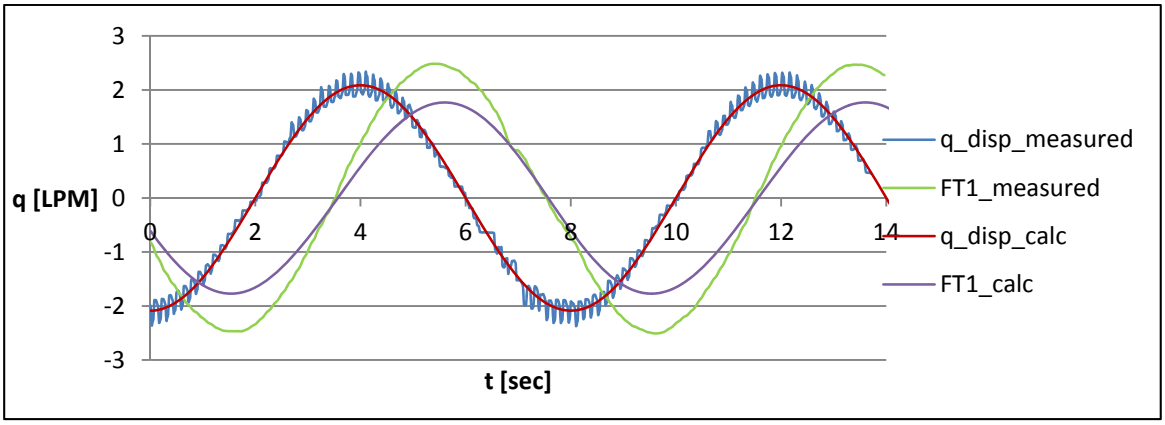

Graph(5.17); Displaced flowrate in the well and at surface for $T_{string} = 8sec.$

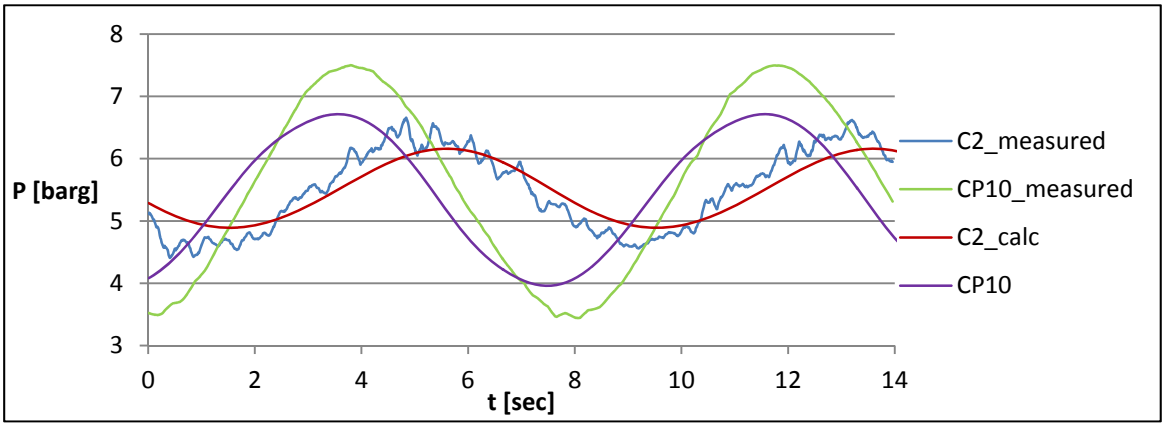

Graph(5.18); Measured and simulated C2 and CP10 for $T_{string} = 8sec.$

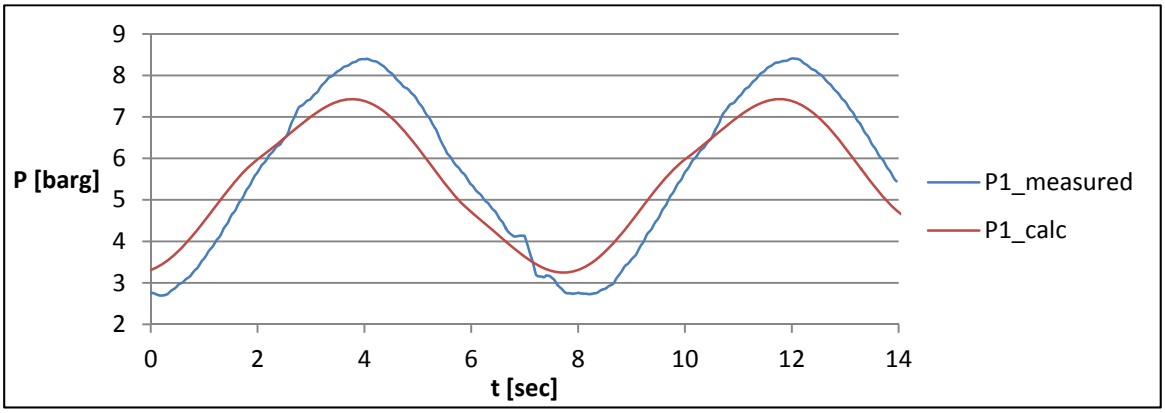

Graph(5.19); Measured and simulated BHP for $T_{string} = 8sec.$

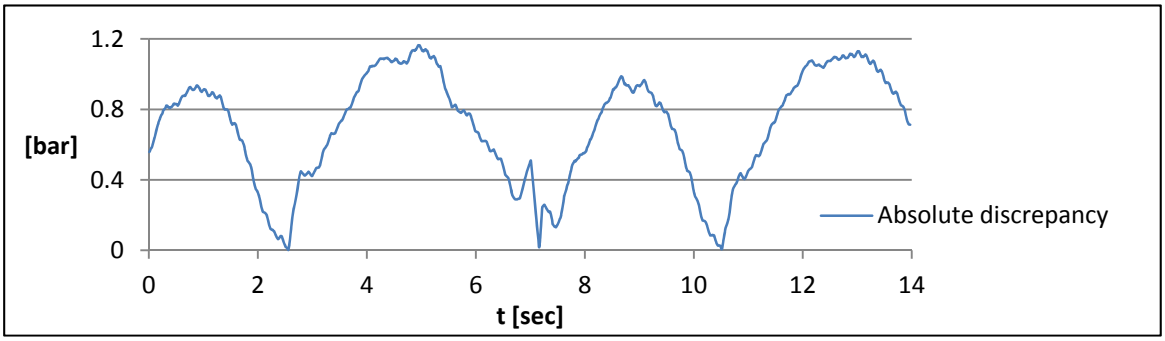

Graph(5.20); Discrepancy between measured and simulated BHP for $T_{string} = 8sec.$

5.1.6 Experiment 6, $T_{string} = 7sec.$

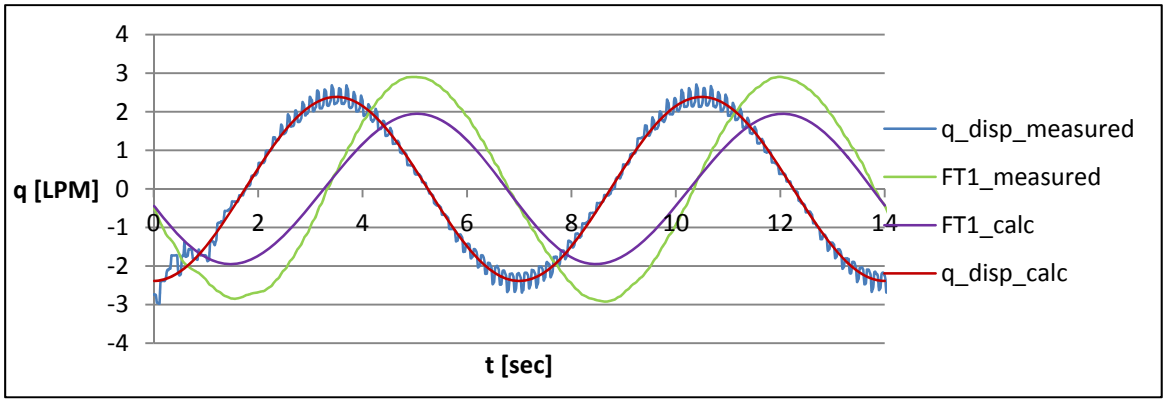

Graph(5.21); Displaced flowrate in the well and at surface for $T_{string} = 7sec.$

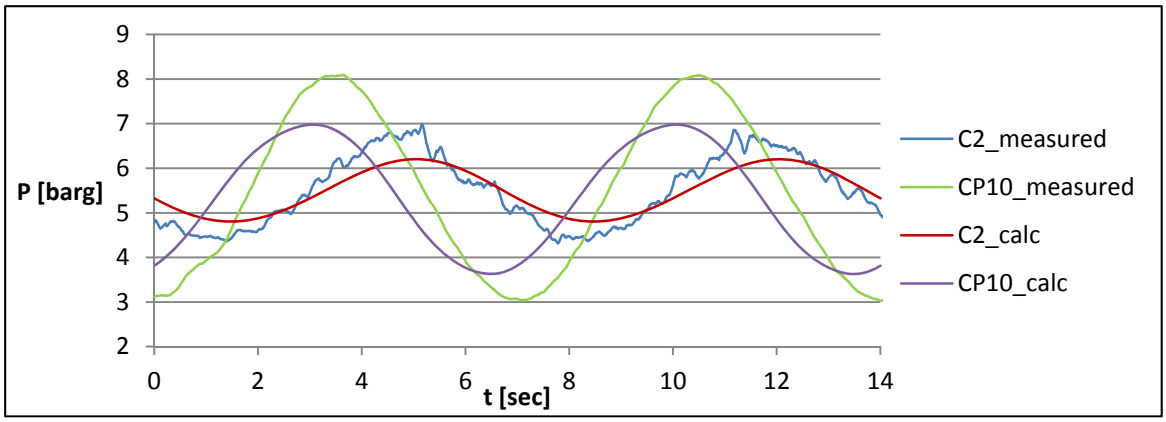

Graph(5.22); Measured and simulated C2 and CP10 for $T_{string} = 7sec.$

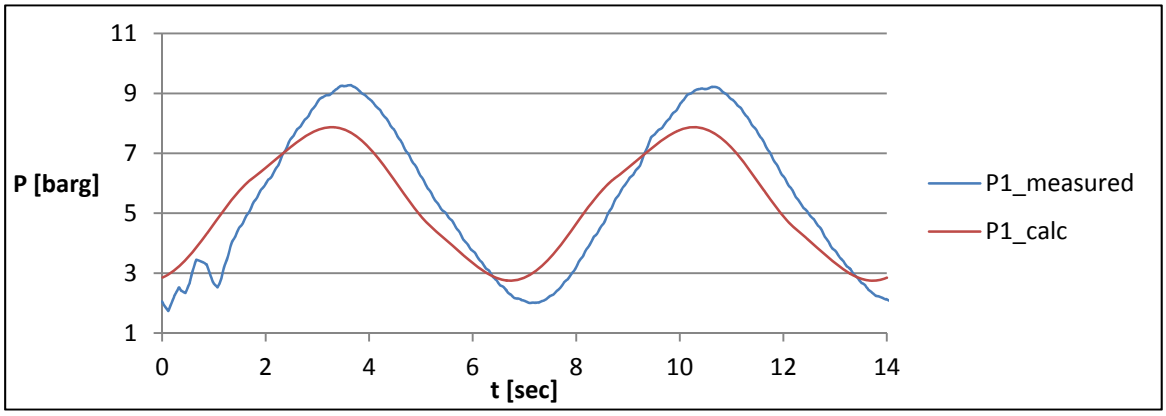

Graph(5.23); Measured and simulated BHP for $T_{string} = 7sec.$

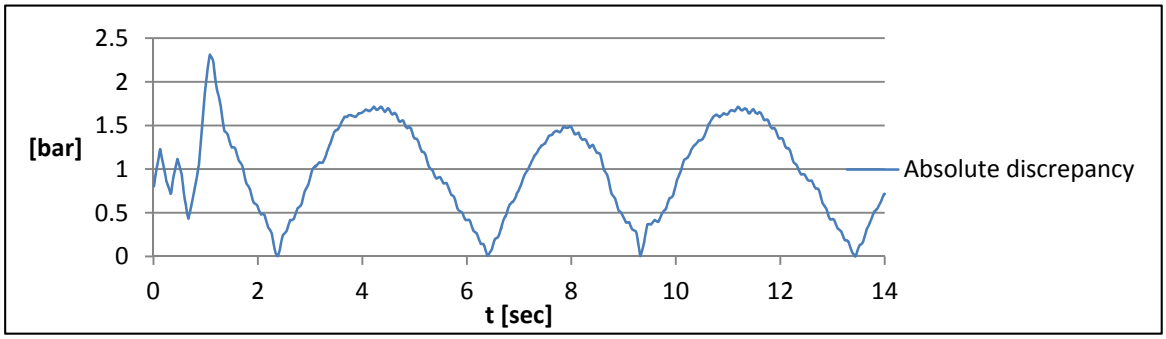

Graph(5.24); Discrepancy between measured and simulated BHP for $T_{string} = 7sec.$

5.1.7 Experiment 7, $T_{string} = 6sec.$

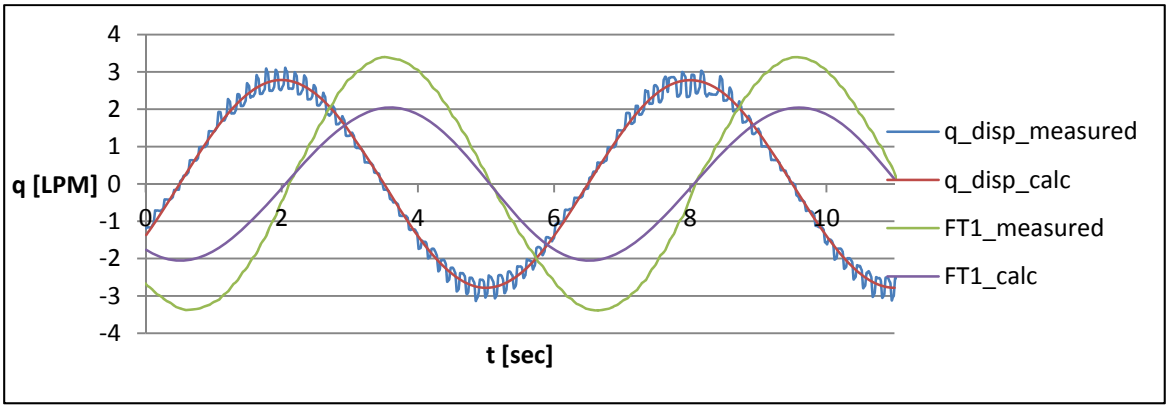

Graph(5.25); Displaced flowrate in the well and at surface for $T_{string} = 6sec.$

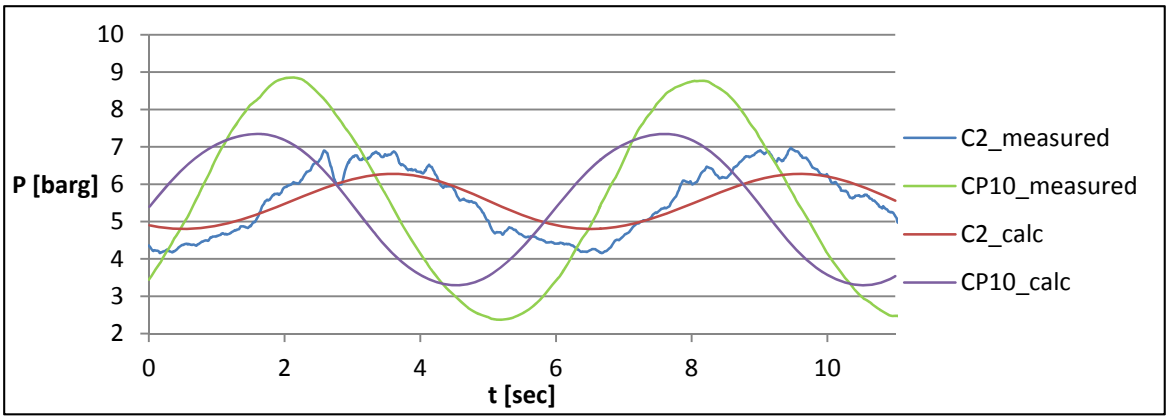

Graph(5.26); Measured and simulated C2 and CP10 for $T_{string} = 6sec.$

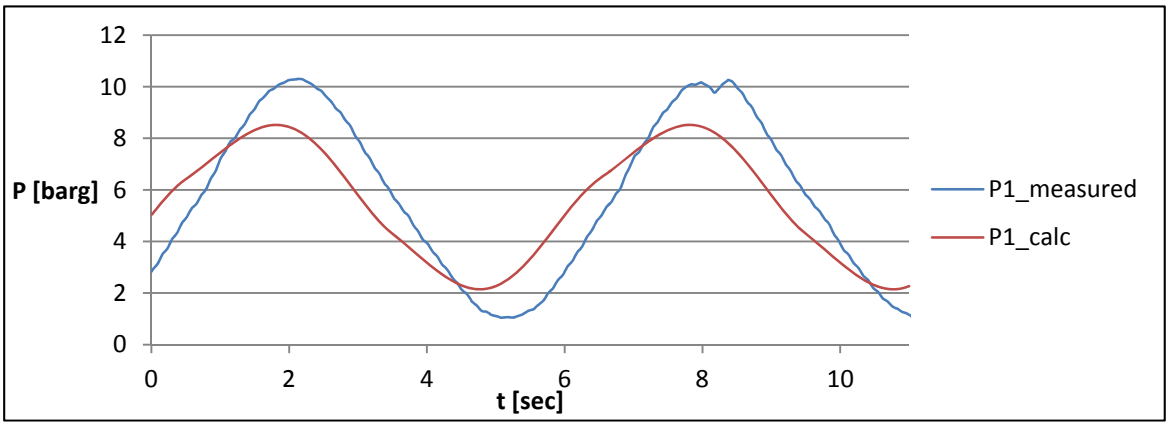

Graph(5.27); Measured and simulated BHP for $T_{string} = 6sec.$

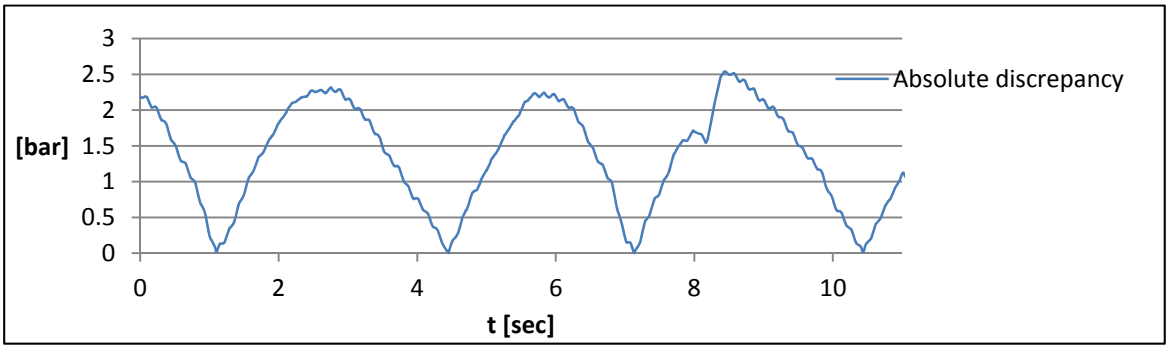

Graph(5.28); Discrepancy between measured and simulated BHP for $T_{string} = 6sec.$

5.1.8 Experiment 8, $T_{string} = 5sec.$

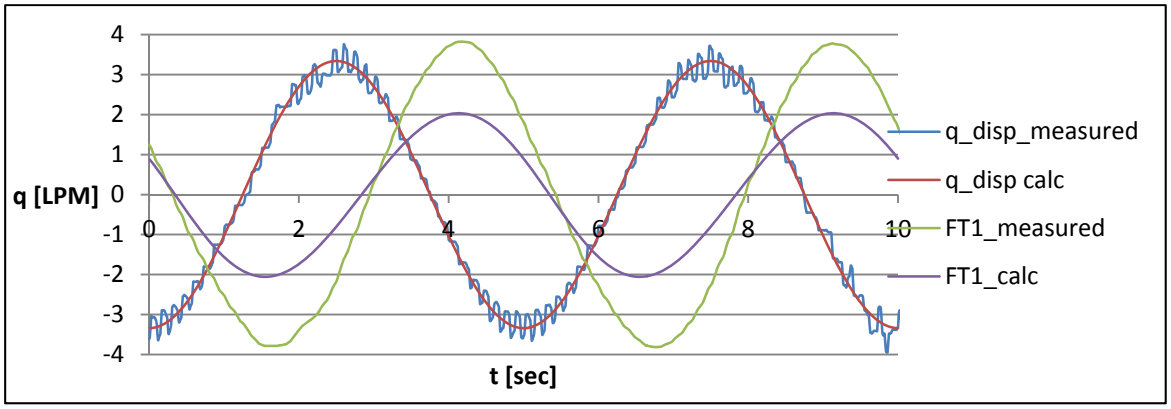

Graph(5.29); Displaced flowrate in the well and at surface for $T_{string} = 5sec.$

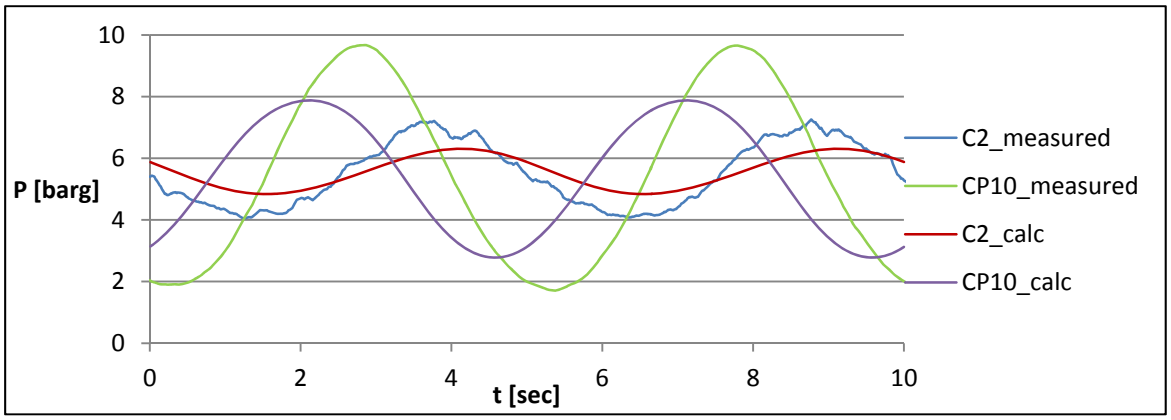

Graph(5.30); Measured and simulated C2 and CP10 for $T_{string} = 5sec.$

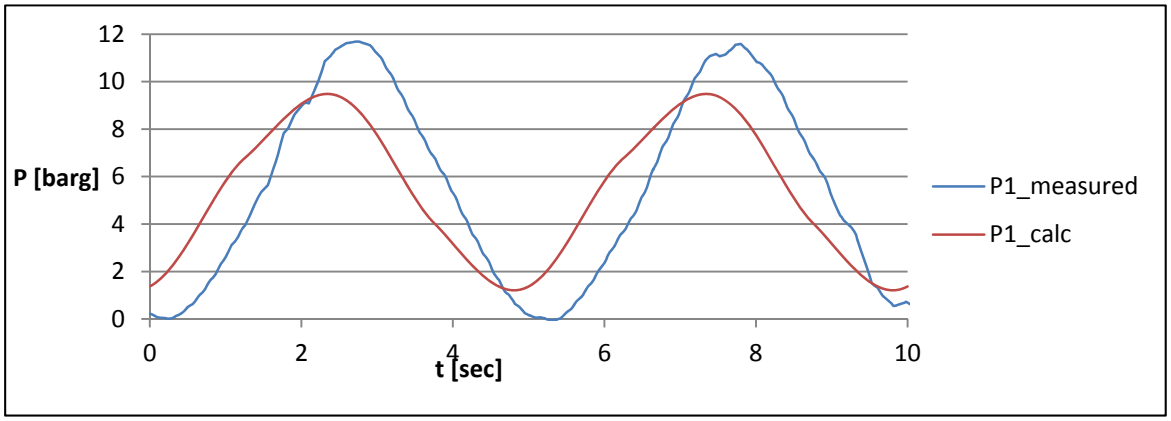

Graph(5.31); Measured and simulated BHP for $T_{string} = 5sec.$

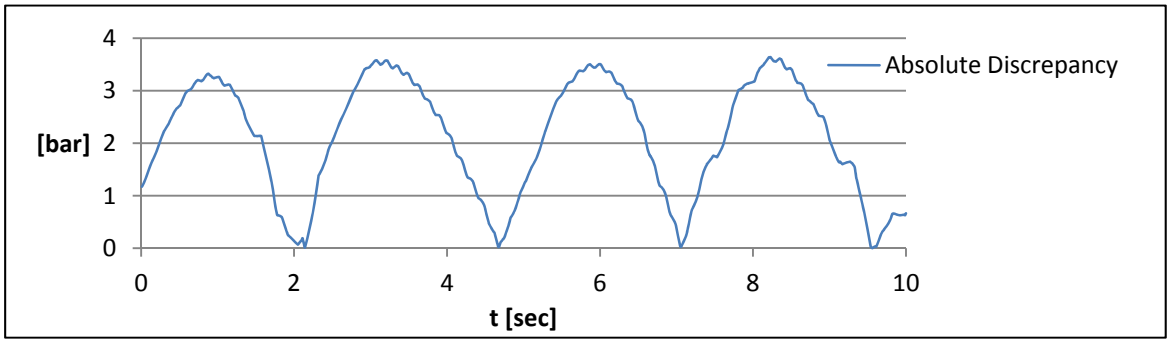

Graph(5.32); Discrepancy between measured and simulated BHP for $T_{string} = 5sec.$

5.2 CBHP Simulation

The overall objective for the MPD Heave Lab is to maintain CBHP while oscillating the BHA string. The BHP is maintained constant by controlling the surface pressure, which is controlled by adjusting the choke angle. It is important to control the surface pressure prior to the actual pressure change downhole due to time delays. The pressure wave created at surface travel with the speed of sound and needs approximately 0.81sec to propagate through the copper pipe, this was discussed in chapter *3.4.* The empirical hydraulic model presented in chapter *4.5* may be used to simulate choke angle to maintain CBHP. By rearranging equation *4.5.6* and substituting with the expression found in equation *4.3.6,* following relationship is found for the choke angle K_v value.

$$K_v = \frac{FT1 \times 3600 + FT2 \times {}^{60}/_{1000}}{\sqrt{P_{BH} - \Delta P_{cp} - \Delta P_{well} - C1}} \quad (5.2.1)$$

FT2, *C1* and P_{BH} are constant in a CBHP operation, while *FT1*, ΔP_{cp} and ΔP_w are variables depending on the heave motion characteristics. These variables needs to be time shifted with 0.81*sec* to maintain CBHP. *FT1* and ΔP_w are found in equation *4.5.1* and *4.5.5* respectively, their time shifted values are given in equation *5.2.2* and *5.2.3*. ΔP_{cp} is a function of both v_{emp} and $a_{emp,}$time shifted values of v_{emp} and a_{emp} are given by equation *5.2.4* and *5.2.5*.

$$FT1_{shifted}(t) = -\frac{2\pi A_{string}}{T_{string}} \cos\left(\frac{2\pi\, t}{T_{string}} - \frac{2\pi\, \Delta t_{flow}}{T_{string}} + \frac{2\pi \Delta t_{p-prop}}{T_{string}}\right) \frac{\pi}{4} \left({D_{ur}}^2 - {D_{lr}}^2\right) \quad (5.2.2)$$

$$\Delta P_{well,shifted}(t) = -1.63 \times \frac{2\pi A_{string}}{T_{string}} \cos\left(\frac{2\pi t}{T_{string}} + \frac{2\pi \Delta t_{p-prop}}{T_{string}}\right) + 0.15 \quad (5.2.3)$$

$$v_{emp,shifted}(t) = -\frac{2\pi A_{string}}{T_{string}} \cos\left(\frac{2\pi t}{T_{string}} - \frac{2\pi \Delta t_{flow}}{2T_{string}} + \frac{2\pi \Delta t_{p-prop}}{T_{string}}\right) \frac{{D_{ur}}^2 - {D_{lr}}^2}{{D_{cp}}^2} \quad (5.2.4)$$

$$a_{emp,shifted}(t) = \left(\frac{2\pi}{T_{string}}\right)^2 A_{string} \sin\left(\frac{2\pi t}{T_{string}} - \frac{2\pi \Delta t_{flow}}{2T_{string}} + \frac{2\pi \Delta t_{p-prop}}{T_{string}}\right) \frac{{D_{ur}}^2 - {D_{lr}}^2}{{D_{cp}}^2} \quad (5.2.5)$$

Equation *5.2.1* together with the time shifted variables presented above is used to calculate the choke K_v value. The choke K_v value is converted to choke angle by equation *5.2.6 (*Phade, A 2013).

$$\theta = (10^{5.08} \times K_v)^{1/2.96} \quad (5.2.6)$$

5.2.1 Simulation Results

A couple of CBHP simulation results are presented below. If the choke angle is kept constant, the BHP will fluctuate according to relationship found in equation *5.2.1*. However; if the choke angle is managed accordingly is it possible to maintain CBHP. Simulations below present two different scenarios: 1. Choke is kept constant 2. BHP is kept constant. Simulations are based on input parameters found in table *5.1*, and $T_{string} = 12, 9$ and $6sec$. For scenario 2 calculations is the BHP equal to $6barg$.

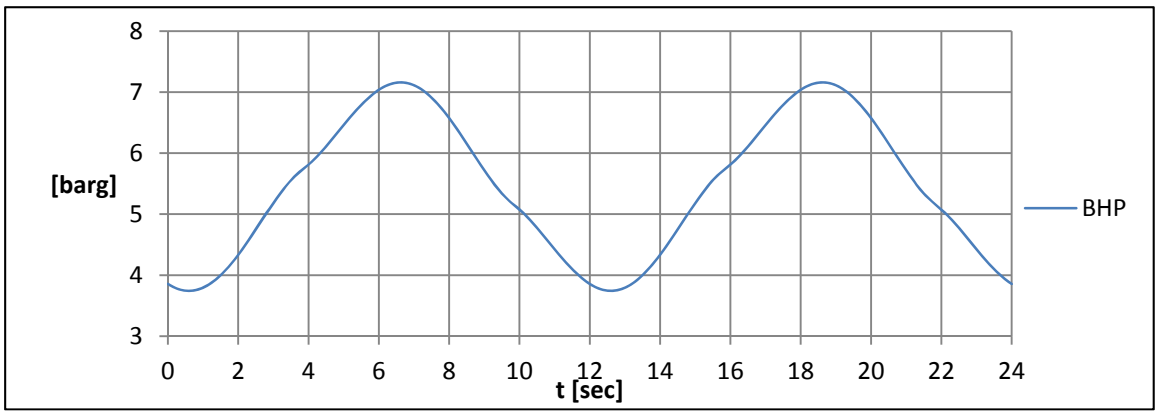

Graph(5.33); Scenario 1 Constant choke angle $K_v = 0.74$ for $T_{string} = 12sec$..

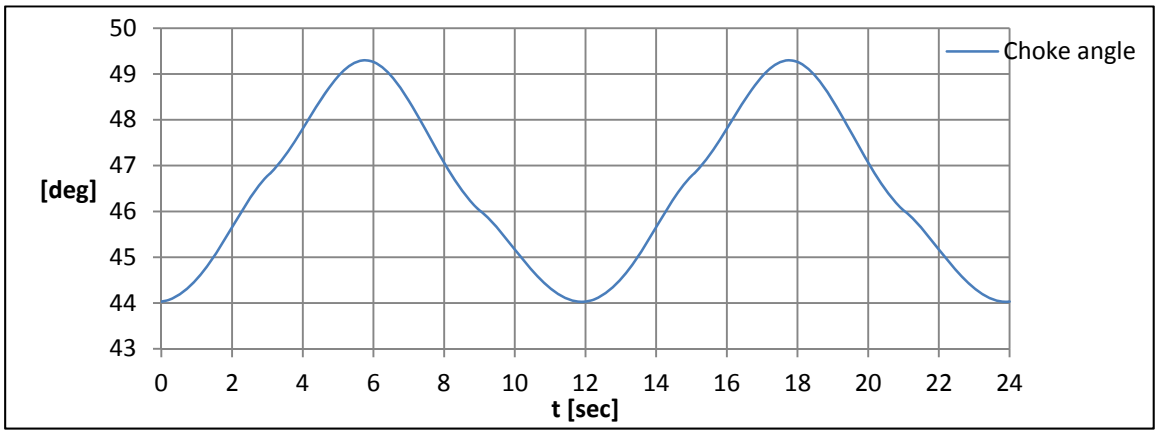

Graph(5.34); Scenario 2 CBHP=6barg for $T_{string} = 12sec$.

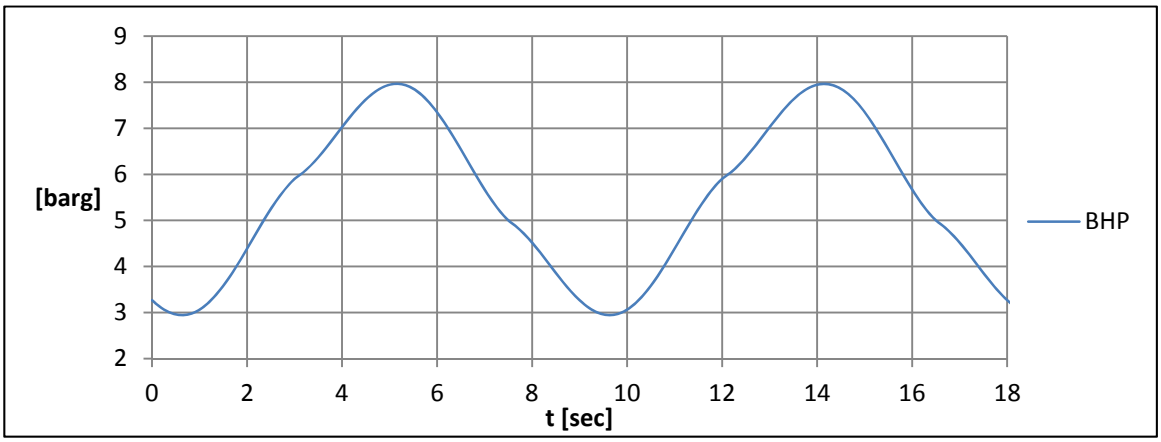

Graph(5.35); Scenario 1 constant choke angle $K_v = 0.74$ for $T_{string} = 9sec$.

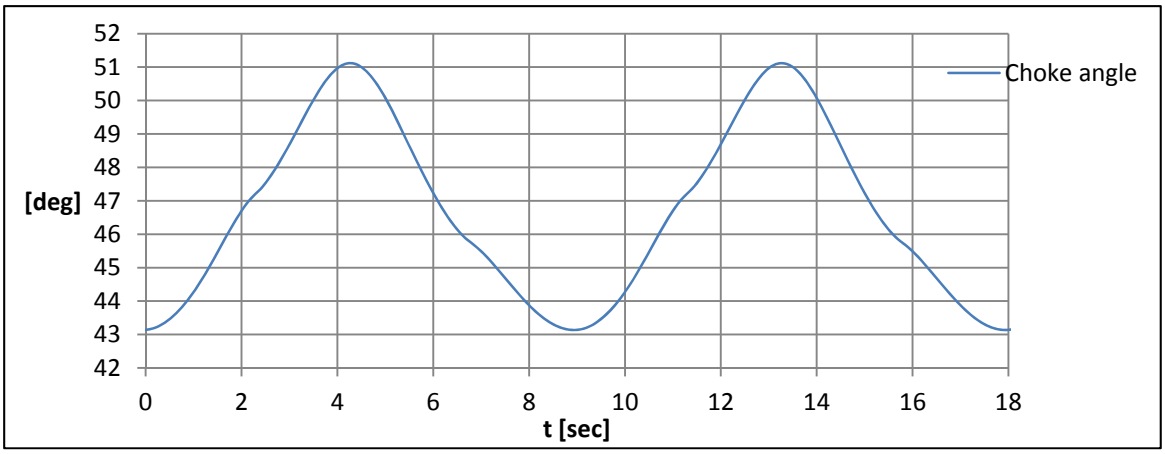

Graph(5.36); Scenario 2 CBHP=6barg for $T_{string} = 9sec$.

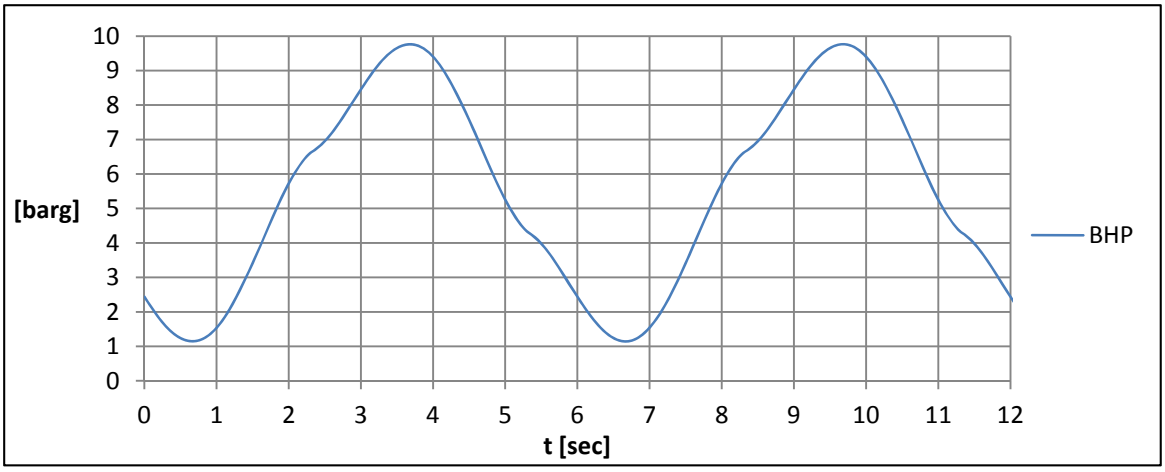

Graph(5.37); Scenario 1 constant choke angle $K_v = 0.74$ for $T_{string} = 6sec$.

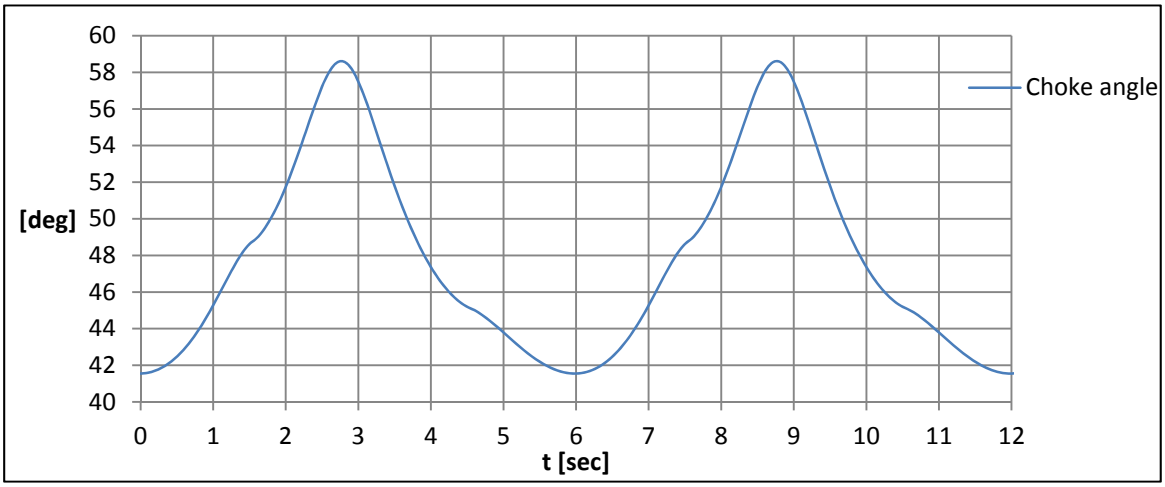

Graph(5.38); Scenario 2 CBHP=6barg for $T_{string} = 6sec$.

6.0 Discussion

In this chapter are results obtained in the MPD heave lab discussed. Chapter *6.2* discuss dynamical properties present in the MPD heave lab. These properties are further discussed in chapter *6.3* for which they are to influence a real drilling situation. Chapter *6.4* suggest further work to be conducted in the MPD heave lab.

6.1 Discussion of Hydraulic Models

6.1.1 Discussion of Empirical Model

Chapter *4* present two different hydraulic models, which both aims to estimate BHP. BHP estimation is in both cases based on heave motion characteristics, flowrate from the backpressure pump, pressure downstream the choke and choke characteristics. The empirical model presented in chapter *4.5* introduces a fairly simple relationship for surface flow, surface pressure and BHP. This model may be used as a hydraulic model to reduce BHP fluctuations in the heave lab. However; it will not be able to maintain CBHP, as the empirical model is not a perfect match to the observed data. The empirical model diverse with 1.46*bar* from observed data, when the BHA string is oscillated with a period of $T_{string} = 5sec$. The discrepancy between the empirical model and observed data equates to approximately 25% of the total pressure fluctuation downhole. Assuming no other sources of error, same accuracy would reduce downhole pressure fluctuation from 300*psi* to 75*psi* in a real drilling operation. In most scenarios would this pressure fluctuation reduction be sufficient for a successful drilling operation, but it requires no other sources of error which is unrealistic. There are several sources or error subjected to an MPD heave compensation operation, this is further discussed in chapter *6.3*. The empirical model is fairly simple to implement, but the model is limited to sinusoidal BHA oscillation only and it is difficult to analyse how different parameters influence the BHP.

6.1.2 Discussion of Numerical Model

Chapter *4.1* through *4.4* derive and presents a 2. hydraulic model which is based on fluid dynamical principles and parameters discussed in chapter *3*. This model is also only valid for sinusoidal BHA oscillation, but it is based on physical parameters which may be analysed. This hydraulic model calculates both flow and pressure throughout the copper

pipe, at surface and in the well. The model is based on the same input parameters as the empirical model discussed above in addition to parameters presented in chapter *3*, such as: friction factor, compressibility and time delay due to pressure propagation. The compressibility factor is used to calculate flowrate through the copper pipe, whilst the friction factor and time delay due to pressure propagation is used to calculate the pressure drop through the copper pipe. There are several limitations in this hydraulic model, which is obvious in simulation results presented in chapter *5.1*. Chapter *4.2* presents how flowrate throughout the copper pipe may be calculated based on compressibility and pressure. The flowrate appears to be further delayed through the copper pipe than calculated. The large Womersley number present in our experiments indicate the flowrate to be influenced by unsteady laminar flow, which likely cause the additional time delay. The hydraulic model accounts for this additional time delay by phase shifting the copper pipe flowrate, but this phase shift is dependent on empirical observation which is an obvious shortcoming in the hydraulic model.

Chapter *3.3* and *3.4* presents friction factor and time delay due to pressure propagation, which are used in chapter *4.4* to derive a pressure model. The pressure drop through the copper pipe is caused by both fluid acceleration and velocity. Acceleration and velocity is by definition phase shifted with $\frac{\pi}{2}$ radians for a sinusoidal flowrate profile. It is important that the pressure contribution from each term is accurate, if not will the pressure profile be wrong in terms of both magnitude and phase (further discussed in chapter *6.2.3*). The hydraulic model assumes the frictional pressure drop to be based on instantaneous fluid velocity only, which is wrong as the fluid acceleration influence the frictional pressure drop (further discussed in chapter *6.2.3*). This assumption results in wrong pressure calculations. The numerical model which is solved iteratively fails to converge due to the phase shift of calculated pressure. Graphs below presents calculated flow and pressure from the Matlab Script, graphs *6.1*, *6.2* and *6.3* illustrate how pressure and flow change for each iteration round.

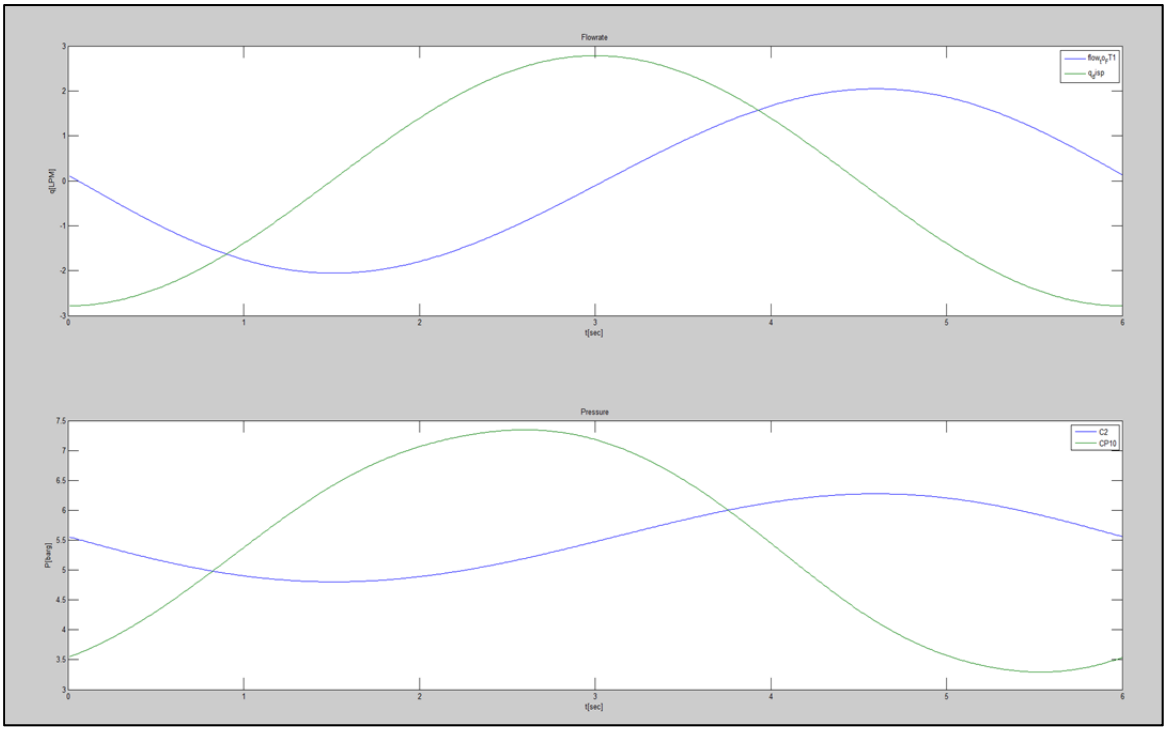

Graph (6.1); Pressure and flow calculations for 1 iteration round. The upper graph represent flowrate, where green line is displaced flowrate in the well and blue line is flowrate at surface displaced through the copper pipe. The lower graph represent pressure, where green line is the pressure at CP10 and blue line is the pressure upstream the choke C2.

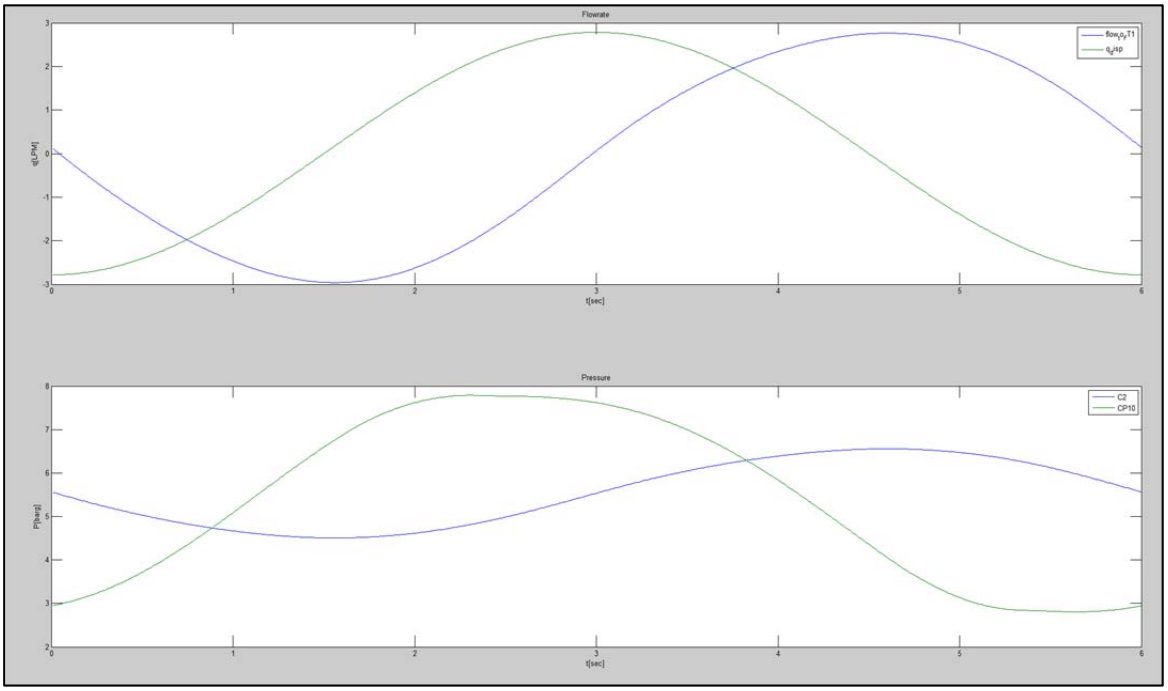

Graph(6.2); Pressure and flow calculations for 2 iteration rounds. The upper graph represent flowrate, where green line is displaced flowrate in the well and blue line is flowrate at surface displaced through the copper pipe. The lower graph represent pressure, where green line is the pressure at CP10 and blue line is the pressure upstream the choke C2.

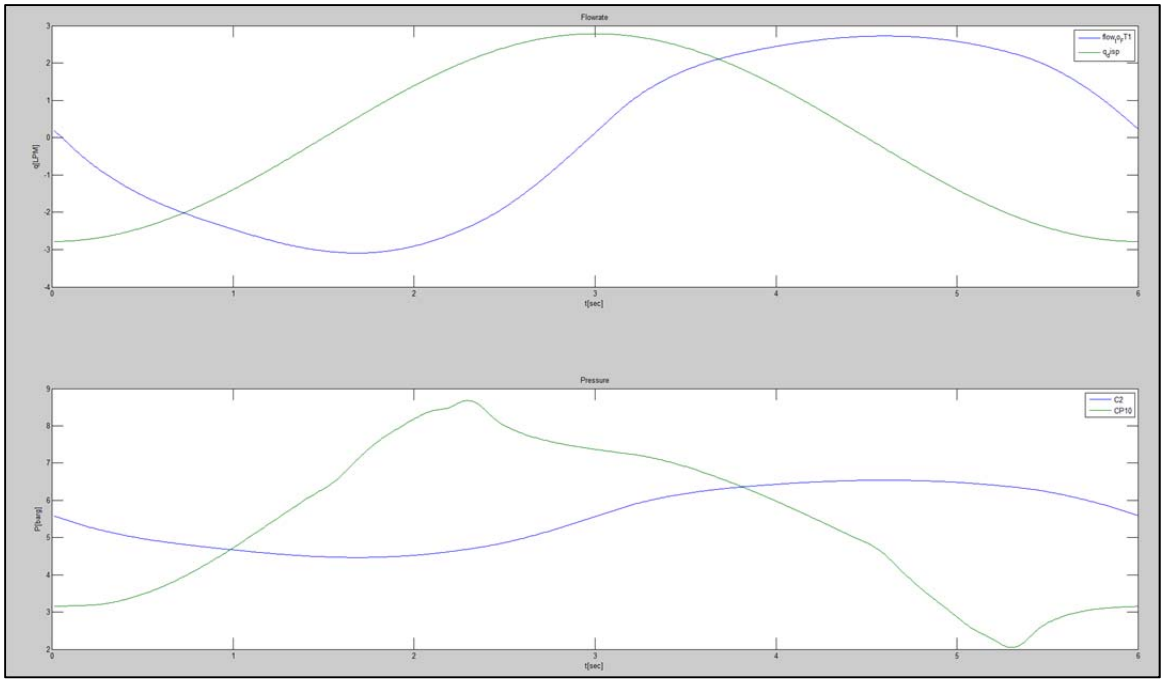

Graph(6.3); Pressure and flow calculations for 3 iteration rounds. The upper graph represent flowrate, where green line is displaced flowrate in the well and blue line is flowrate at surface displaced through the copper pipe. The lower graph represent pressure, where green line is the pressure at CP10 and blue line is the pressure upstream the choke C2.

Graphs *6.1*, *6.2* and *6.3* above illustrate that the iterative model does not converge. However; this model is used to further analyse the fluid dynamics present in our system and highlight important modelling challenges for a real case MPD Heave Compensation operation.

6.2 Discussion of Results

6.2.1 Discussion of Flowrate

One of the variables that are presented in chapter *5.1* is the fluid flowrate. The displaced flowrate in the well is calculated from equation *4.2.1*, the displaced volume flows through the copper pipe and is measured at surface after a certain time delay. The calculated displaced flowrate in the well coincide with measured flowrate for all experiments presented in chapter *5.1*. However; there is a source of error within the measured flowrate in the well. The measured flowrate is based on the string velocity measurement, which displaces the fluid volume. There are uncertainties associated with the upper and lower rod diameters, which introduces an uncertainty regarding the displaced flowrate. A downhole flow measurement would be preferred to evaluate the

flowrate, but *FT4* still remains to be installed. The upper and lower rod diameters have been measured in detail, and found to be very close to 25*mm* and 22*mm*. There are therefore very small uncertainties associated with the measured displaced flowrate in the well. Results presented of measured displaced flowrate seem to contain large amounts of signal noise. The string velocity is calculated from the derivative of string position. Derivation always amplifies signal noise, and therefore causes the flowrate peaks to appear like heavy noise.

FT1 is installed just upstream the choke and is an important measurement to calculate pressure upstream the choke. Chapter *4.2* presents a method of how to calculate flowrate throughout the copper pipe. This calculation approach is based on a known pressure profile, which is solved by iteratively calculate both pressure and flow. Results found in chapter *5.1* are obtained by only one iteration round due to iteration divergence. The calculated *FT1* values presented in chapter *5.1* are therefore based on the initial pressure guess (ref: graph *4.10*), which is slightly incorrect for most experiments. The initial pressure guess is close to actual pressure for $T_{string} \geq 9sec$, this appears also clear when comparing measured and calculated flowrate. The calculated value of *FT1* is fairly close to the measured value of *FT1* for $T_{string} \geq 9sec$, but there is a huge discrepancy for $T_{string} = 5sec$. For $T_{string} = 5sec$ is the calculated maximum value of *FT1* equal to 2*LPM*, whilst the measured maximum value approaches 4*LPM.* In addition to the iteration problem encountered, does the measured value of *FT1* exceed the calculate value of *FT1* independent of oscillation period T_{string}. This is likely caused by the compressibility assumptions made in chapter *4.2*, where it was chosen to use the system compressibility factor rather than copper pipe compressibility factor and thereby neglecting the volumetric effect of the rubber hoses. This would be a correct assumption if the pressure variation was constant throughout the entire system. However; in our system is the pressure variation largest closest to the well, where a 3.55*m* long rubber hose is connecting the well and the copper pipe. This highly expandable rubber hose section will accumulate and release fluid, especially for higher pressure variations. The later issue would be reduced by installing new lesser flexible rubber hoses.

Flow calculations presented in chapter *5.1* have been phase shifted to match measured data. This calculations approach is an obvious shortcoming in the numerical model, this have already been discussed in the previous chapter. A possible explanation for the additional time delay is presented in sub-chapter *4.2.2.* Modelling of additional time delay induced by unsteady laminar flow has not been conducted in this thesis, and is left as further work.

6.2.2 Discussion of Choked Flow

The choke installed at surface is an important component in any CBHP MPD operation, as this component is installed to physically adjust surface pressure which again determines BHP. Surface pressure depends on flowrate through the choke, pressure downstream the choke and choke opening. Flowrate through the choke consists of flowrate from the pump and flowrate displaced from the well (*FT1* measurement). Flowrate from the pump was discussed in chapter *4.1.2*, and is assumed to be constant. The calculated value of *FT1* presented in chapter *5.1* was discussed in previous chapter. The discrepancy between calculated and measured *FT1* values for $T_{string} < 9sec$ affects the calculated *C2* value, as calculated *C2* value is based on calculated *FT1* value. Graph 5.30 clearly illustrate that the calculated *C2* value vary less than measured *C2* value.

Experiments presented in chapter *5.1* are performed with a 50*deg* choke opening. The choke characteristic for a 50*deg* choke opening was evaluated just prior to experiments execution. Choke evaluation result is found in chapter *4.3.1*, where a K_v value of 0.70 is calculated. However; results presented in chapter *5.1* are based on a K_v value of 0.74, which is found from curve matching. Graph *6.4* below compares measured *C2* and calculated *C2* based on $K_v = 0.7$ for $T_{string} = 9sec$. Graph *6.4* illustrate that the calculated *C2* value exceed the measured *C2* value with approximately 0.6*bar* for the entire period. This was also the case for all other experiments presented in chapter *5.1*. There are several reasons that might have caused the mismatch between the K_v values. The initial experiment presented in chapter *4.3.1* is subjected to uncertainty. Both flow and pressure were measured to evaluate the choke

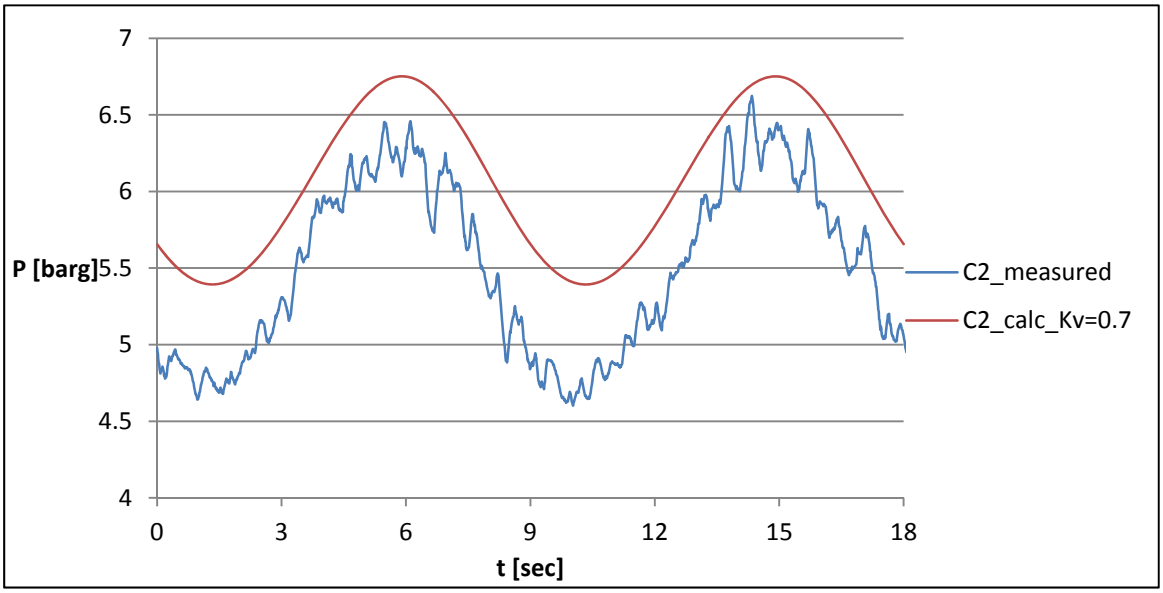

Graph(6.4); Measured and calculated C2 based on $K_v = 0.70$ for $T_{string} = 9sec$.

characteristic, these measurements contain a certain uncertainty which again affects the choke characteristic calculation. The pressure sensor is accurate within 0.1*bar* and the

flow sensor is accurate within 1% of maximum flow which is 100*LPM*. The calculation uncertainty associated with uncertain input parameters may be calculated from the law of Gaussian error propagation. Given an uncertainty of 0.1*bar* for pressure measurements and 1*LPM* for flow measurement, uncertainty associated with K_v equates to 0.027 (detailed calculation found in Appendix B). Choke characteristics evaluation presented in chapter *4.3.1* was performed over a 45*sec* interval. An average value was used to calculate the choke characterization parameter, which should eliminate error caused by natural variation within the measurement device. A more likely explanation for the choke characterization parameter deviation is uncertainty regarding the choke repeatability. After performing the initial choke characteristic evaluation for a 50*deg* choke opening was the choke opening changed to 90*deg*, before it again was adjusted back to 50*deg* to execute experiments found in chapter *5.1*. There is a possibility that the choke never reached the exact same position as it had initially. Challenges regarding choke repeatability introduce an important concept. In any MPD operation may the choke opening be initially calculated based on a K_v value concept, but it is important to measure the actual choke pressure and adjust for model discrepancy.

6.2.3 Discussion of Copper Pipe Pressure

The surface choke is the boundary condition for copper pipe pressure. An important factor that needs to be addressed when modelling copper pressure is the effect of time delay. Chapter *6.2.1* discussed how flowrate is delayed through the copper pipe, graph *5.29* illustrate that surface flowrate flow the well is still negative when flowrate in the well reaches its maximum. The non-uniform flow profile through the copper pipe imposes an important aspect to pressure drop; pressure drop depends on both position and time. A numerical approach have been used to calculate pressure drop through the copper pipe, this is presented in chapter *4.3*.

Chapter *6.1.2* briefly introduce modelling challenges for pressure drop through the copper pipe. Pressure drop depends on both fluid acceleration and velocity, which are by definition phase shifted by $\frac{\pi}{2}$ radians for a sinusoidal flow profile. Total pressure drop is the sum of frictional pressure drop and pressure required to accelerate the fluid, if one of these terms are incorrect will the total pressure drop be wrong in terms of both magnitude and phase. Graph *6.5* below illustrate how an incorrect frictional pressure drop phase shifts the total pressure drop through a 1*m* long tubing section when $T_{string} = 9sec$.

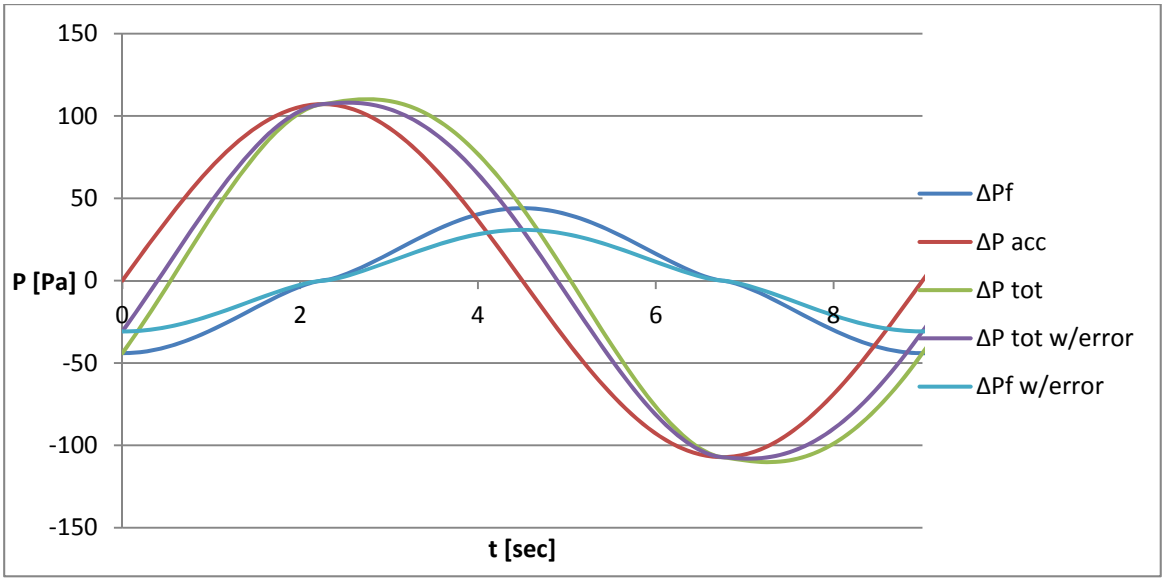

Graph(6.5); phase shift of total pressure drop through a 1m long tubing section for $T_{string} = 9sec$.

Graph *6.5* illustrate how the total pressure drop is shifted to left when the frictional pressure drop is estimated to be lesser than what it really is. All *CP10* results presented in chapter *5.1* are more or less wrong in terms of both magnitude and phase. The discrepancy in terms of magnitude is partly caused by an incorrect flowrate, previously discussed in chapter *6.2.1*. Graph *6.6* below presents *CP10* as presented in chapter *5.1* and *CP10* calculated from a correct flowrate for $T_{string} = 9sec$. The correct flowrate has been obtained by data matching.

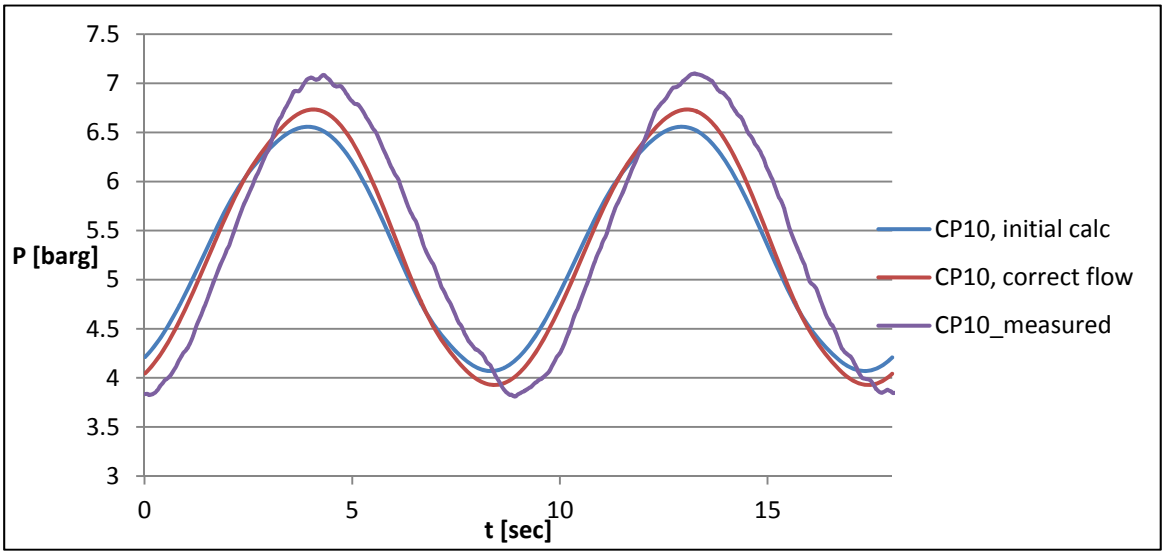

Graph(6.6); CP10 as presented in chapter 5.1, measured CP10 and CP10 based on correct flow for $T_{string} = 9sec$.

Graph *6.6* shows that the *CP10* calculation improves when correcting the flowrate. However; the calculated pressure is still shifted left compared to the measured pressure. Graph *6.5* illustrate how the total pressure is shifted to left when a too low frictional

pressure drop is used, it is likely that the frictional pressure drop is too low for all results presented in chapter *5.1*. The frictional pressure drop through the coiled copper pipe was carefully investigated in chapter *3.3*. The friction factor measured in the lab was found to be very close to correlations by White, C.M and Ito, H. Furthermore was a simplified friction factor correlation derived that is valid for both laminar and turbulent flow. The numerical model calculates frictional pressure drop based on instantaneous velocity, which seems to be a shortcoming in the model.

Wall shear stress which is proportional to the frictional pressure drop depends on initial Reynolds number and rate of acceleration for accelerating turbulent flow (He, S. et. Al 2011). Experimental comparison of steady wall shear stress providing quasi steady curves with unsteady wall shear stress has shown a significant effect of fluid acceleration to wall shear stress. The unsteady wall shear stress development may be divided into 3 different stages. Experimental results presented by He,S. et. al shows that stage 1 (acceleration start) which extends up to a Reynolds number of 125 000 depends primarily on fluid inertia. In stage 1 is the unsteady wall shear stress found to initially exceed the quasi steady value, before it again undershoots the quasi steady value. For results presented in chapter *5.1* is the flow laminar, transitional and turbulent. Similar to experiment results by He, S. et. Al is it likely that the effect of fluid inertia in the heave lab cause the unsteady wall shear stress to exceed the quasi steady wall shear stress (instantaneous velocity wall shear stress) for turbulent flow and partly transitional flow. This would explain why measured pressure drop through the copper pipe exceed the calculated pressure drop.

6.2.4 Discussion of BHP

Pressure drop over the BHA is found to be determined by string velocity and the effect of clinging is an important factor for pressure drop over the BHA (Boge, A 2012). The relative short well in the MPD heave lab simplifies pressure calculations in the well compared to copper pipe calculations. The displaced flowrate within the well is independent of position, and a numerical model is therefore not needed to calculate pressure drop over the BHA. Furthermore is an empirical correlation found in chapter *4.3.2* to estimate pressure loss through the connection point; well – copper pipe. This correlation is also independent of position. Estimation of *P1* and *P2* is not part of the iterative process presented in chapter *4.4 P1* and *P2* are simply added to *CP10* after the iteration process.

Calculation error for pressure drop over the BHA is relative small, illustrated in graph *6.7* (adapted from: “MPD Heave Lab: Experimental Work and Modelling of Surge and Swab Effects” by Boge, A 2012).

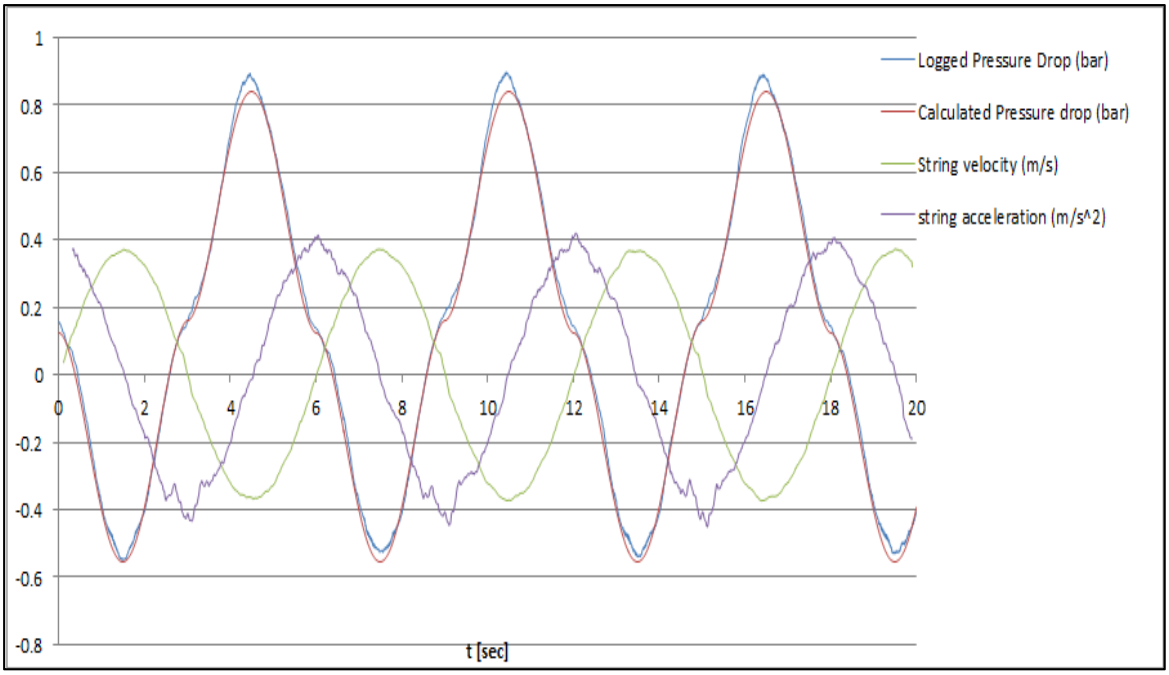

Graph (6.7); String velocity, string acceleration, logged pressure drop and calculated pressure drop,T=6sec.

Logged pressure drop presented above is found from the difference between *P1* and *P2*. The calculated value coincide with the measured value, the same pressure drop formula is used to calculate BHP presented in chapter *5.1*. BHP results presented in chapter *5.1* illustrate significant deviation between measured and calculated BHP. This deviation is mostly caused by calculation error associated with copper pipe pressure discussed in previous chapter.

6.2.5 Discussion of CBHP Simulations

Chapter *5.2* presents CBHP simulations based on the empirical model found in chapter *4.5*. Simulations presents how the BHP would fluctuate for a constant choke angle, and how the choke angle is required to change to maintain CBHP. The choke angle needs to be adjusted prior to the actual pressure change downhole as it takes time for the pressure wave to propagate through the copper pipe. Scenario 2 simulations illustrate how the choke angle is adjusted 0.81*sec* prior to the pressure change found in scenario 1 simulations. The empirical model has not been used as an active controller in the MPD heave lab, CBHP simulations are therefore not compared to lab results.

There are several factors that may affect a controller using this hydraulic model. First of all is this hydraulic model not a perfect match to measured data, largest discrepancy between measured BHP and calculated BHP equates to 1.46*bar.* The empirical model is matched and found for a given dynamic system, by introducing an automatic controlled

choke system will the boundary condition change. The automatic operated choke will now create an additional pressure wave propagating in the opposite direction of the BHA induced pressure wave. The flowrate from the pump *FT2* is assumed constant for all experiments and calculations performed with a fixed choke angle. By introducing an automatic controlled choke will the surface pressure fluctuate quite heavier, this is again expected to affect flowrate from the pump making it less stable.

A linear controller has been implemented and tested in the heave lab, the controller has been evaluated for various BHA frequencies. BHP fluctuation was successfully reduced from $\pm 1.5bar$ to $\pm 0.5bar$ for a 10*sec* string period and reduced from $\pm 1.75bar$ to $\pm 1bar$ for a 3*sec* string period. Graph *6.8* below (adapted from "Disturbance Attenuation in Managed Pressure Drilling" by A. Albert 2013)illustrates BHP fluctuation with an without an active controller for a 10*sec* string period.

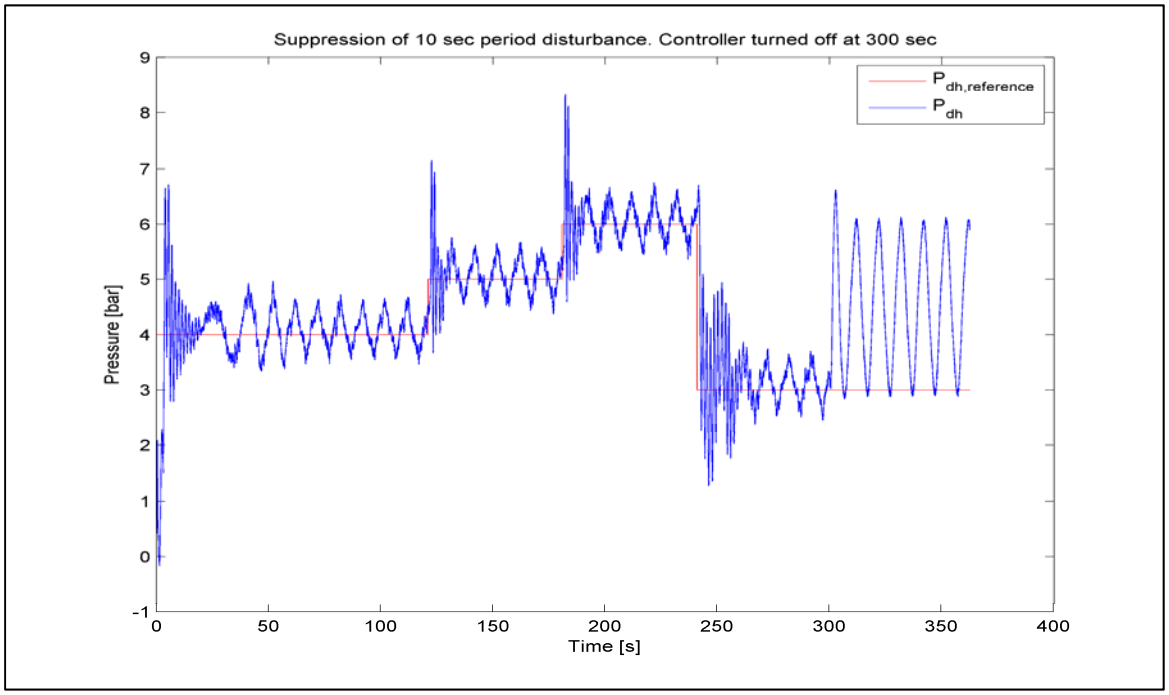

Graph(6.8); BHP with and without an active controller, $T_{string} = 10sec.$

6.2.6 Sources of Error

Previous chapters present several sources of error in terms of calculation procedures. The largest source of error is assumed to be the friction factor for the numerical model. Underestimating the frictional pressure drop through the copper pipe cause the numerical model to diverge, which again cause inaccurate flow modelling. The empirical model is not a perfect match to measured data and is therefore an obvious source of error. In addition to these calculation errors are there uncertainties associated with input parameters and the actual lab measurements.

There are several input parameters estimating the BHP, especially for the numerical model. Chapter *6.2.1* presents a source of error regarding the displaced flowrate in the

well. The displaced flowrate in the well is based on string velocity and upper and lower rod diameters. Upper and lower rod diameters have been measured and found to be close to 25*mm* and 22*mm* respectively, but there are uncertainties associated with these values. It is recommended to install a flowmeter *(FT4)* to measure the displaced flowrate in the well, but as of June 2013 has this flowmeter not been returned from the manufacturer. Installing a flowmeter to measure displaced flow in the well would reduce the uncertainty associated with this measurement. Length and diameter of the copper pipe are important parameters to evaluate pressure drop through the copper pipe. The nominal diameter of the copper pipe equates to 16mm, and is assumed correct. Copper pipe length has been measured by counting number of windings and coil circumferences. Number of windings was counted several times and is found to be 133, while the coil circumference approximates 677*cm*. A representative coil circumference was measured, but each coil winding vary slightly from the next one. Picture *6.1* below is a picture of the actual MPD heave lab copper pipe, it illustrates how each coil winding differ from the other. The copper pipe and well was drained and measured to evaluate diameters and lengths. This is discussed in chapter *3.1.1* where a difference of only 1.1% is found between measured and calculated system volume.

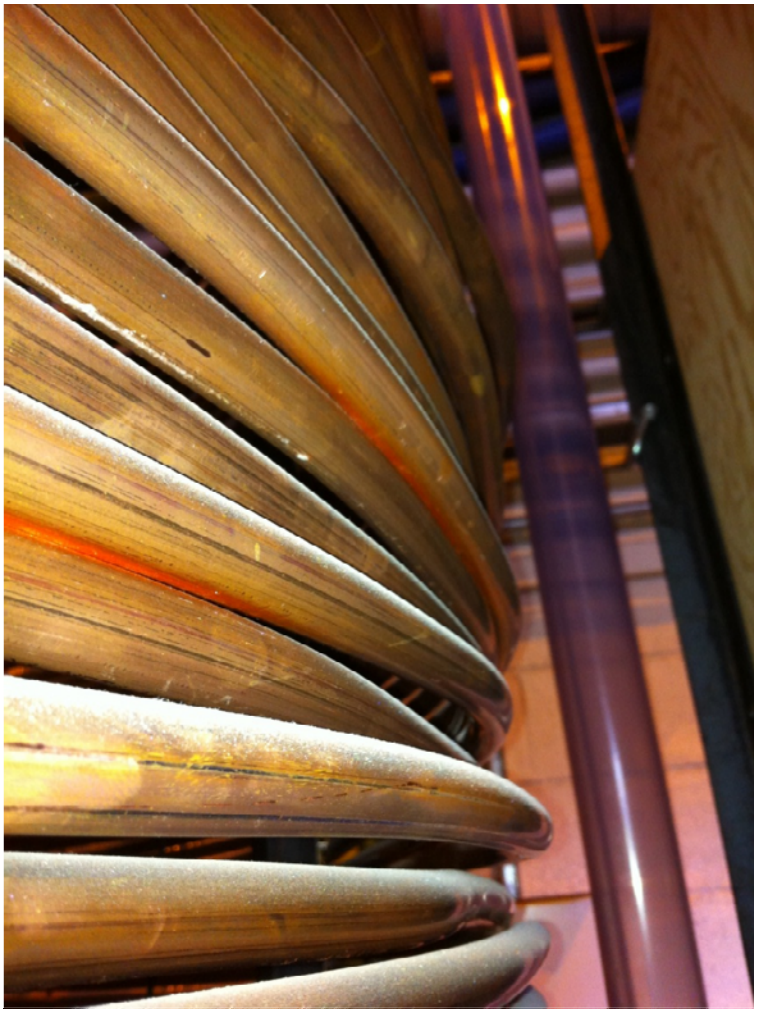

Picture 6.1; non-uniform copper pipe circumference.

Several input parameters such as compressibility, friction factor, choke characteristics and time delay due to pressure propagation are estimated from measured values. There are factors that influence the accuracy of these values and the actual results presented in chapter 5. Experimental sources of error may be divided into 3 groups; personal careless error, systematic error and random error.

Personal careless error is due to experimenter “sloppiness”, most experiments performed in the MPD heave lab is controlled by the computer and digital measured. These experiments are subjected to low personal careless error. However, experiments such as compressibility determination introduce the human factor. The amount of water drained from the system in this experiment is subjected to risk in terms of spilling. Sufficient circulation prior to experiment execution is another source of error caused by personal careless error. It is important that all air bubbles are circulated out of the system before conducting any experiment. Presence of air bubbles will have a significant effect on compressibility.

Systematic error is caused by such as poorly calibrated instruments and uncertainty that is inherent in the measurement device. Chapter *3.1.2* and *3.1.3* present calibration of pressure sensors and flowmeters respectively. Systematic error has been reduced by calibrating all sensors. However; systematic error would be further reduced if sensors were periodically calibrated.

Most measurement errors within the MPD heave lab are random error or unsystematic error. Random error is caused by natural variation in the measurement and variation in experimental condition. The electrical signal transmitted from the measurement device is affected by background noise, this will cause the sensor to vary over time. The actual sensor accuracy is also an obvious random error. The pressure sensors are accurate within 0.1*bar* and the flowmeters are accurate within 1% of the upper measurement limit. Random error is reduced by repeated measurements. Parameters presented in chapter 3 are estimated based on several measurements to reduce the random error.

6.3 Discussion of A real case MPD Heave Compensation Operation

6.3.1 Discussion of Input Parameters

Chapter *6.2* discusses several parameters essential for a successful MPD Heave compensation operation, such as: fluid properties, type of flow and hydraulic friction factor. Fluid compressibility was investigated and measured in the MPD heave lab, in a real drilling operation is it more difficult to get accurate wellbore compressibility data. The effective compressibility factor in the MPD heave lab was found to be approximately four times the value of water, this is due to copper pipe expansion. In a real drilling operation are there several factors that will influence the effective compressibility, such as: pressure, temperature, formation bulk modulus, influx of and loss of fluids. Fluid compressibility is an important factor for the actual fluid flow through the annulus and speed of sound through the fluid. The bottom hole compressibility factor may be estimated by use of MWD tools, but compressibility through the well needs to be estimated. Unsteady laminar flow and flow inertia is assumed to cause an additional flow delay through the MPD heave lab copper pipe. Womersley number was calculated to evaluate the flow profile within the copper pipe. Womersley number is only valid for a Newtonian fluid, and can therefore not be used for a real drilling fluid as most drilling fluids are non-Newtonian. However; it is important to evaluate the actual drilling fluid flow characteristics, as drilling fluids also may be subjected to modelling challenges such as fluid inertia.

Common drilling practice is to estimate the hydraulic friction factor in the annulus throughout the drilling operation. In presence of a downhole pressure device may this hydraulic friction factor be estimated rather accurate. The quasi steady friction factor was used to estimate the frictional pressure drop through the copper pipe in the MPD heave lab. This friction factor was obtained from lab experiments, but proves to be insufficient for fixed choke heave experiments. The presence of unsteady wall shear stress is likely to be a challenge also for a real drilling operation. Even though models may predict the unsteady wall shear stress, will it be difficult to apply such models to a drilling environment where parameters such as geometry and formations properties are relatively unknown.

6.3.2 Discussion of Modelling Approach

There are primarily two different methods of how to estimate the change in downhole pressure due to heave motion. The pressure change may be estimated based on either predicting pipe movement or measuring topside flow and pressure. There are several challenges and limitations subjected to both approaches. Models presented in this thesis estimates downhole pressure based on pipe movement. Pipe movement is a given input for all experiments performed in the MPD heave lab, pipe movement is therefore predictable for the next time period. In a real drilling environment performed

from a floating rig subjected to heave motion is pipe movement a rather difficult phenomena. There are several parameters influencing pipe movement such as: length of pipe, material properties of the drillstring and frictional drag along the string. Graph *6.9* below illustrate drillbit heave response to rig heave excitation for a given drag coefficient, ROA is the relation between drillbit amplitude and rig amplitude.

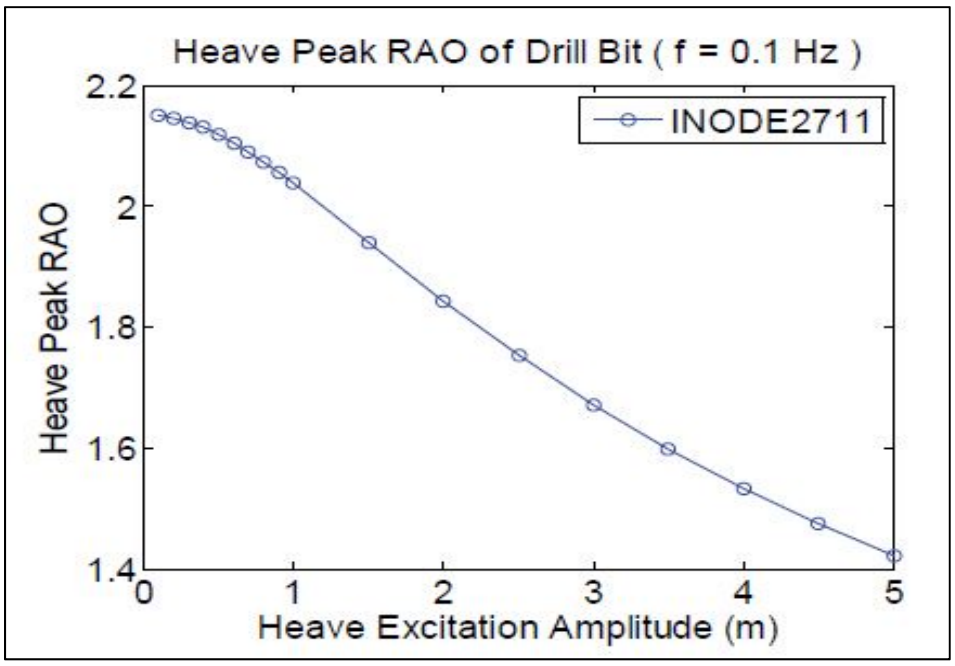

Graph(6.9); Drillbit heave response to rig heave excitation (Huang, L. et. Al 2011).

Graph *6.9* illustrate that even the rig heave excitation amplitude has a huge impact on the drillbit heave response. Furthermore is it required to predict the drillstring heave excitation before the actual movement, as the surface pressure needs to be controlled prior to the actual downhole pressure change. A buoy located 500-1000*m* from the floating rig is an alternative to measure wave amplitude and period affecting the rig for the next period. A hydraulic model based on pipe movement is associated with several uncertainties. Rig heave needs to be predicted for the next period, drillbit heave response needs to be estimated before pressure change is calculated based on input parameters discussed above.

A somehow simpler approach is to utilize topside pressure and flow measurements to reduce downhole pressure fluctuation. Chapter *6.2.1* discuss how displaced fluid flows through the copper pipe and eventually is measured at surface. Table *4.1* lists time delay from displacement downhole until flow is observed at surface. Table *4.1* shows that it takes approximately 1.6*sec* before flowrate and pressure change is observed at surface. For a 4000*m* MD long well would it take approximately 6.4*sec* from pipe movement until flow and pressure change is registered at surface, when assuming all other properties equal. In addition to this flow delay, will it take an additional $\frac{4000m}{1400^{m}/_{s}} = 2.85sec$ before any pressure change at surface is registered dowhole due to time delay caused by pressure propagation (assuming speed of sound= $1400\,^{m}/_{s}$ in the drilling fluid). Total

time from pressure change downhole until corrective action is registed equates to 9.25sec. It takes one fourth of a period before pressure change has gone from zero to its maximum. If the heave period is lesser than $9.25 \times 4 = 37sec$ is it pointless to do any corrective actions, as maximum pressure fluctuation is already reached. MPD heave compensation based on surface readings is therefore only an option for longer heave periods.

6.3.3 Downhole pressure monitoring

The model approach used in this thesis is based on pipe movement. Previous chapter presents and discusses several challenges and uncertainties associated with such a model approach. Recent technology provides real time downhole pressure monitoring through a fibre optical cable. The Intelliserv Network by NOV provides transmission rates up to 57 600 bits per second, which is outstanding compared to conventional mud pulse telemetry with a general throughput of 16-24 bits per second. This technology makes it possible to monitor, calibrate hydraulic model to match actual pressure and control surface pressure directly from BHP. Similar to surface reading model discussed above are there some restrains by controlling surface directly from BHP. The implied pressure change will lag approximately 3sec behind the actual downhole pressure change. For rapidly changing pipe position will such model be insufficient. The advantage of being able to calibrate the hydraulic model by use of downhole pressure device is huge when weather is stable. By aid of downhole pressure monitoring is it possible to assure an acceptable downhole pressure variation before drilling through weak layers. However; if weather is changing more rapidly is it difficult to adapt the hydraulic model to each heave situation. If the hydraulic model were to fail when drilling through a layer with narrow pressure limits is well failure and collapse likely.

6.4 Further Work

As of june 2013 have the entire MPD heave lab been tested. All pressure and flowsensors are intact and successfully tested except *FT4* which has currently not been installed. Installation and testing of *FT4* is left as further work. This thesis presents a numerical model for flow and pressure. This model deviates slightly from measured data, suggested explanations are discussed such as; unsteady laminar flow and unsteady wall shear stress. These effects have not been quantitatively analysed, and is left as further work.

The empirical model presented in this thesis has not been implemented in the MPD heave lab to automatically control the choke opening. It is left as further work to implement this non-linear model and identify the accuracy of the model.

Both models presented in this thesis are based on string motion. Chapter *6.3.2* discuss a second model approach based on surface readings. Such a model approach may also be implemented and tested in the heave lab. Derivation of this model is left as further work.

Independent of which automatic controller is used in MPD heave lab; is a counteracting pressure wave created at surface propagating to the well. This pressure wave aims to maintain CBHP, however; large pressure variations are expected further up through the copper pipe. It is left as further work to investigate pressure variations in the copper pipe while running the system with an automatic controller. This is important in a real drilling situation if large pressure variations are found where the wellbore is not sealed off by casing.

The BHA string was initially designed to move with a period of $T_{string} = 3sec$, experiments presented in this thesis are not performed with any period lower than $T_{string} = 5sec$, as pressure became too high. The lower rod currently installed holds an OD of 22mm. This lower rod OD needs to be bigger to perform any heave experiments with a period of $T_{string} = 3sec$ and $A_{string} = 0.4m$.

Conclusion

Chapter *3* presents three important system parameters; compressibility, copper pipe friction factor and time delay due to pressure propagation.

- Water is usually assumed incompressible, in our system was effective fluid compressibility found to be approximately four times bigger than water compressibility. The compressibility magnitude has a significant impact on flow through the copper pipe.
- Copper pipe friction factor is obtained through several steady flow experiments. Measured friction factor coincide with coiled pipe friction factor correlation given by White, C. M. and Ito, H.
- Time required for a pressure pulse to propagate through the copper pipe is fairly constant.

A numerical model has been developed to evaluate pressure and flow in the MPD heave lab. Fixed choke opening experiments presented in chapter *5.1* shows that the numerical model fails to accurately calculate BHP.

- Womersley number evaluation of the copper pipe indicates presence of unsteady laminar flow. Fluid inertia cause fluid flow to lag behind the applied pressure which cause an additional time delay.
- Frictional pressure loss is based on instantaneous fluid velocity in the numerical model. Experimental results from He, S. et. Al 2011 illustrates a significant difference between wall shear stress for accelerating flow and its quasi steady form. This modelling shortcoming cause calculated BHP to fluctuate lesser than measured BHP.

A non-linear model is presented in this thesis, this model is derived from curve matching. The non-linear model has not been implemented and tested in the heave lab. However; a linear controller has been tested in the MPD heave lab, this controller has successfully reduced BHP fluctuation with 46-64% depending on the BHA frequency (Albert, A 2013).

There are several uncertainties associated with a real case MPD heave compensation operation. A hydraulic model based on string movements needs to predict next period heave motion and responding drillbit excitation. Furthermore is it difficult to get accurate along wellbore parameters, such as; unsteady hydraulic friction factor, fluid compressibility and speed of sound through the fluid. It is advisable to perform MPD heave compensation operations with wired drillpipe enabling real-time BHP readings.

Nomenclature

ΔA_{ur-lr}	Differential cross-sectional area between upper rod and lower rod, m^2
Δh	Vertical height difference, *m*
Δh_{P2-CPi}	Height difference between P2 and i'*th* pressure sensor, *m*
ΔP_{acc}	Pressure difference due to fluid acceleration, *Pa*
ΔP_{hyd}	Hydrostatic pressure difference, *Pa*
ΔP_L	Frictional pressure loss, *Pa*
ΔP_w	Pressure drop over BHA, *Pa*
Δt_{flow}	Delay of flow through copper pipe, *sec*
$\Delta t_{p-prop,cv}$	Pressure pulse propagating time through CV, *sec*
Δt_{step}	Calculation time step, *sec*
α	Womersley number
α_{cp}	Copper pipe expansion factor, $^{m^3}/_{m\ Pa}$
ε	Equivalent roughness value
ε_{error}	Absolute error
η_t	Total pump efficiency
ρ	Fluid density, $^{kg}/_{m^3}$
τ	Fluid shear stress, *Pa*
μ	Fluid viscosity, *Pa s*
ν	Kinematic viscosity, $^{m^2}/_{s}$
ω	Angular frequency, s^{-1}
a	Speed of sound
a_f	Fluid acceleration, $^{m}/_{s^2}$
a_{string}	String acceleration, $^{m}/_{s^2}$
A_{string}	String amplitude, *m*
BHA	Bottom hole assembly
BHP	Bottom hole pressure
CBHP	Constant bottom hole pressure
$c_{f,cp}$	Effective fluid compressibility in copper pipe, $^{1}/_{Pa}$
$c_{f,hose}$	Effective fluid compressibility in rubber hose, $^{1}/_{Pa}$
$c_{f,system}$	Effective fluid compressibility for system, $^{1}/_{Pa}$
c_w	Compressibility of water, $^{1}/_{Pa}$
D_{cp}	Copper pipe inner diameter, *m*
D_{hose}	Rubber hose diameter, *m*
D_{lr}	Lower rod diameter, *m*
D_{ur}	Upper rod diameter, *m*
DG	Dual gradient
E_{string}	String equilibrium, *m*
f	Darcy-Weisbach friction factor
f_{CL}	Darcy-Weisbach friction factor for coiled laminar flow
f_{CT}	Darcy-Weisbach friction factor for coiled turbulent flow
f_{emp}	Empirical friction factor

f_{SL}	Darcy-Weisbach friction factor for straight laminar flow
f_{ST}	Darcy-Weisbach friction factor for straight turbulent flow
g	Gravitational acceleration, $^{m}/_{s^2}$
h_{ground}	Height from ground level, *m*
ID	Inner diameter
K_v	Choke characteristic parameter
L_{cp}	Copper pipe length, *m*
L_{cv}	Length of control volume
L_{hose}	Rubber hose length, *m*
MPD	Managed Pressure Drilling
NPT	Non productive time
N_{De}	Dean number
OD	Outer diameter
P	Undefind pressure, *Pa*
P_{pump}	Pump effect, *w*
PMCD	Pressurized mud-cap drilling
PVC	Polyvinyl chloride
q_{disp}	Displaced flowrate, $^{m^3}/_{s}$
R_c	Coil radius, *m*
R_{cp}	Radius of copper pipe, *m*
Re	Reynolds number
SD	Standard deviation
T_{string}	BHA string period, *sec*
U	Voltage, *volt*
v_f	Fluid velocity, $^{m}/_{s}$
v_{hose}	Fluid velocity through rubber hose, $^{m}/_{sec}$
v_{string}	String velocity, $^{m}/_{s}$
V_{cp}	Copper pipe volume, m^3
V_{hose}	Rubber hose volume, m^3
x_{cp}	Copper pipe fractional volume
x_{hose}	Rubber hose fractional volume
z_{string}	String position, *m*

References

Ahlbrandt, T. S., and P. J. McCabe (2002). http://www.geotimes.org/nov02/feature_oil.html

Becker, C. L. (2012). http://www.dn.no/forsiden/borsMarked/article2474855.ece

Brooks, A. G. (1982). Swab and Surge Pressures in Non-Newtonian fluids. SPE.

Boge, A. (2012). MPD Heave Lab: Experimental Work and Modelling of Surge and Swab Effects.

Bourgoyne, A. T., M. E. Chenevert, K. K. Millheim, and J. F. S. Young (1986). Applied Drilling Engineering. SPE Textbook Series, Vol 2.

Burkhardt J. A. (1961). Wellbore Pressure Surges Produced by Pipe Movement. SPE.

Cardwell, W. T. Pressure Changes in Drilling Wells Caused by Pipe Movement.

Caro, C. G., T. J. Pedley, R. C. Schroter, W. A. Seed and K. H. parker (2013) The Mechanics of the Circulation. Cambridge University Press

Cengel, Y. A., and J.M. Cimbala (2010). Fluid Mechanics, Fundamentals and Applications. Seconds Edition in SI UNITS. Mc Graw Hill Higher Education.

Gjenghseth, C (2012). Lab for heave motion during managed pressure drilling.

Gjengseth, C and T Svenum (2011). Heave compensated managed pressure drilling: A lab scaled rig design.

Glad, J (2013). Conversation.

Guardian (2009). http://www.guardian.co.uk/environment/datablog/2009/nov/10/energy-statistics-oil-coal

Gudmundsson, J. S. (2010). http://www.ipt.ntnu.no/~jsg/undervisning/prosessering/kompendium/5%20Pumper%20(utkast%202010).pdf TPG4135

Hannegan, D (2011). Managed Pressure Drilling Applications on Offshore HPHT Wells. SPE

He, S., C. Ariyaratne and A. E. Vardy (2011) Wall Shear stress in accelerating turbulent pipe flow. Cambridge University Press.

Huang, L., V. T. Galin, and C. Yusong (2011). Investigation of Drill Bit Heave Response to Drill Rig Heave Excitation. ISOPE.

Johansen, S. T. (2013). Conversation.

Landet, I. S., H. Mahdianfar, A. Pavlov and O. M. Aamo (2012). Modeling for MPD Operations with Experimental Validation. IADC/SPE

McCann R. C. and C. G. Islas (1996). Frictional Pressure Loss During Turbulent Flow in Coiled Tubing. SPE.

NOV 2013. http://www.nov.com/Downhole/Telemetry_Drill_Strings /Frequently_Asked_Questions.aspx

Rasmussen, O. S. and S. Sangesland (2007). Managed Pressure Drilling and Underbalanced Operations. IADC/SPE

Rehm. B., J. Schubert, A. Haghshenas, A. S. Paknejad and J. Hughes (2008). Managed Pressure Drilling, Gulf Publishing Company.

Samyak, J., N. Singhal, and S. N. Shah (2004). Effect of Coiled Tubing Curvature on Friction Pressure Loss of Newtonian and Non-Newtonian Fluids – Experimental and Simulation Study. SPE

Sangesland, S (2013). Conversation.

Skalle, P (2013). Conversation.

Skalle, P (2012). Drilling Fluid Engineering, 3. Edition

Statistics 512, Purdue University. http://www.stat.purdue.edu/~jennings/stat514 /stat512notes/topic3.pdf

Steen, A. (2008). http://www.offshore.no/sak/21958_undervurderes_behovet_for_olje

Svenum, T. (2012). Lab for heave motion during managed pressure drilling.

Zhou, Y. and S. N. Shah (2002) Fluid Flow in Coiled Tubing: A Critical Review and Experimental Investigation. Petroleum Society.

APPENDIX A

```
function loop=Lcv3(T,Astring,Kv,FT2_LPM,C1_barg)


cv=81;%number of control volumes
time_lapse=0.01;%sec
Estring=0.4;%m
D_upper_rod=0.025;%m
D_lower_rod=0.022;%m
L_BHA=0.35;%m
D_BHA=40.89/1000;%m
t_cling=0.18/1000;%m
D_cling=D_BHA+t_cling;%m
D_well=0.04253;%m
P_hyd=14300;%bar
alpha_cp=2.7E-13; %m3/m Pa
D_cp=0.016;%m
D_rubberhose=0.019;%m
L_cp=893.6;%m
Rho=998.2;%kg/m3
My=0.001; %Pas
Delta_L_cp=L_cp/81;%m
C1=C1_barg*100000;%Pag
FT2=FT2_LPM*60/1000;%m3/hr
time_delay_cv=1;%1/100 sec

time=time_lapse:time_lapse:T;
A=0.05;
time_delay_emp=1.5;


for t=1:T*100; %string properties and displaced fluid
  string_pos(t)=Astring*sin(2*pi()*(t/100)/T)+Estring;
  string_vel(t)=2*pi()*Astring/T*cos(2*pi()*(t/100)/T); %[m/s]
  string_acc(t)=-(2*pi()/T).^2*Astring*sin(2*pi()*(t/100)/T);
  q_disp(t)=-string_vel(t)*pi()/4*(D_upper_rod.^2-D_lower_rod.^2); %[m3/s]
  v_cp(t)=q_disp(t)/(pi()/4*D_cp.^2);
end


for t=1:T*100 %initial guess, calculates amplitude of control volume
pressure
    for i=2:cv+1
      if t<=round(time_delay_emp*100)

      C2(t)=((q_disp(T*100-(round(time_delay_emp*100)-
t))*3600+FT2)/Kv).^2*100000+C1;
      CP(t,1)=C2(t)+0.92*9.81*Rho;
```

```
      CP_ini(t,2)=CP(t,1)+A*(v_cp(T*100-(round(time_delay_emp*100)-
t)))*100000-0.032*9.81*Rho;
      CP_ini(t,i)=CP_ini(t,i-1)+A*(v_cp(T*100-(round(time_delay_emp*100)-
t)))*100000-0.032*9.81*Rho;

      else
      C2(t)=((q_disp(t-
round(time_delay_emp*100))*3600+FT2)/Kv).^2*100000+C1;
      CP(t,1)=C2(t)+0.92*9.81*Rho;

      CP_ini(t,2)=CP(t,1)+A*(v_cp(t-round(time_delay_emp*100)))*100000-
0.032*9.81*Rho;
      CP_ini(t,i)=CP_ini(t,i-1)+A*(v_cp(t-
round(time_delay_emp*100)))*100000-0.032*9.81*Rho;

      end
   end
end


for t=1:T*100    %initial guess, phase shifts all pressures based on
empirical time delay
    for i=2:cv+1

      if t>T*100-round((i-1)/81*time_delay_emp*100)
      CP(t,i)=CP_ini(t-T*100+round((i-1)/81*time_delay_emp*100),i);
      else
      CP(t,i)=CP_ini(t+round((i-1)/81*time_delay_emp*100),i);
      end

    end
end



for Y=1:1   %number of iteration rounds

 for t=1:T*100 %average pressure change within each cv
      for i=1:cv

        if t==1
        Delta_P_pr_sec_i(t,i)=(((CP(t+1,i+1)+CP(t+1,i))-
(CP(T*100,i+1)+(CP(T*100,i))))/2)/(time_lapse*2);

        elseif t==T*100
        Delta_P_pr_sec_i(t,i)=(((CP(1,i+1)+CP(1,i))-(CP(t-1,i+1)+(CP(t-
1,i))))/2)/(time_lapse*2);

        else
        Delta_P_pr_sec_i(t,i)=(((CP(t+1,i+1)+CP(t+1,i))-(CP(t-
1,i+1)+(CP(t-1,i))))/2)/(time_lapse*2);

        end
```

```
      end
 end


 for t=1:T*100 %accumulated volume
    for i=1:cv

Delta_volum_pr_sec_i(t,i)=Delta_P_pr_sec_i(t,i)*alpha_cp*Delta_L_cp;
    end
 end


 for t=1:T*100 %flowrate through each cv boundary
    flow_to_i(t,cv)=q_disp(t);
      for i=cv-1:-1:1

      flow_to_i(t,i)=flow_to_i(t,i+1)-Delta_volum_pr_sec_i(t,i+1);

      end
    flow_to_FT1(t)=flow_to_i(t,1)-Delta_volum_pr_sec_i(t,1);
 end



 for t=2:T*100-1 % locate max FT1_calc to evaluate compressibility effect
on time delay

     if flow_to_FT1(t)>flow_to_FT1(t-1) &&
flow_to_FT1(t)>flow_to_FT1(t+1);
     max_t=t;
     end

 end

    inertia_effect=T/2+time_delay_emp-max_t/100;


 for t=1:T*100 %phase shift flowrate to match empirical time delay
    for i=cv:-1:1
        if t<=round((81-i)/81*inertia_effect*100)
           flow_to_i_rep(t,i)=flow_to_i((T*100+t)-round((cv-
i)/cv*inertia_effect*100),i);
        else
           flow_to_i_rep(t,i)=flow_to_i(t-round((cv-
i)/cv*inertia_effect*100),i);
        end
    end
        if t<=round(inertia_effect*100)
           flow_to_FT1_rep(t)=flow_to_FT1((T*100+t)-
round(inertia_effect*100));
        else
           flow_to_FT1_rep(t)=flow_to_FT1(t-round(inertia_effect*100));
        end
```

```
end

for t=1:T*100
    for i=cv:-1:1
       flow_to_i(t,i)=flow_to_i_rep(t,i);
       flow_to_FT1(t)=flow_to_FT1_rep(t);
    end
end



for t=1:T*100 %average flowrate through cv
    for i=2:cv
        average_flow_i(t,1)=(flow_to_i(t,1)+flow_to_FT1(t))./2;
        average_flow_i(t,i)=(flow_to_i(t,i)+flow_to_i(t,i-1))./2;
    end
end


for t=1:T*100 %average flow velocity through cv
   for i=1:cv

   average_flow_velo_i(t,i)=average_flow_i(t,i)/(pi()/4*D_cp.^2);

   end
end



for t=1:T*100 %Reynolds number for each cv
   for i=1:cv

      Re_i(t,i)=abs(Rho*average_flow_velo_i(t,i)*D_cp)/My;

   end
end

for t=1:T*100 %Darcy friction factor for each cv
    for i=1:cv
       f_darcy_i(t,i)=10.^0.705./(Re_i(t,i).^0.569);
    end
end


for t=1:T*100 %pressure drop based on instantaneous velocity over cv
    for i=1:cv
       if average_flow_i(t,i)>0

Delta_P_velo_i(t,i)=f_darcy_i(t,i)*Delta_L_cp*Rho*average_flow_velo_i(t,i)
.^2/(2*D_cp);
        else
          Delta_P_velo_i(t,i)=-
f_darcy_i(t,i)*Delta_L_cp*Rho*average_flow_velo_i(t,i).^2/(2*D_cp);
        end
```

```
    end
end



for t=1:T*100 %average fluid acceleration through cv
    for i=1:cv

       if t==1
          hose_acc_i(t,i)=(average_flow_velo_i(t+1,i)-
average_flow_velo_i(T*100,i))/0.02;
       elseif t==T*100
          hose_acc_i(t,i)=(average_flow_velo_i(1,i)-
average_flow_velo_i(t-1,i))/0.02;
       else
          hose_acc_i(t,i)=(average_flow_velo_i(t+1,i)-
average_flow_velo_i(t-1,i))/0.02;
       end
    end
end



for t=1:T*100 %Pressure drop based on acceleration over cv
   for i=1:cv
       Delta_P_acc_i(t,i)=Rho*Delta_L_cp*hose_acc_i(t,i);
   end
end






for t=1:T*100 %calculates pressure throughout the copper pipe
      C2(t)=((flow_to_FT1(t)*3600+FT2)/Kv).^2*100000+C1;
      CP(t,1)=C2(t)+0.92*9.81*Rho;
end

for i=2:cv+1
    for t=1:T*100

      if t>T*100-time_delay_cv
        CP(t,i)=CP(t-T*100+time_delay_cv,i-1)+Delta_P_acc_i(t,i-
1)+Delta_P_velo_i(t,i-1)-0.032*9.81*Rho;
      else
        CP(t,i)=CP(t+time_delay_cv,i-1)+Delta_P_acc_i(t,i-
1)+Delta_P_velo_i(t,i-1)-0.032*9.81*Rho;
      end
    end
end


end
```

```
 for t=1:T*100 %P2 based on empirical relation
       if q_disp(t)>0

P2(t)=CP(t,cv+1)+100000*(10*(q_disp(t)/(pi()/4*D_rubberhose.^2)).^1.75-
0.15);
       else
         P2(t)=CP(t,cv+1)-
100000*(10*(abs(q_disp(t)/(pi()/4*D_rubberhose.^2))).^1.75+0.15);
       end
 end



%calculating pressure drop between P1 and P2
for t=1:T*100;
    if string_vel(t)>0;
        fortegn=-1;
        rod1=D_upper_rod;
        rod2=D_lower_rod;
    else;

        fortegn=1;
        rod1=D_lower_rod;
        rod2=D_upper_rod;
    end


    q_disp_BHA(t)=-string_vel(t)*pi()/4*(D_BHA.^2-D_lower_rod.^2);
    q_cling(t)=-(string_vel(t)/2)*pi()/4*(D_cling.^2-D_BHA.^2);
    q_eff(t)=q_disp_BHA(t)+q_cling(t);
    v_fluid_ave_eff(t)=q_eff(t)/(pi()/4*(D_well.^2-D_cling.^2));



P_fric(t)=0.1582*fortegn*Rho.^0.75*My.^0.25*L_BHA*(abs(v_fluid_ave_eff(t))
).^1.75/((D_well-D_cling).^1.25);
    P_entrance_loss(t)=fortegn*0.42*(1-((D_well-D_cling).^2/(D_well-
rod1).^2))*v_fluid_ave_eff(t).^2/2*Rho;
    P_exit_loss(t)=fortegn*(1-((D_well-D_cling).^2/(D_well-
rod2).^2)).^2*v_fluid_ave_eff(t).^2/2*Rho;
    P_acc_upper_rod(t)=-Rho*string_acc(t)*(0.675+Astring-
string_pos(t))*(D_cling.^2-D_lower_rod.^2)/(D_well.^2-D_upper_rod.^2);
    P_acc_BHA(t)=-Rho*string_acc(t)*L_BHA*(D_cling.^2-
D_lower_rod.^2)/(D_well.^2-D_cling.^2);
    P_acc_lower_rod(t)=-Rho*string_acc(t)*(0.675-
Astring+string_pos(t))*(D_cling.^2-D_lower_rod.^2)/(D_well.^2-
D_lower_rod.^2);
```

```
P_w(t)=P_fric(t)+P_entrance_loss(t)+P_exit_loss(t)+P_acc_upper_rod(t)+P_ac
c_BHA(t)+P_acc_lower_rod(t)+P_hyd;

    P1(t)=P2(t)+P_w(t);
end
```

```
  for t=1:T*100
         [P1_barg(t)]=P1(t)/100000;
         [P2_barg(t)]=P2(t)/100000;
         [C2_barg(t)]=C2(t)/100000;
         [CP1_barg(t)]=CP(t,1)/100000;
         [CP2_barg(t)]=CP(t,10)/100000;
         [CP3_barg(t)]=CP(t,19)/100000;
         [CP4_barg(t)]=CP(t,28)/100000;
         [CP5_barg(t)]=CP(t,37)/100000;
         [CP6_barg(t)]=CP(t,46)/100000;
         [CP7_barg(t)]=CP(t,55)/100000;
         [CP8_barg(t)]=CP(t,64)/100000;
         [CP9_barg(t)]=CP(t,73)/100000;
         [CP10_barg(t)]=CP(t,82)/100000;
         [q_disp_LPM(t)]=q_disp(t)*60000;
         [FT1_LPM(t)]=flow_to_FT1(t)*60000;

  end
```

```
    subplot(3,1,2)
    plot(time,FT1_LPM,time,q_disp_LPM)
    legend('flow_to_FT1','q_disp')
    subplot(3,1,3)
    plot(time,C2_barg,time,CP10_barg,time,P1_barg,time,P2_barg)
    legend('C2','CP10','P1_barg','P2_barg')
```

```
time=time(:);
P1_barg=P1_barg(:);
P2_barg=P2_barg(:);
C2_barg=C2_barg(:);
CP1_barg=CP1_barg(:);
CP2_barg=CP2_barg(:);
CP3_barg=CP3_barg(:);
CP4_barg=CP4_barg(:);
CP5_barg=CP5_barg(:);
CP6_barg=CP6_barg(:);
CP7_barg=CP7_barg(:);
CP8_barg=CP8_barg(:);
CP9_barg=CP9_barg(:);
CP10_barg=CP10_barg(:);
q_disp_LPM=q_disp_LPM(:);
FT1_LPM=FT1_LPM(:);
```

```
title={'Pressure and flow calculations for MPD Heave Lab'};
row_header1={'String period [sec]'};
row_header2={'String Amplitude [m]'};
row_header3={'Pump flowrate [LPM]'};
row_header4={'Choke cooeficient kv'};
row_header5={'Pressure downstream choke C1 [barg]'};
row_header6={'total time delay empirical [sec]'};
row_header7={'time delay inertial effect [sec]'};
col_header1={'time [sec]'};
col_header2={'q_disp [LPM]'};
col_header3={'FT1 [LPM]'};
col_header4={'C2 [barg]'};
col_header5={'CP1 [barg]'};
col_header6={'CP2 [barg]'};
col_header7={'CP3 [barg]'};
col_header8={'CP4 [barg]'};
col_header9={'CP5 [barg]'};
col_header10={'CP6 [barg]'};
col_header11={'CP7 [barg]'};
col_header12={'CP8 [barg]'};
col_header13={'CP9 [barg]'};
col_header14={'CP10 [barg]'};
col_header15={'P1 [barg]'};
col_header16={'P2 [barg]'};

xlswrite('output',title,'sheet1','A1:A1')
xlswrite('output',row_header1,'sheet1','A3:A3')
xlswrite('output',row_header2,'sheet1','A4:A4')
xlswrite('output',row_header3,'sheet1','A5:A5')
xlswrite('output',row_header4,'sheet1','A6:A6')
xlswrite('output',row_header5,'sheet1','A7:A7')
xlswrite('output',row_header6,'sheet1','A8:A8')
xlswrite('output',row_header7,'sheet1','A9:A9')
xlswrite('output',T,'sheet1','B3:B3')
xlswrite('output',Astring,'sheet1','B4:B4')
xlswrite('output',FT2_LPM,'sheet1','B5:B5')
xlswrite('output',Kv,'sheet1','B6:B6')
xlswrite('output',C1_barg,'sheet1','B7:B7')
xlswrite('output',time_delay_emp,'sheet1','B8:B8')
xlswrite('output',inertia_effect,'sheet1','B9:B9')



xlswrite('output',col_header1,'sheet1','A11:A11')
xlswrite('output',time,'sheet1','A12:A1212')
xlswrite('output',col_header2,'sheet1','B11:B11')
xlswrite('output',q_disp_LPM,'sheet1','B12:B1212')
xlswrite('output',col_header3,'sheet1','C11:C11')
xlswrite('output',FT1_LPM,'sheet1','C12:C1212')
xlswrite('output',col_header4,'sheet1','D11:D11')
xlswrite('output',C2_barg,'sheet1','D12:D1212')
xlswrite('output',col_header5,'sheet1','E11:E11')
xlswrite('output',CP1_barg,'sheet1','E12:E1212')
xlswrite('output',col_header6,'sheet1','F11:F11')
```

```
xlswrite('output',CP2_barg,'sheet1','F12:F1212')
xlswrite('output',col_header7,'sheet1','G11:G11')
xlswrite('output',CP3_barg,'sheet1','G12:G1212')
xlswrite('output',col_header8,'sheet1','H11:H11')
xlswrite('output',CP4_barg,'sheet1','H12:H1212')
xlswrite('output',col_header9,'sheet1','I11:I11')
xlswrite('output',CP5_barg,'sheet1','I12:I1212')
xlswrite('output',col_header10,'sheet1','J11:J11')
xlswrite('output',CP6_barg,'sheet1','J12:J1212')
xlswrite('output',col_header11,'sheet1','K11:K11')
xlswrite('output',CP7_barg,'sheet1','K12:K1212')
xlswrite('output',col_header12,'sheet1','L11:L11')
xlswrite('output',CP8_barg,'sheet1','L12:L1212')
xlswrite('output',col_header13,'sheet1','M11:M11')
xlswrite('output',CP9_barg,'sheet1','M12:M1212')
xlswrite('output',col_header14,'sheet1','N11:N11')
xlswrite('output',CP10_barg,'sheet1','N12:N1212')
xlswrite('output',col_header15,'sheet1','O11:O11')
xlswrite('output',P1_barg,'sheet1','O12:O1212')
xlswrite('output',col_header16,'sheet1','P11:P11')
xlswrite('output',P2_barg,'sheet1','P12:P1212')




end
```

APPENDIX B

Calculation uncertainty based on uncertain input parameters may be calculated from Gaussian error propagation. Calculation uncertainty is given by equation B.1

$$\delta K_v = \sqrt{\left(\frac{dK_v}{dq}\delta q\right)^2 + \left(\frac{dK_v}{d\Delta P}\delta \Delta P\right)^2} \quad \text{(B.1)}$$

This equation is used to evaluate uncertainty for K_v discussed in chapter 6.2.2.

$$K_v = \frac{q}{\sqrt{\Delta P}} \quad \text{(B.2)}$$

The partially derivative of equation B.2 with respect to flow *q* and pressure drop *ΔP* , are found below.

$\frac{dK_v}{dq} = \frac{1}{\sqrt{\Delta P}}$ and $\frac{dK_v}{d\Delta P} = \frac{-q}{2\Delta P^{3/2}}$

The partially derivative are substituted into equation B.1, to find the expression for K_v uncertainty.

$$\delta K_v = \sqrt{\left(\frac{1}{\sqrt{\Delta P}}\delta q\right)^2 + \left(\frac{-q}{2\Delta P^{\frac{3}{2}}}\delta \Delta P\right)^2} \quad \text{(B.3)}$$

Where parameters denote following:

$\delta K_v = calculation\ uncertainty.$

$\delta q = flow\ uncertainty$

$\delta \Delta P = Pressure\ drop\ uncertainty$

$\Delta P = Pressure\ drop$

$q = flowrate$

Equation B.3 is used to find calculation uncertainty for $\Delta P = 5.16bar, q = 5.16m3/hr, \delta \Delta P = 0.1bar\ and\ \delta q = 0.06m3/hr.$

$$\delta K_v = \sqrt{\left(\frac{1}{\sqrt{\Delta P}}\delta q\right)^2 + \left(\frac{-q}{2\Delta P^{\frac{3}{2}}}\delta \Delta P\right)^2} = \sqrt{\left(\frac{1}{\sqrt{5.16}}\ 0.06\right)^2 + \left(\frac{-1.59}{2\times 5.16^{\frac{3}{2}}}\ 0.1\right)^2} = 0.027.$$

APPENDIX C

Method of least squares

Simple linear regression is a method to fit a linear curve between a set of points, minimizing the squared error term ε (distance between the data points and the fitted line). A general linear equation including the error term ε is stated in equation C1.

$$Y_i = \beta_0 + \beta_1 X_i + \varepsilon_i$$

(C.1)

In matrix form the linear equation can be written as follow;

$$\begin{bmatrix} Y_1 \\ Y_2 \\ \vdots \\ Y_n \end{bmatrix} = \begin{bmatrix} 1 & X_1 \\ 1 & X_2 \\ \vdots & \vdots \\ 1 & X_n \end{bmatrix} \begin{bmatrix} \beta_0 \\ \beta_1 \end{bmatrix} + \begin{bmatrix} \varepsilon_1 \\ \varepsilon_2 \\ \vdots \\ \varepsilon_n \end{bmatrix}$$

(C.2)

In equation C.2, $\boldsymbol{X}$ is the design matrix, $\boldsymbol{Y}$ is called the response vector, $\boldsymbol{\beta}$ is the vector of parameters and $\boldsymbol{\varepsilon}$ is called the error vector.

$$\boldsymbol{X} = \begin{bmatrix} 1 & X_1 \\ 1 & X_2 \\ \vdots & \vdots \\ 1 & X_n \end{bmatrix}, \boldsymbol{Y} = \begin{bmatrix} Y_1 \\ Y_2 \\ \vdots \\ Y_n \end{bmatrix}, \boldsymbol{\beta} = \begin{bmatrix} \beta_0 \\ \beta_1 \end{bmatrix} \quad \boldsymbol{\varepsilon} = \begin{bmatrix} \varepsilon_1 \\ \varepsilon_2 \\ \vdots \\ \varepsilon_n \end{bmatrix}$$

Method of least squares is used to solve equation (), the error vector $\boldsymbol{\varepsilon}$ can be rewritten to; $\boldsymbol{\varepsilon = Y - X\beta}$. By minimizing the sum of squared error terms in equation C.3, the parameter vector $\boldsymbol{\beta}$ can be determined.

$$\sum {\varepsilon_i}^2 = \begin{bmatrix} \varepsilon_1 & \varepsilon_2 & \cdots & \varepsilon_n \end{bmatrix} \begin{bmatrix} \varepsilon_1 \\ \varepsilon_2 \\ \vdots \\ \varepsilon_n \end{bmatrix} = \boldsymbol{\varepsilon}^T \boldsymbol{\varepsilon} = (\boldsymbol{Y - X\beta})^T (\boldsymbol{Y - X\beta})$$

(C.3)

In equation C.3 the raised notation *T* denotes the transpose of the matrix. Equation C.3 is minimized by finding the derivative with respect to β and setting it equal to zero. The derivative can be found with the chain rule; $\frac{d\,((\boldsymbol{Y-X\beta})^T(\boldsymbol{Y-X\beta}))}{d\boldsymbol{\beta}} = -\boldsymbol{X}^T(\boldsymbol{Y - X\beta}) - \boldsymbol{X}^T(\boldsymbol{Y - X\beta}) = -\boldsymbol{2X}^T(\boldsymbol{Y - X\beta})$. When setting the derivative equal to zero, vector parameter $\boldsymbol{\beta}$ is expressed as follows; $-2\boldsymbol{X}^T(\boldsymbol{Y - X\beta}) = \boldsymbol{0} \xrightarrow{\boldsymbol{yields}} \boldsymbol{X}^T\boldsymbol{Y} = (\boldsymbol{X}^T\boldsymbol{X})\boldsymbol{\beta}$.

$$\boldsymbol{\beta} = (\boldsymbol{X}^T\boldsymbol{X})^{-1}\boldsymbol{X}^T\boldsymbol{Y}$$

(C.4)